Effect of Pore Geometry on Membrane Flux Decline due to Pore Constriction by Particles in Ultra and Micro Filtration

By:

Mohammad Hosein Faghihi

A thesis submitted to the

Faculty of Graduate and Postdoctoral Studies

In partial fulfillment of the requirements for the degree of

Master of Applied Science in Chemical Engineering

Department of Chemical & Biological Engineering

Faculty of Engineering

University of Ottawa

STATEMENT OF CONTRIBUTIONS OF COLLABORATORS

I hereby declare that I am the sole author of this Masters' thesis. All articles in this thesis are co-authored with my research supervisor Dr. André Y. Tremblay. All the experimental, simulations and analytical work related to these articles was performed by me under the supervision of professor Tremblay.

My supervisor, Dr. Tremblay, provided me with an excellent collaboration throughout this work with regular meetings, discussions, supports and editorial comments for all of my written work. As a result the quality of this thesis has been tremendously improved through his guidance.

Signature:

Date: May 28, 2013

Mohammad H. Faghihi

To my mother

ABSTRACT

Membrane separation is known as an economic and environmental friendly mode of separation and is used in various types of separation processes. The major challenges regarding membrane separation are the internal and external fouling of the membrane which reduces the permeate flux of the membranes by inducing extra resistance to flow.

Synthetic membranes are designed and implemented to separate solutes or particles in a feed stream by rejecting them and permitting the liquid to pass through the membrane pores; however, most of the feed streams, such as wastewaters, contain more than one type of solute. This yields a distribution of particle sizes in the feed. Many wastewaters contain supracolloidal particles (1-100µm). Most membrane separations aim to remove these particles from the feed solution. Wastewaters also contain colloidal particles (0.001-1µm). These particles are less concentrated than supracolloidal particles in the feed but they are more problematic since they are able to penetrate into the membrane pores and cause internal fouling which is the main source of irreversible flux decline.

Fouling mechanisms are traditionally classified into four types. Among these mechanisms, standard pore blocking (pore constriction) refers to internal fouling while the other types model external fouling. On the effect of pore geometry, as a morphological factor, studies to date have been limited to external membrane fouling. However, it is believed that up to 80% of the permeate flux can be affected by pore constriction which is caused by particle penetration and deposition into membrane pores (internal fouling).

The effect of pore geometry, as a factor, in flux decline due pore constriction of membranes was investigated in this work. Pore constriction by particles was approximated by maximum particle deposition onto the interior wall of the pores and simulated using MATLAB image processing toolbox (MIPT). Sixteen different basic geometries were considered for the simulation of pore constriction by particles. These include circular pores, 3 groups of rectangular, triangular and oval geometries at four different aspect ratios (3, 7, 15 and 30) and three combined geometries of star, cross and a rectangle with rounded ends. The

simulation of maximum particle deposition onto pore walls was carried out for a range of particle diameters to pore hydraulic diameters (λ) of 0.1 to the complete rejection of the particle by the pore. As the result of the simulation, the ratio of the available pore cross-sectional area after pore constriction to initial pore cross-sectional area (α) and the ratio of pore channel hydraulic diameter after pore constriction to initial pore hydraulic diameter (β) were measured and recorded. It was observed that for λ<0.2 (small particles compared to pore size) some geometries showed the same values of α and β. However, for λ>0.2, other geometries showed different values of α and β. It was also observed that several geometries reject the particle at different λ ratios.

Using the values of α and β, the fluxes of membranes having different pore geometries, after pore constriction by particles, were calculated and compared. These results show that for a very small particle size, compared to pore size, there is no preference for a specific geometry over another; however, for intermediate particle sizes, membranes having triangular and star pore shapes provide higher fluxes compared to other membranes. The effect of pore aspect ratio (PAR) on the flux of membranes after pore constriction was also examined.

In order to compare the combined effect of pore geometry on particle rejection and pore constriction, fluxes of membranes having different pore shapes were compared in light of several pore size distributions (PSDs). For this part of the study, the pore geometries of circular, rectangular, triangular and oval were considered at four PARs. Different values for the hydraulic diameter of the largest rejecting pore ($D_{H,LRP}$) were observed for different geometries. Rectangular pores showed the largest values of $D_{H,LRP}$, at a constant PAR, which affirms their superior rejection behavior. The overall flux of the membranes after pore constriction was determined by a combination of three effects: the position of $D_{H,LRP}$ in the PSD, the pore constriction behavior of the pore geometry and the shape of the PSD. Generally, for the PSDs for which most of the pores in the membrane physically reject the particles, membranes having rectangular pores showed higher fluxes, due to the greater rejection of particles. However, for PSDs for which a major number of pores are constricted by the particles, membranes with triangular pores offered higher flux after membrane pore constriction. The results of this work indicate a new direction for the design of membranes having defined pore geometries.

RÉSUMÉ

La séparation par membrane est un procédé qui est utilisé dans différents types de séparations. Les défis majeurs concernant la séparation membranaire sont l'encrassement interne et externe de la membrane. Le colmatage des membranes réduit le flux de perméat. Ceci peut se produire soit en raison du dépôt des particules à la surface externe de la membrane et couvrant la surface active de la membrane (encrassement externe), ou en raison de la pénétration et du dépôt de particules dans la structure intérieure des membranes (encrassement interne).

Les membranes synthétiques sont conçues et mises en œuvre pour séparer des solutés ou des particules en solution en les rejetant ce qui permet au liquide seul de passer à travers des pores de la membrane. Plusieurs alimentations, telles que les eaux usées, contiennent plus d'un type de soluté. Cela donne une distribution de tailles de particules dans l'alimentation. Les eaux usées sont fortement concentrées en particules supracolloidales (1-100 microns). La plupart des séparations par membrane visent à éliminer ces particules. Les eaux usées contiennent aussi des particules colloïdales (0,001-1μm). Ces particules sont moins concentrées que les particules supracolloidales dans l'alimentation, mais elles sont plus problématiques car elles sont capables de pénétrer dans les pores de la membrane et provoquer un encrassement interne qui est la source principale de la baisse du flux irréversible observé lors de l'opération des membranes.

Les mécanismes d'encrassement sont traditionnellement classés en quatre types. Parmi ces mécanismes, le blocage des pores dit «standard» (constriction des pores) réfère à l'encrassement interne alors que les autres sont utilisés pour modéliser l'encrassement externe. L'étendue et l'intensité de l'encrassement à l'extérieur de la membrane sont influencées par la morphologie de la membrane. Les études faites sur ce type d'entartrage ont été limitées aux phénomènes qui se produisent à l'extérieur des pores. Toutefois, on estime qu'une réduction de 80% du flux de perméat peut être causée par la constriction des pores qui est dû à la pénétration et le dépôt des particules dans les pores de la membrane.

L'objet de cette étude était de déterminer l'effet de la géométrie des pores sur le déclin du flux due à la constriction des pores. La constriction des pores par des particules a été modélisée par le dépôt maximal de particules sur la paroi intérieure des pores et simulées à l'aide de MATLAB image processing toolbox (MIPT).

Afin d'étudier l'effet de la forme des pores, 16 géométries de base ont été considérées pour la simulation de la constriction des pores par des particules. Il s'agit notamment de pores circulaires, 3 groupes de géométries rectangulaires, triangulaires ou ovales à quatre rapports d'aspect différents (3, 7, 15 et 30) et trois géométries combinées des étoiles, croix et un rectangle avec des bouts arrondis. La simulation de dépôt maximal de particules sur les parois des pores a été effectuée pour chaque géométrie, pour une gamme de diamètres de particules de diamètres hydrauliques des pores (λ) comprise entre 0,1 et le rejet complet de la particule par le pore. Le rapport de l'aire de section transversale de pore disponible après la constriction des pores et de la surface de section transversale de pore initiale (α) ainsi que le rapport du diamètre hydraulique des pores après la constriction des pores et du diamètre hydraulique de pores initial (β) ont étés mesurés et enregistrés. Les valeurs de α et β sont tracées par rapport à λ. Il a été observé que pour λ <0,2 (petites particules par rapport à la taille des pores) toutes les géométries prédisent les mêmes valeurs de α et β. Cependant, pour λ> 0,2, les valeurs de α et β sont différentes.

Le flux de membranes ayant différentes géométries de pores, après la constriction des pores par des particules, ont été calculés et comparés. Le flux des membranes après constriction des pores par des particules montre que pour la filtration de petites particules (0,01 µm), il n'y a pas de préférence pour une géométrie spécifique plutôt qu'une autre, mais pour des tailles de particules intermédiaires, des membranes ayant des formes triangulaires et en étoile fournissent des flux supérieurs à ceux des autres membranes. L'effet du rapport d'aspect des pores (PAR) sur le flux des membranes après constriction des pores a également été examiné.

Afin de comparer l'effet combiné de la géométrie des pores sur le rejet de particules et la constriction des pores, les flux de membranes ayant des formes différentes de pores ont été comparés à la lumière de plusieurs distributions de taille des pores (DTP). Pour cette partie de l'étude, les géométries des pores de la circulaire, rectangulaire, triangulaire ou ovale ont été examinées à quatre RAP. Différentes valeurs du diamètre hydraulique du plus grand pore rejetant une particule d'intérêt ($D_{H,\ LRP}$) ont été observées pour différentes géométries. Les pores rectangulaires ont montré les plus grandes valeurs de $D_{H,LRP}$, à une valeur constante du PAR, ce qui confirme leur comportement de rejet supérieur. Le flux global des membranes après la constriction des pores a été déterminé par une combinaison des trois effets: la position de $D_{H,LRP}$ dans la distribution des pores de la membrane, la constriction des pores dû à la géométrie des pores et de la forme de la DTP. En général, pour les DTP pour laquelle la plupart des pores dans la membrane rejettent physiquement les particules, les membranes ayant des pores rectangulaires ont montrés des flux plus élevés, en raison du plus grand rejet de particules. Cependant, pour des DTP pour lesquels un nombre important de pores sont rétrécis par les particules, les membranes ayant des pores triangulaires offrent un flux plus élevé que toutes autres géométries. Les résultats de cette étude indiquent de nouvelles directions pour la conception de membranes, ayant des pores de géométrie fixe, pour augmenter leur durée de vie.

ACKNOWLEDGMENTS

Hereby I wish to express my sincere appreciation and gratitude from the bottom of my heart to my research supervisor, Dr. André Tremblay, for his excellent guidance and generous supervision throughout this research. I gained a lot of knowledge during our lively and friendly discussions and had the greatest opportunity to profit such a professional and pure supervision to improve my research skills. I thank him for his boundless support and patience during the completion of this thesis. I will always remember and appreciate his support which was far beyond the regular requirement for an academic supervisor.

I also wish to thank my father, Asadollah Faghihi, for his complete support and encouragement during my studies and for teaching me the way to believe in myself; and finally I wish to thank my lovely wife, Sara Barghi, who is always beside me with her endless kindness and understanding.

.

NOMENCLATURE

A	Pore area(L^2)
D	Diameter (L)
D_H	Hydraulic diameter (L)
f	Pore frequency
J	Membrane flux (MT^{-1})
l	Membrane thickness (L)
n	Number of pores per unit area of the membrane(L^{-2})
p	Pore diameter (L)
ΔP	Pressure difference across the membrane thickness ($ML^{-1}T^{-2}$)
Q	Flow rate (L^3T^{-1})

Subscripts

$clean$	Clean membrane
$constricted$	Constricted membrane
i	Pore index

Greek Symbols

α	Ratio of constricted pore's area to clean pore's area
β	Ratio of constricted pore's hydraulic diameter to clean pore's hydraulic diameter
ϵ	Membrane porosity
λ	Ratio of particle diameter to pore hydraulic diameter
μ	Permeate viscosity ($ML^{-1}T^{-1}$)
σ	Standard deviation

ABBREVIATIONS

AAF	Accumulative area frequency
AF	Area frequency
BP	Back pulsing
cP	Centipoise
lmh	Liters per meter square hour
LRP	Largest rejecting pore
MF	Microfiltration
MIPT	MATLAB image processing toolbox
MWCO	Molecular weight cut-off
PSD	Pore size distribution
RO	Reverse osmosis
RP	Rejecting pores
SEM	Scanning electron microscopy
SF	Shape factor
TMP	Trans membrane pressure
UF	Ultrafiltration

TABLE OF CONTENTS

LIST OF TABLES

LIST OF FIGURES

CHAPTER II (Paper 1)

CHAPTER I

Introduction

According to a definition provided by Hsieh [1996], a membrane is a semipermeable barrier which preferentially blocks one or more desired species in a mixture and permits the rest to pass through it due to a driving force. This driving force might be a gradient of pressure, concentration or electrical voltage along the membrane thickness. The rejected components are called retentate, and the components passing through are called permeate or solvent.

Membranes are used in variety of industrial, environmental, medical and agricultural applications. In industrial applications, they are used for various separation processes such as catalyst recycling and reuse and material processing, to name a few. Membranes are also used for municipal and industrial wastewater treatment, water purification, brackish and sea water desalination. Examples of agricultural application of membranes are micro-organism removal from dairy products or concentrating proteins from milk whey. Membranes are also used in medical and pharmaceutical applications such as dialysis, drug delivery systems and artificial organs [Baker, 2004; Baker *et al.*, 1991; Hwang and Lin, 2002].

Membrane separation processes are operated in two major modes according to the direction of feed flow towards the membrane. These modes are known as dead-end filtration and cross-flow filtration. In dead-end filtration the feed flow is perpendicular to the membrane surface while in cross-flow filtration the feed stream is flowing tangential to the membrane surface [HSIEH, 1996].

Baker [2004] classifies industrial membrane separations in different groups based on the size of the solutes to be separated. These groups are microfiltration (MF), ultrafiltration (UF), reverse osmosis (RO), pervaporation, electrodialysis and gas separation. This research is mainly focused on MF and UF based on the range of particle sizes used in the study. MF membranes are used to separate suspended particles in diameter ranges from 0.1 to 10 µms. MF membranes are used in sterile filtration of pharmaceuticals, sterilization of wine and beer and drinking water treatment. UF membranes are used for separation of water and micro-solutes from macromolecules and colloids. The average pore diameter of a UF membrane is between 10 and 1000 $\dot{A}$. UF membranes are used in the food industry (cheese production), clarification of fruit juice, oil–water emulsions and process water and product recycling [Baker, 2004].

Membrane fouling

Membrane fouling is the main factor limiting almost all membrane separation processes and is known to be the primary source of decline in permeate flux. The clean membrane flux, in its initial moments of application, is usually high compared to the steady state flux of the membrane. One source of this decline in flux is a phenomenon called concentration polarization. Concentration polarization causes the rejected solutes to deposit on the surface of the membrane and cause membrane fouling. The dense layer of agglomerated particles, commonly known as cake layer, reduces the flux by provoking extra resistance to permeate flow [Baker, 2004]. Another source of fouling are molecular interactions (hydrophobic interactions, van der Waals attraction, *etc.*) between the solutes and membrane material which causes the adsorption and attachment of solutes to membrane surface [Strathmann, 2006].

Hermia [1982] defined four fouling mechanisms which are extensively used in the literature to model membrane flux decline behavior [Chang *et al.*, 2011; Wang, X. *et al.*, 2012; Wang, C. *et al.*, 2012; Mah *et al.*, 2012]. These mechanisms and the explanations are as follows [Wang and Tarabara, 2008]:

1. Standard pore blocking (also known as pore constriction): particles penetrate through the pores and deposit into the pore walls causing a reduction in available pore volume to flow.
2. Complete pore blocking: particles block the entrance of the pores without overlaying each other.
3. Cake filtration: particles do not block the pores individually but the cake made by the aggregation of the particles is a barrier to flow. This happens in the case of dense

membranes or membranes with very small pores compared to the particles being separated.

4. Intermediate blocking: some particles block the entrance of the pores and some other particles overlay each other to form a cake.

It is always desired to minimize membrane fouling since it can affect many aspects of the separation operation in a plant. The amount of energy consumed by a treatment plant, number of required membrane modules, membrane replacement, *etc.* and the consequent costs, all can be affected by the type and extent of fouling [Jacquemet *et al.*, 2006].

Membrane fouling cannot be prevented but there has been efforts to reduce and control it by different methods e.g. morphology and surface modification, optimization of the system design and modules, setting regular cleaning protocols, *etc.* [Judd and Jefferson, 2003; Baker, 2004].

One of the cleaning procedures which is commonly used in membrane separations is back-flushing. By this mean, a portion of declined flux due to fouling is recoverable by periodic back-flushing of the permeate; but, the amount of the recovered flux will decrease after a certain time of operation. This permanent decline in flux is mainly due to the internal fouling of the membrane. Internal fouling is caused by the solutes that penetrate into the membrane and deposit in the interior structure of the membrane [Baker, 2004]. This corresponds to the first fouling mechanism mentioned above (pore constriction). It has been shown that up to 80% of the permeate volume can be affected by pore constriction [Wang and Tarabara, 2008]; therefore, minimizing pore constriction and its contribution to membrane flux decline can extensively impact the economic viability of membrane separation by increasing membrane life and productivity.

Factors affecting membrane fouling

There are numerous factors determining the extent and intensity of membrane fouling. These factors are including but not limited to: membrane material and morphology, solutes to be separated, mutual interaction of membrane material and solutes [Hwang and Lin, 2002; Baker, 2004; Fane and Fell, 1987; Lim and Bai, 2003].

Among different factors affecting the fouling behavior of the membranes, membrane morphology is of interest to researchers. Understanding the effect of membrane morphology on the fouling behavior of membranes can lead to the design of membranes with enhanced performance and fouling resistance. Morphological factors like porosity, asymmetricity, pore inter-connectivity, homogeneity, pore geometry, *etc.* all have shown to affect the fouling behavior of the membranes [Ho and Zydney, 1999; Zydney and Ho 2003; Hwang and Lin, 2002; Brans *et al.*, 2006; Chandler and Zydney, 2006].

Pore geometry

Amongst these morphological factors, the effect of pore geometry has been investigated to a lesser extent. Chandler and Zydney [2006] compared the rate of flux decline due to particle deposition at the entrance of the membrane pores for two membranes each having a unique pore shape. They showed that membranes having long slotted pores offer slower rates of flux decline compared to membranes having circular pores. In another study, Brans *et al.* [2006] studied membranes having different pore shapes of circular, rectangular, oval and triangular to compare the ease of release of the particles deposited at the entrance of the membrane pores. Their result showed that triangular pores facilitate particle release by the external cross-flow on the surface of the membrane. Almost all published articles on this subject assume all of the pores on the surface of the membrane to completely reject the particle existing in the feed solution. This disregards the effect of geometry when there is a particle penetration through the membrane pores; while, as mentioned before, up to 80% of the membrane's permeate volume can be affected by pore constriction which is a direct result of particle penetration into the pores [Wang and Tarabara, 2008].

Distribution of particle sizes found in feed streams

Many membrane separation processes treat feed solutions containing a mixture of particles with different sizes. Seawater contains suspended particulate matter with multimodal diameter distribution of 2 to 128μm [Sheldon *et al.*, 1967]. In wastewater streams, there is a mixture of particulates, soluble inorganic and organic substances which cover a range of particle sizes [Levine *et al.*, 1985]. The particle in wastewater streams can be categorized as dissolved (<0.001μm), colloidal (0.001-1μm), supracolloidal (1-100μm) and settleable (>100μm). The size distribution of particles in these streams varies depending on the type and source of the stream. A substantial portion of the organic matter in wastewaters are in the colloidal and supracolloidal sizes [Levine *et al.*, 1991]. Oily wastewaters are mostly produced in oil and gas production and are usually concentrated in hydrocarbon constitutes and different salts [Pendashteh *et al.*, 2012]. Different size ranges for the particles and colloids found in oily wastewaters are reported in literature. Some examples of the reported particle diameter ranges are 0.07-1.5μm [Salahi *et al.*, 2010], 0.05-0.3μm [Chang *et al.*, 2001] and 0.3-30μm [Pendashteh *et al.*, 2012]. Peng *et al.* [2005] used UF and MF for filtration of bilge water containing a bimodal particle distribution. The smaller particle sizes were 0.07, 0.089 and 0.1μm; while the larger ones were between 2 and 5 μm.

Problem definition

Wang and Tarabara [2008] showed that up to 80% of the permeate flow through a membrane can be affected by pore constriction which is a direct consequence of particle penetration into membrane pores. This is compatible with the fact that many wastewater streams contain a distribution of particle sizes instead of a unique size. The particle size distribution of these solutions is often bimodal. The smaller particles are in the sub-micron range and can be colloids, humic acids, proteins, or partially dissolved solids. The larger particles can be for example: oil droplets, debris or suspended matter.

If in the filtration of these mixtures, a membrane with very small pores is used to reject all particles a high operating pressure will be required. This will negatively affect process economics. A suitable membrane to separate such mixtures is one with a pore size just below the desired cut-off where separation is to be achieved. Often this is a pore size just below the smaller particle size or in between the two particle sizes in a feed containing a bimodal particle size distribution. In choosing a membrane with an intermediate pore size, the larger particles are rejected by the membrane, as the process intended, but the smaller ones are able to penetrate into the structure of the membrane and cause gradual internal fouling.

Membranes have a distribution of pore sizes instead of a unique pore size. The internal fouling process may also happen for a unimodal distribution of particles where there is a distribution of pore sizes for these membranes. In this distribution, some pores are physically larger than the particles. These larger pores are the main contributors to membrane flow but they are also susceptible to particle penetration and internal fouling. A question of major interest, and the incentive of this research, is: What would be the effect of pore geometry be on the deposition of particles within membrane pores (pore constriction) and the effect on flux decline? The best geometry would lead to the design of membranes with improved productivity and service life.

Thesis objectives

The main purpose of this research is to compare the effect of different pore geometries on the extent of internal fouling by particles. This was carried out by simulating maximum particle deposition onto pore walls. This was done using the MATLAB image analysis toolbox.

The objective of this thesis can be divided to three sections:

1) Designing a general algorithm for the simulation of maximum particle deposition onto the interior perimeter of a membrane pore. This was used to represent pore constriction by particles. This method is applicable to any regular or irregular shaped pore geometry.

2) Comparing the flux of membranes having different basic pore geometries but the same hydraulic diameter, after maximum particle deposition onto pore walls to examine the effect of geometry on the flux decline due to pore constriction. This was carried out using the calculated values of the hydraulic diameter and the available area for flow of the pores, before and after particle deposition.

3) Investigating the combined effect of pore constriction by particles and particle rejection by the pores, in the case of the existence of a distribution of pore sizes, to compare the fouled flux of the membranes having similar pore size distributions but different pore geometries.

Organization of the thesis

Two papers have been prepared for publication. These papers are presented in chapters II and III.

The objective of paper 1 was to investigate the effect pore geometry on pore constriction by particles penetrating into membrane pores and to compare the flux decline due to this phenomenon for membranes having unique pore sizes but different pore geometries. The size of the smaller particle in the feed stream was set at 0.1 microns.

The objective of paper 2 was to investigate the combined effect of different particle rejection characteristics and constriction behavior of different pore geometries in light of various pore size distributions of membranes filtering a feed stream a particle size of 0.1 microns.

In both cases the larger particles were assumed to be fully rejected by the membrane pores and did not penetrate within the membrane.

References

Baker, R. W., E. L. Cussler, W. Eykamp, W. J. Koros, R. L. Riley, and H. Strathmann. 1991. *Membrane Separation Systems: Recent Developments and Future Directions* Noyes Data Corporation.

Baker, Richard W. 2004. *Membrane Technology and Applications*. Membrane Technology and Research, Inc. Menlo Park, California: John Wiley & Sons Ltd.

Brans, G., R. G. M. van der Sman, C. G. P. H. Schroën, A. van der Padt, and R. M. Boom. 2006. "Optimization of the Membrane and Pore Design for Micro-Machined Membranes." *Journal of Membrane Science* 278 (1–2): 239-250.

Chandler, Martin and Andrew Zydney. 2006. "Effects of Membrane Pore Geometry on Fouling Behavior during Yeast Cell Microfiltration." *Journal of Membrane Science* 285 (1–2): 334-342.

Chang, E. -E, Sung-Yueh Yang, Chin-Pao Huang, Chung-Huei Liang, and Pen-Chi Chiang. 2011. "Assessing the Fouling Mechanisms of High-Pressure Nanofiltration Membrane using the Modified Hermia Model and the Resistance-in-Series Model." *Separation and Purification Technology* 79 (3): 329-336.

Chang, In-Soung, Chang-Mo Chung, and Seung-Ho Han. 2001. "Treatment of Oily Wastewater by Ultrafiltration and Ozone." *Desalination* 133 (3): 225-232.

Hermia, J. 1982. "Constant Pressure Blocking Filtration Laws – Application to Power-Law Non-Newtonian Fluids." *Trans. IChemE* 60: 183.

Ho, Chia-Chi and Andrew L. Zydney. 1999. "Effect of Membrane Morphology on the Initial Rate of Protein Fouling during Microfiltration." *Journal of Membrane Science* 155 (2): 261-275.

Ho, Chia-Chi and Andrew L. Zydney. 1999. "Theoretical Analysis of the Effect of Membrane Morphology on Fouling during Microfiltration." *Separation Science and Technology* 34 (13): 2461-2483.

Hsieh, H. P. 1996. *Inorganic Membranes for Separation and Reaction*. Membrane Science and Technology Series, 3. ELSEVIER.

Hwang, Kuo-Jen and Tsung-Ting Lin. 2002. "Effect of Morphology of Polymeric Membrane on the Performance of Cross-Flow Microfiltration." *Journal of Membrane Science* 199 (1–2): 41-52.

Jacquemet, Valérie, Gilberte Gaval, Elena-Carmen Gherman, and Jean-Christophe Schrotter. 2006. "Deeper Understanding of Membrane Fouling Issues on a Full Scale Water Plant." *Desalination* 199 (1–3): 78-80.

Judd, Simon and Bruce Jefferson, eds. 2003. *Membranes for Industrial Wastewater Recovery and Re-use*: Elsevier.

Levine, Audrey D., George Tchobanoglous, and Takashi Asano. 1985. "Characterization of the Size Distribution of Contaminants in Wastewater: Treatment and Reuse Implications." *Journal (Water Pollution Control Federation)* 57 (7): 805-816.

Levine, Audrey D., George Tchobanoglous, and Takashi Asano. 1991. "Size Distributions of Particulate Contaminants in Wastewater and their Impact on Treatability." *Water Research* 25 (8): 911-922.

Mah, Shee-Keat, Chong-Kheng Chuah, W. P. Cathie Lee, and Siang-Piao Chai. 2012. "Ultrafiltration of Palm oil–oleic acid–glycerin Solutions: Fouling Mechanism Identification, Fouling Mechanism Analysis and Membrane Characterizations." *Separation and Purification Technology* 98 (0): 419-431.

Pendashteh, Ali Reza, Luqman Chuah Abdullah, A. Fakhru'l-Razi, Sayed Siavash Madaeni, Zurina Zainal Abidin, and Dayang Radiah Awang Biak. 2012. "Evaluation of Membrane Bioreactor for Hypersaline Oily Wastewater Treatment." *Process Safety and Environmental Protection* 90 (1): 45-55.

Peng, H., A. Y. Tremblay, and D. E. Veinot. 2005. "The use of Backflushed Coalescing Microfiltration as a Pretreatment for the Ultrafiltration of Bilge Water." *Desalination* 181 (1–3): 109-120.

Salahi, Abdolhamid, Mohsen Abbasi, and Toraj Mohammadi. 2010. "Permeate Flux Decline during UF of Oily Wastewater: Experimental and Modeling." *Desalination* 251 (1–3): 153-160.

Sheldon, R. W., T. P. T. Evelyn, and T. R. Parsons. 1967. "On the Occurrence and Formation of Small Particles in Seawater." *Limnology and Oceanography* 12 (3): 367-375.

Strathmann, Heiner, Lidietta Giorno, and Enrico Drioli. 2006. *An Introduction to Membrane Science and Technology* CONSIGLIO NAZIONALE DELLE RICERCHE ROMA.

Wang, Caixia, Qiang Li, Huang Tang, Daojiang Yan, Wei Zhou, Jianmin Xing, and Yinhua Wan. 2012. "Membrane Fouling Mechanism in Ultrafiltration of Succinic Acid Fermentation Broth." *Bioresource Technology* 116 (0): 366-371.

Wang, Fulin and Volodymyr V. Tarabara. 2008. "Pore Blocking Mechanisms during Early Stages of Membrane Fouling by Colloids." *Journal of Colloid and Interface Science* 328 (2): 464-469.

Wang, Xiuyan, Sha Chen, Wenyue Dong, Zhan Wang, Liying Yang, Xuejie Xi, Qian Zhang, and Longyue Shi. 2012. "Contribution of Main Pollutants in Oilfield Polymer-Flooding Wastewater to the Total Membrane Fouling Resistance." *Separation Science and Technology* 47 (11): 1617-1627.

Zydney, Andrew L. and Chia-Chi Ho. 2003. "Effect of Membrane Morphology on System Capacity during Normal Flow Microfiltration." *Biotechnology and Bioengineering* 83 (- 5): 537.

CHAPTER II

Effect of pore shape on membrane pore constriction by particles

M.H. Faghihi, A.Y. Tremblay*

Department of Chemical and Biological Engineering, University of Ottawa

161 Louis Pasteur Street, Ottawa, ON, K1V 6N5, Canada

Abstract

Irreversible flux decline is a problem facing many membrane separation processes which decreases useful membrane life and often affects the selection of synthetic membranes as a competitive separation technology. The accumulation of particles inside membrane pores can be linked to the irreversible flux decline experienced in many systems. Particle accumulation within membrane pores and the residual open area for flow in a membrane pore were studied in light of several pore geometries and λ (ratios of particle diameter to pore hydraulic diameter) of 0.1 to full particle rejection. Pore constriction was approximated by maximum particle deposition onto membrane pore walls and simulated using MATLAB Image Processing Toolbox. Sixteen pore geometries including basic pore shapes (oval, rectangular and triangular), and combined shapes (star, cross and rounded ends rectangle) having different aspect ratios (1, 3, 7, 15 and 30) were examined and compared. The effect of different geometries on area lost after pore constriction was the same for small particles compared to pore size ($\lambda < 0.2$). However, for larger values of λ, different pore geometries yielded different amounts of area lost due to pore constriction by particles. The flux of membranes having the aforementioned pore geometries was calculated after pore constriction at five different particle to pore size ratios. All parameters affecting the membrane flow, such as membrane porosity, pore size, membrane thickness, *etc.*, were held constant to avoid their effect on the flow and result in an identical clean membrane flux for all membranes. For small particles compared to membrane pore size, all membranes showed almost the same flux. However, for intermediate particle sizes, the flux of membranes having triangular and star shape pores was higher compared to other pore geometries. Increasing the aspect ratio of the triangular and oval pore shapes caused the fouled flux of the membrane to increase; while, the fouled flux of the membranes having rectangular pores decreased by increasing the aspect ratio of the pores. The effect of aspect ratio leveled off at aspect ratios of 15. In general, the results of this work indicate that membranes with triangular and star shape pores be recommended for applications where particle penetration into membrane structure and consequent pore constriction by particles is most likely to occur.

Keywords: pore constriction, pore geometry, aspect ratio, internal fouling

1. Introduction

Synthetic membranes are utilized in many separation processes. Membrane cross-flow filtration is known to be an economic and environmentally friendly process for separation of colloids and particulates in numerous separation applications. These applications include but are not limited to waste water treatment, water purification, micro-organism removal from dairy products, catalyst recycling, dialysis, material processing [1-2].

The major challenges regarding membrane separation processes are the short term and long term fouling of the membranes [1-2]. These undesired phenomena cause a reduction in permeate flux by inducing extra resistance to flow and are responsible for irreversible fouling and reducing long term membrane operability [3-5]. This greatly affects the economic viability of membrane separations as it affects the energy consumption of the process and also membrane life and operating costs [5-7]. There are numerous inherent characteristics of membranes, and the solutes they separate, that determine the extent and intensity of membrane fouling and its effect on long-term flux decline. Factors such as membrane material and morphology, porosity, membrane-particle mutual interaction, to name a few, have all been found to affect membrane flux decline. [1-3,5].

The fouling mechanisms are traditionally classified into four different types; cake filtration and three kinds of pore blocking, known as standard pore blocking (pore constriction), complete pore blocking (pore sealing), and intermediate pore blocking. The last two types of pore blockings occur on the entrance of the pores while pore constriction occurs inside the pores when the particles are smaller than pores [5,8,9]. Studies have shown that up to 80% of the permeate volume can be affected by this type of fouling [9].

One of the important characteristics of membranes is their morphology which can have a significant influence on the membrane's performance and fouling behavior. Morphological factors such as porosity, pore interconnectivity, pore geometry, pore size distribution, and homogeneity affect the long term flux decline of membranes. Ho and Zydney [10] studied the initial rate of flux decline due to protein fouling in Ultrafiltration. They found that membrane porosity affected the flux decline for micro-machined membranes having straight through pores. For low porosities, the initial rate of fouling decreased with increasing porosity. However, at higher porosities flux decline did not show dependency on porosity. They also showed the importance of pore interconnectivity on the initial rate of fouling. Membranes with interconnected pores exhibited a significantly lower rate of flux decline compared to membranes with straight-through pores having the same porosity. In another study, they investigated the role of membrane morphology on the system capacity during microfiltration. They showed that the interconnectivity of the pores reduces the flux decline due to pore blockage and consequently results in membranes with higher capacities [11]. Ho and Zydney also performed theoretical modeling on different membranes with interconnected and straight-through pore structures using Darcy's law. Their calculations predicted slower rates of flux decline for interconnected pores due to less hydraulic resistance after partial internal fouling [12].

Chandler and Zydney [13] studied the flux decline and fouling behavior of two micro-patterned membranes, each of which possessed a unique pore shape. They compared the fouling behavior of these membranes while for all membranes the pore sizes (6 μm) where smaller than the particle size range (6.5-11.5 μm). Their results showed that, the rate of flux decline for membranes with circular pores was faster than membranes with slotted pores. Yeast cells at the surface of the membrane with circular pores covered the whole area of the pores leading to a fast decline in membrane flow; while in the membrane with slotted pores, initial deposition of yeast cell covers only a small portion of the pores; therefore, there is still a large enough space for liquid to flow on the sides of the deposited particles and penetrate beneath them into the membrane pores. This phenomenon, occurring at the entrance of the pore, leads to a slower rate of flux decline for slotted pores compared to circular pores. In another study, Brans *et al.* used CFD simulations to calculate the exerted drag and pressure forces on particles deposited at the entrance of the pores. They compared four different basic pore geometries and showed that triangular pores offered the best particle release at the entrance of the pores under the influence of cross-flow [14].

Most of the studies in this area assume that all the particulate sizes in the feed are larger than the pores in the membrane (100% rejection) while fouling studies have shown that up to 80% of permeate volume of membranes can be affected by pore constriction [9] which has been always one of the limiting factors of membrane separation. In many membrane applications the particles have a size distribution. In wastewater streams, contaminants are a complex mixture of particulates and soluble inorganic and organic substances covering a broad range of sizes [15]. These particles are traditionally categorized to dissolved (<0.001µm), colloidal (0.001-1µm), supracolloidal (1-100µm) and settleable (>100µm). The distribution of particle size existing in wastewater streams depends on the constituents and the origin of the stream; however, a significant portion of the organic matter are the range of colloidal and supracolloidal categories [16]. Oily wastewater is mostly produced in oil and gas production and is highly concentrated in hydrocarbon constitutes and various salts [17]. There are different size ranges reported in literature for the particles and colloids in oily wastewaters. Some examples of the reported particle diameter ranges are 0.07-1.5µm [18], 0.05-0.3µm [19] and 0.3-30µm [17]. Peng *et al.* [20] used UF and MF to filter bilge water containing a bimodal particle distribution. The smaller particle sizes were 0.07, 0.089 and 0.1µm; while the larger ones were between 2 and 5 µm. The smaller particles are most often less concentrated, but more problematic, than the larger ones. On selecting a pore size for a membrane, an intermediate pore size is often used in order to obtain reasonable permeate flux. In such a case, the larger particles tend to be excluded from the pores and the smaller ones can penetrate the pores causing gradual long term internal fouling. As previously stated, this fouling causes extra resistance to flow and is commonly known as "pore constriction" resistance. The smaller particles can be either hydro-dynamically entrapped or adsorbed onto the pore walls within the membrane. Pore constriction is the result of the penetration and deposition of particles, inside the membrane walls which causes internal fouling and can be an important contributor to irreversible flux decline leading to costly membrane replacement [2].

The steady state flux of ultra and microfiltration membranes are usually an order of magnitude less than the initial flux (clean membrane flux). Even after chemical cleaning, the steady state flux of the membrane tends to decrease over time due to surface and internal fouling. A portion of the declined flux due to this type of fouling can be recovered by back-flushing the permeate to release the particles in the pores; but, eventually particles will be physically entrapped within the reticulated geometry of the pore. These particles cannot be dislodged by more aggressive physical or chemical cleaning without imparting serious structural damage to the membrane material. At this point in its operation, the membrane must be replaced representing substantial operating costs.

As mentioned previously, pore geometry has been shown to affect the filtration of particles at the entrance of a pore [10-14]; however, the effect of pore geometry on flux decline due to particles that have entered the pores has not been examined to a great extent. Studying the role of pore geometry as a factor affecting the flux decline could help us design and fabricate membranes with higher long-term productivity. This will extend the useful life of membranes and in some cases make membranes a viable economic option compared to other separation techniques.

The objective of this study is to investigate the effect of geometrical characteristics of membrane pores such as pore shape and aspect ratio on the membrane's flow after pore constriction by smaller particles in the feed stream. Furthermore, the effect of pore shape on the amount of pore cross-sectional area loss after constriction by particles was examined. This will help to determine which geometries will provide easier release of constricting particles by periodic back-flushing.

2. Simulation Process and Calculation Method

2.1. Geometries

Numerous factors determine the permeation of fluids through a membrane. Factors such as porosity, membrane thickness, pore size distribution, and pressure will play important roles. In order to understand the effect of pore shape, all the parameters affecting membrane flux should be held constant except the pore shape.

Fifteen model membranes with different pore geometries were studied to understand the effect of pore shape and aspect ratio on membrane flux after maximum surface coverage of the interior pore wall. These geometries are listed in Table 1.

Table 1. Geometry and Aspect ratio of the pores studied.

Geometry	rectangular	triangular	oval	circular	cross	star	Rounded ends rectangle
Aspect ratios	3,7,15,30	3,7,15,30	3,7,15,30	1	7	7	30

The aspect ratios for different geometries were defined as follows:

rectangular: $\frac{\text{length}}{\text{width}}$, triangular: $\frac{\text{height}}{\text{base}}$, oval: $\frac{\text{larger diameter}}{\text{smaller diameter}}$

A cross with aspect ratio of 7 was represented by combining four rectangles with aspect ratios of 3 with a square (1:1) in the middle. Similarly the star was built by a combination of four triangles with aspect ratio of 3 with a square (1:1) in the middle. A rectangle with rounded ends with aspect ratio of 30 was represented as a rectangle with aspect ratio of 29, with semicircles at both ends.

2.2. Simulation

A two dimensional simulation of a monolayer particle deposition into pore wall was carried out using MATLAB image processing toolbox. A specific geometrical algorithm was developed to simulate maximum particle attachment into pore walls and also to measure different pore characteristics before and after the attachment of particles. These characteristics include pore cross-sectional area, perimeter and hydraulic diameter of the flow channel. The algorithm is general and can be applied to any regular and irregular pore geometries. It maximizes the number of particles that can be attached to the inside perimeter of a membrane pore. This algorithm assumes the particles to be rigid and spherical with a unique diameter. For a given pore size and geometry the program calculates the entire open area, perimeter and hydraulic diameter of the clean and fouled pore. In its calculation of area and perimeter, the algorithm accounts for the exposed semi-circular shape of the particles adsorbed onto the surface of the pore. This procedure is then repeated for each particle diameter to pore hydraulic diameter ratio (λ) from 0.1, with an interval of 0.01, up to the complete rejection of the particle.

The measured values for area and hydraulic diameter for each pore after particle deposition were divided by the values for clean pore to find the ratios of area and hydraulic diameter after particle deposition to the initial area and hydraulic diameter (α and β) where;

$$\alpha(\lambda) = \frac{A_{constricted}}{A_{clean}} \quad , \tag{1}$$

$$\beta(\lambda) = \frac{D_{H\ constricted}}{D_{H\ clean}} \quad , \tag{2}$$

$$\lambda = \frac{particle\ diameter}{pore\ hydraulic\ diameter\ (D_H)} \quad , \tag{3}$$

In which D_H is the pore hydraulic diameter, defined as four times the pore area over the wetted perimeter of the pore [21-22].

$$D_H = \frac{4A}{p} \quad , \tag{4}$$

If the particle is big enough to be excluded from the pore, i.e. the particle is rejected by the pore, both α and β will equal 1. The calculated values of α and β were used to calculate the flow through fouled pores (pore after maximum particle deposition into the walls) which will be explained later.

The pore size of membranes is usually characterized by bubble point porometry. The definition of pore hydraulic diameter, as stated above, will yield the same value of pore size measured by bubble point porometry [23].

Figure 1 shows a graphical illustration of the maximum particle deposition onto internal pore wall and also the available area for flow after particle deposition at λ ratios equal to 0.3 and 0.4 for cross and star shape pores. Samples results for other geometries are presented in discussions. λ was defined as the ratio of particle diameter to pore hydraulic diameter. In Figure 1, open surfaces defined by the space between the pore wall and the edges of the particles, including the convoluted shape of the adsorbed particle layer, represent the area available for flow. For the calculation of the available area and hydraulic diameter after maximum particle deposition, the area surrounded by the pore wall and edges of the particles adsorbed on its internal walls, is considered to be unavailable for flow if it is significantly smaller than particles' cross-sectional area. The available and unavailable areas described above can be seen in Figure 1.

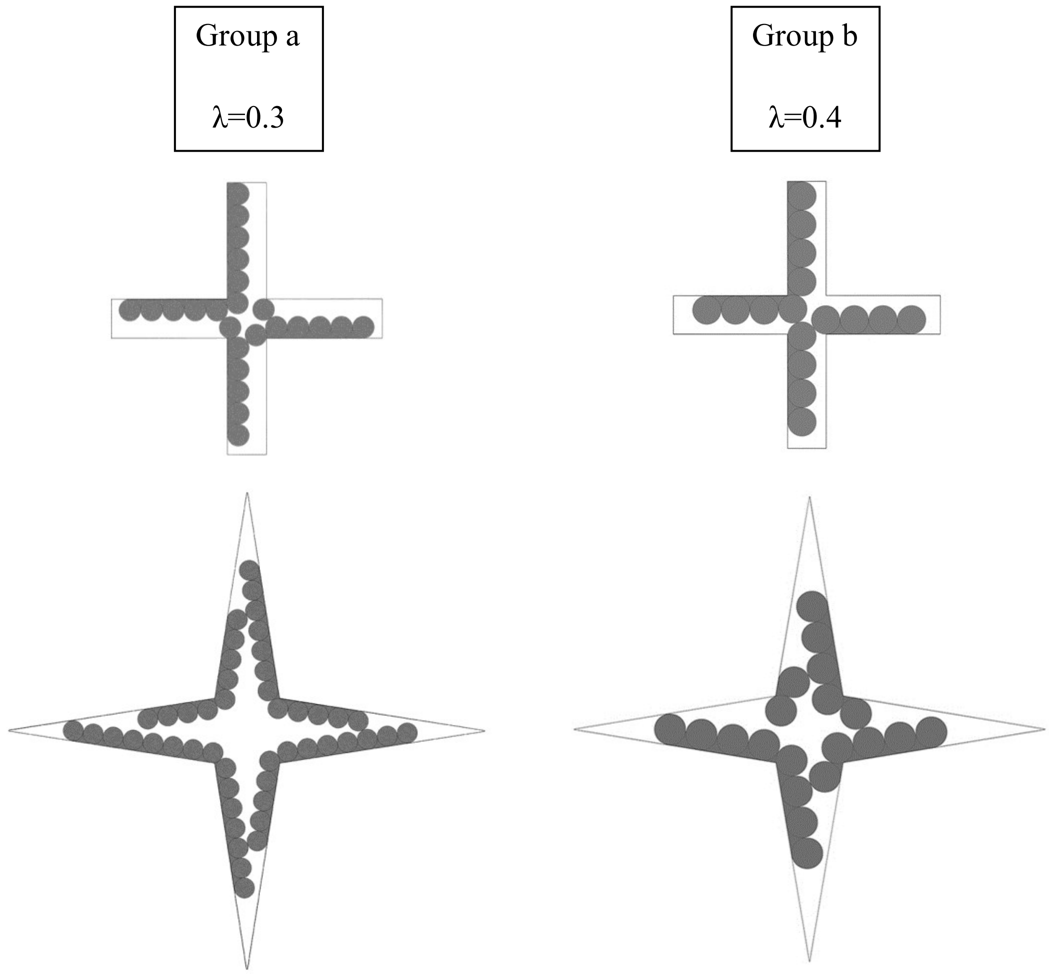

Figure 1. Sample simulation results and available area after particle deposition for cross and star shape pores in two different values of λ. Group "a" represent $\lambda = 0.3$ and "b" represent $\lambda = 0.4$. The aspect ratio is 7 for all shapes. The pore hydraulic diameter is unique and identical for both groups. All geometries in a group have identical particle diameter. The geometries and particles are drawn to scale.

2.3.Flux calculation

In order to compare the flux of membranes having different pore geometries, after pore constriction by particles, a set of constant design and operational parameters were considered. This helps to avoid the effect of other parameters on the flux of membranes and enables us to focus on the effect of pore geometry alone. The constant parameters for flux calculations are summarized in Table 2.

Table 2. Constant parameters for flux calculations.

Pressure difference across the membrane thickness (ΔP)	2 bar
Viscosity of the permeate (μ)	$1\ cP$
Membrane skin layer thickness (l)	$50\ \mu m$
Porosity (ϵ)	20%
Membrane pore size (bubble point)	$0.1\ \mu m$
Particle Size (diameter)	0.01, 0.025, 0.05, 0.075 and 0.1 μm

A unique pore size of 0.1µm was considered for all membranes as it was shown by Cheryan and Rajagopalan [24] that 0.1µm MF membranes are effective in separation of oily wastewater and recovery of the existing surfactant in the feed. This size represents the pore hydraulic diameter which is the same value yielded by bubble point porometry [23]. It was assumed that the pore geometry does not change on the surface of the membrane.

As represented in Table 2, a porosity of 20% is assumed for all the membranes. Porosity was defined by the ratio of accumulative pore cross-sectional area over unit area of membrane. Dividing the cumulative pore cross-sectional area to a single pore cross-sectional area yields the number of pores available at the surface of the membrane. Considering the fact that two different geometries with the same hydraulic diameter will have different cross-sectional areas, the number of pores on the membrane surface will be different for different pore geometries in order to maintain a constant porosity.

Five different particle sizes were considered for calculation of flux after pore constriction, each corresponding to a value of λ amongst 0.1, 0.25, 0.5, 0.75 and 1. Clean and fouled membrane fluxes of all different membranes were calculated by the following procedure after being challenged by these particles separately. It was assumed that the larger particles (>0.1µm) available in the feed are rejected and do not contribute in pore constriction and its consequent flux decline.

Using the Hagen-Poiseuille equation, the flow rate through one clean single pore can be calculated as follows:

$$Q_{clean} = D_{H\,clean}^2\, A_{clean}\, \frac{\Delta P}{32\mu l} \tag{5}$$

In which Q_{clean} is the flow rate through a clean single pore, $D_{H\,clean}$ the pore hydraulic diameter, A_{clean} the cross-sectional area perpendicular to the flow and l pore length (membrane thickness) [25]. ΔP is the pressure difference across the membrane thickness and μ is the viscosity of the solvent (water). Membrane thickness is considered as a constant parameter for all geometries. All calculations were carried out for a unit area (1 m^2) of membranes. Therefore, the clean membrane flux can be calculated as:

$$J_{clean} = n \times Q_{clean} \tag{6}$$

Where n represents the number of pores in 1 m^2 of the membrane. The calculated value of the clean membrane flux was 900 (L/m^2h) using the parameters listed in Table 2. This clean flux was the same for all membranes.

After particle deposition into the pore walls, both hydraulic diameter and cross-sectional area decrease due to pore constriction by the particles, causing a reduction in permeate flow. The following equations can be written for the internally fouled pores:

$$Q_{fouled} = D_{H\,constricted}^2\, A_{constricted}\, \frac{\Delta P}{32\mu l} \tag{7}$$

$$J_{constricted} = n \times Q_{constricted} \tag{8}$$

Knowing the clean pore cross-sectional area and having the values of α and β as the results of the simulation, A_{fouled} and $D_{H\,fouled}$ can be calculated by equations 1 and 2 respectively for each particle trial.

3. Results and discussion

3.1. α and β vs. λ

The values of α vs λ was plotted in Figure 2.a) for rectangles, Figure 2.b) triangles, Figures 2.c) ovals and Figure 2.d) for circle and combined shapes. Values of β followed a similar pattern to α and are not presented here for reasons of space. As we can see at low values of λ, where particle diameter is small compared to the pore hydraulic diameter, α follows a similar pattern for all geometries. For rectangular geometries, it starts from $\alpha \approx 0.7$ for $\lambda = 0.1$, and linearly decreases to $\alpha \approx 0.4$ for $\lambda = 0.2$, with a slope of -3.2. Similarly, for triangular geometries, $\alpha \approx 0.7$ for $\lambda = 0.1$, but it drops to $\alpha \approx 0.5$ for $\lambda = 0.2$, with a slope of -2.8. For oval geometries however it starts from $\alpha \approx 0.64$ for $\lambda = 0.1$, and linearly decreases to $\alpha \approx 0.4$ for $\lambda = 0.2$, with a slope of -3.3. This similar behavior for $\lambda < 0.2$ is due to the adsorption of a monolayer of particles onto the pore walls. This region of λ corresponds to the situations where particle diameter is small compared to pore hydraulic diameter. In this case the maximum particle deposition onto pore walls leads to a layer of particles attached to the interior wall of the pore. This thin layer does not change the general geometry of the pores and consequently causes a similar decrease in pore area for various geometries. Therefore, for $\lambda < 0.2$ the amount of area loss by deposition of small particles will be independent of the pore geometry. The dotted linear fit in Figures 2.a) to 2.d) indicates that for an infinitely small λ, corresponding to infinitely small particles, α equals 1 as expected.

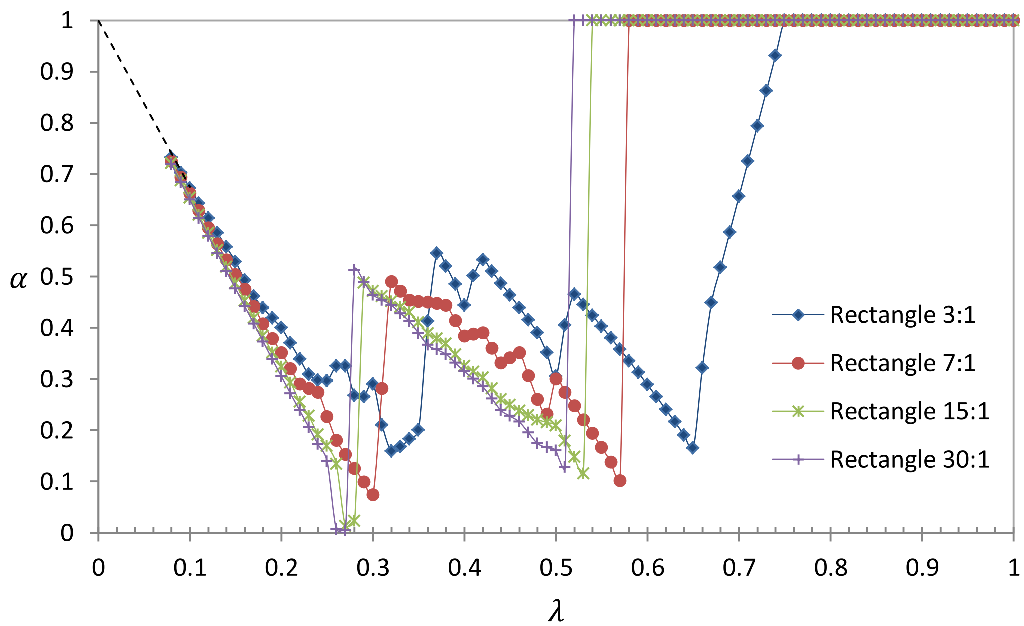

Figure 2.a) ratio of the area available for flow after maximum particle binding inside pores to initial pore area for rectangular shapes

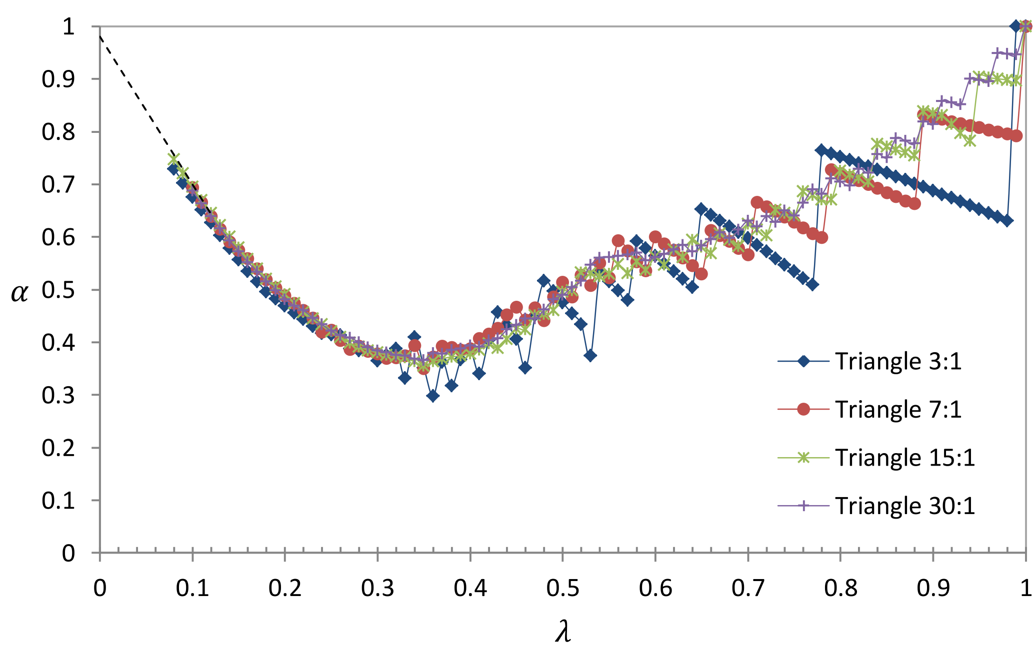

Figure 2.b) ratio of the area available for flow after maximum particle binding inside pores to initial pore area for triangular shapes

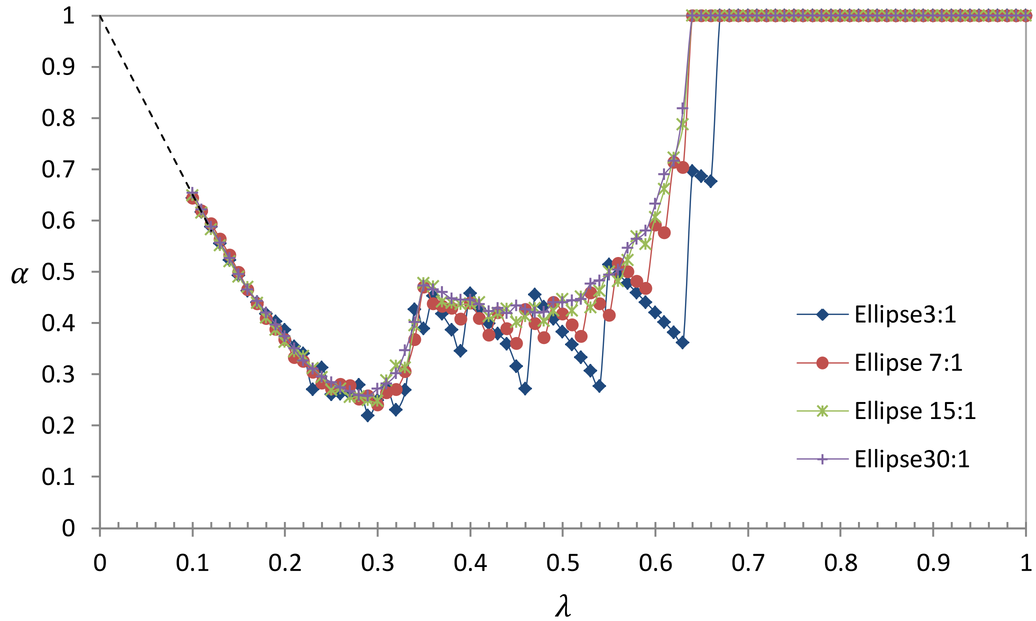

Figure 2.c) ratio of the area available for flow after maximum particle binding inside pores to initial pore area for oval shapes

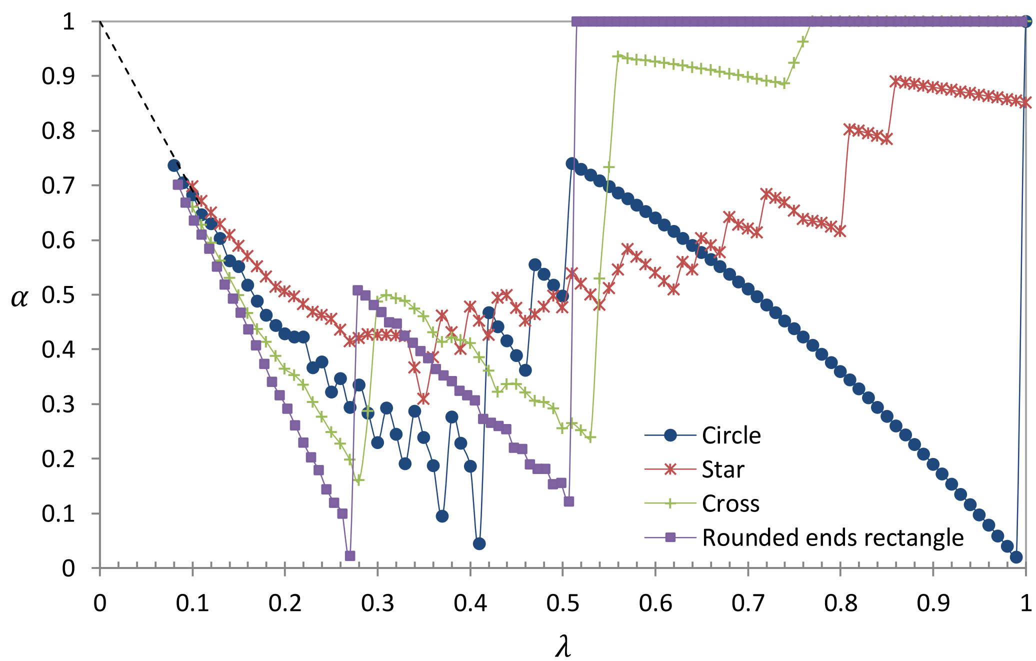

Figure 2.d) ratio of the area available for flow after maximum particle binding inside pores to initial pore area for circle and combined shapes

The effect of different geometries on available area after maximum particle binding to pore walls can be seen for $\lambda > 0.2$. As we can see in figures 2.a), 2.b), 2.c) and 2.d), all geometries in the same group exhibited the same overall trend of α vs. λ while the values are not exactly the same because of different aspect ratios. However this general form is different for different groups of geometries. For example, all rectangular geometries showed two minimums of α at $\lambda \approx 0.27$ and $\lambda \approx 0.6$ followed by a sudden increase while the general trend of α vs. λ for triangular pores includes only one minimum at $\lambda \approx 0.34$. To understand and specify the sources of these differences all different groups will be discussed in detail as follows.

In figure 2.a) for all rectangular pores the value of α reaches to its minimum at $\lambda \approx 0.27$. For longer rectangles, (aspect ratios of 15 and 30) the value of α drops to zero. For a rectangular pore with aspect ratio of 15, calculations show that $\lambda = 0.28$ corresponds to the situation in which the particle diameter is 0.54 times the rectangle's width. In this case the maximum particle binding to pore walls results in the maximum particle packing in the pore which covers the whole cross sectional area of the pore. Figure 3 shows the available area after maximum particle binding at $\lambda = 0.28$ for a rectangular pore with aspect ratio of 15.

Figure 3. Available area after maximum particle binding to pore walls for a rectangular pore with aspect ratio of 15 at $\lambda = 0.28$.

As previously mentioned, for all rectangular pores there is a sudden increase in values of α after $\lambda \approx 0.27$. This is due to the fact that a slight increase in λ (increase in particle size compared to pore hydraulic diameter) makes it impossible for the particles to maintain both maximum packing structure and maximum surface coverage inside the pore. At this point, the maximum particle packing reverts to maximum surface coverage. Here, particles are attached just to one side of the pore walls because they are just slightly larger than the size suitable for maximum packing. This explains the sudden increase in the value of α and β after the first minimum in figure 2.a). Figure 4 represents this situation for a rectangular pore with aspect ratio of 15 at $\lambda = 0.29$.

Figure 4. Available area after maximum particle binding to pore walls for a rectangular pore with aspect ratio of 15 at $\lambda = 0.29$.

Moving to larger values of λ (> 0.29) in figure 2.a), we see that α vs. λ starts to decrease again up to the second minimum of the graph. At this point the particle diameter is the exact same size as the rectangle's width; therefore particles cover the whole cross-sectional area of the pore and build maximum particle packing for the second time. Figure 5 shows this situation for a rectangular pore with aspect ratio of 15 at $\lambda = 0.53$.

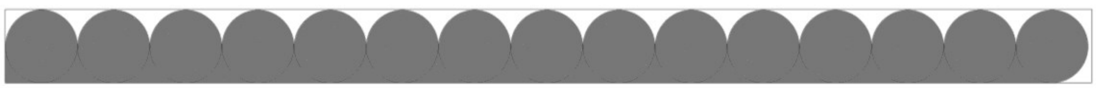

Figure 5. Available area after maximum particle binding to pore walls for a rectangular pore with aspect ratio of 15 at $\lambda = 0.53$.

For all rectangular geometries, after the second minimum, there is a sudden increase in the value of α to 1 and they are constant for all larger values of λ. This means that for all values of λ larger than this point, the particles cannot penetrate into the pores and are rejected by the pores.

Figure 2.b) shows the values of α vs. λ for triangular pores with different aspect ratios. As mentioned before, the overall trend of the graph for all triangular pores with different aspect ratios is similar. Comparing the results for different triangles shows no significant difference in the values of α for $\lambda < 0.2$ due to the effect of thin monolayer of particles. The effect of different aspect ratios can be seen for $\lambda > 0.2$. Generally, triangles with higher aspect ratio exhibited higher values of α at a constant λ. However, all of them showed an absolute minimum of α at $\lambda \approx 0.35$. The lowest value of α for all triangular shapes was always greater than 0.3. Unlike rectangular pores, the value of α never reaches zero at any λ. This is due to the asymmetric geometry of a triangle compared to a rectangle. The asymmetrical geometry of a triangle makes it impossible for particles to maintain both maximum particle packing and maximum particle binding to walls of the pore. Figure 6 shows a triangular pore

with aspect ratio of 15 at $\lambda = 0.35$ which corresponds to its lowest available area after maximum particle binding (minimum α in figure 2.b)).

Figure 6. Available area after maximum particle binding to pore walls for a triangular pore with aspect ratio of 15 at $\lambda = 0.35$.

Figure 2.c) shows the values of α vs. λ for oval shape pores with different aspect ratios. For ovals, the lowest value of α corresponds to $\lambda \approx 0.3$. Again unlike rectangular geometries, the value of α never reaches zero for any λ. Again, this is due to the fact that non-uniform thickness of an oval does not provide required area for the particles to build a maximum packing structure and maximum binding into oval pore walls at the same time to cover the whole cross-sectional area of the pore.

Values of α vs. λ for a circular pore are presented in figure 2.d). There are a few differences between the pattern of α for circular pore and other geometries. For circular geometry relative minimum values of α correspond to the situations where all penetrated particles come into contact with each other. These relative minimums are more intense at $\lambda = 0.37\ and\ 0.41$. At $\lambda = 0.37$, five particles are attached together covering most of the cross-sectional area of the pore. At $\lambda = 0.41$ the same structure is built by four particles. Figure 7 shows the available area after maximum particle binding to pore at these two λ. There is also an absolute minimum of α which happens at $\lambda = 1$. This is the point that particle diameter is equal to the circular pore's diameter and it covers the whole cross-sectional area of the pore ($\alpha = 0$).

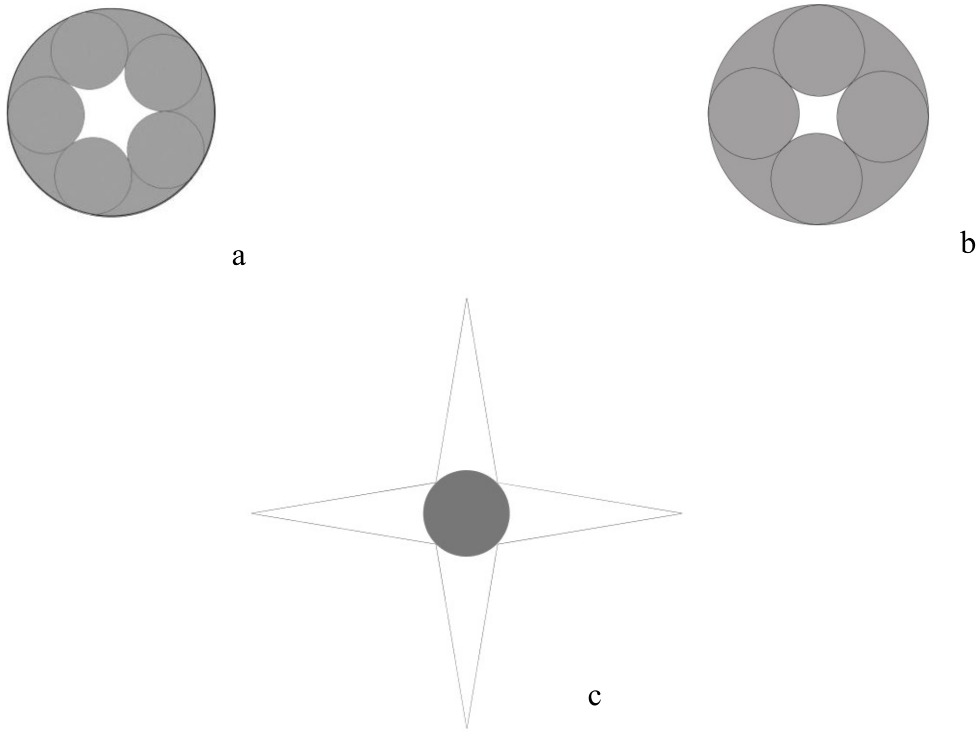

Figure 7. Available area after maximum particle binding to pore walls for a circular pore at $\lambda = 0.37$ (a) and $\lambda = 0.41$ (b) and for a star shape pore at $\lambda = 1.24$ (c).

Figure 2.d) also shows the α vs. λ for cross and star shape pores. It is interesting that for a star shape pore, values of α is not equal to 1 for $\lambda > 1$. It means that a star shape pore does not reject the particles with the same diameter as its hydraulic diameter. For this geometry, λ_{pr} equals 1.24. Figure 7.c) shows the available area after maximum particle binding into a star shape pore at $\lambda = 1.24$.

3.2. Membranes' fluxes after particle binding to pore walls

Figures 8.a) to 8.e) show the overall flux of the membranes with mentioned pore shapes with pore size of 0.1 μm (bubble point porometry) filtering five different particle diameters of 0.1, 0.075, 0.05, 0.025 and 0.01 μm, separately. As mentioned before, the clean flux of all the membranes was 900 lmh regardless of their pore shape.

Figure 8.a) corresponds to the situation where particles are very small compared to pore hydraulic diameter. In this case, all membranes with different geometries show almost similar fluxes after pore constriction by particles (≈ 180 lmh). As mentioned before, for very small particles compared to pore size, the amount of area lost after particle binding into pore walls is the same. This causes a same fouled pore flux for all geometries.

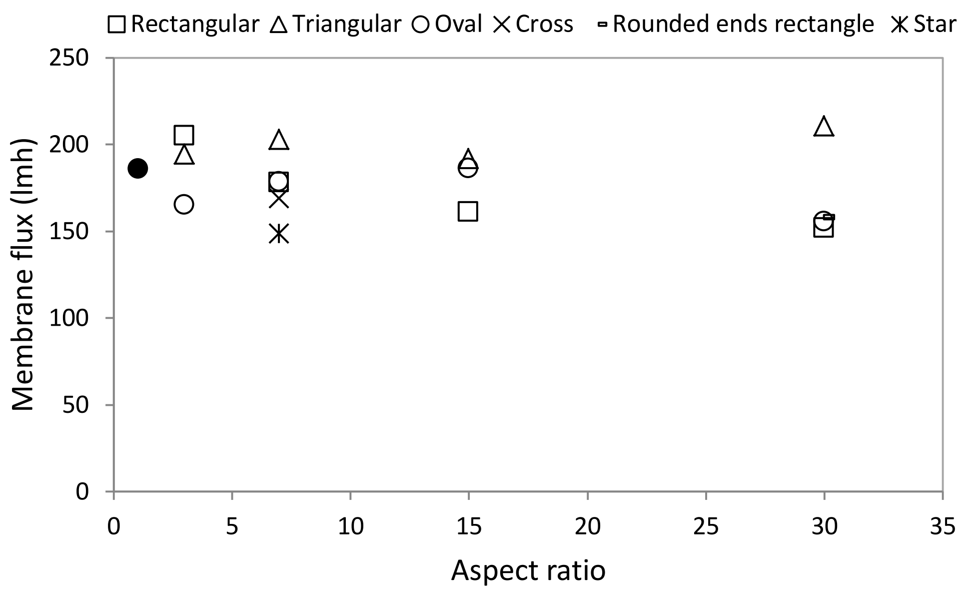

Figure 8.a) Membranes' fluxes after pore constriction by 0.01 μm particles (λ = 0.1).

As we increase the particle size, in figures 8.b) and 8.c) for 0.025 and 0.05 μm particles respectively ($\lambda = 0.25$ and 0.5), we can see all flux values decrease compared to previous particle size trial. This is mainly due to the fact that deposition of larger particles causes larger area loss in the pores. In these figures, the fluxes of membranes with triangular pores and star shape pores are higher compared to other geometries. These geometries provide larger available area after particle deposition at intermediate λ ratios. Comparing these results with values of α vs. λ for different geometries in figures 2.a) to 2.d), we can see that the overall available area after particle binding is higher for triangular geometries and is the lowest for rectangular geometries. The results for oval geometries were in between rectangular and triangular geometries.

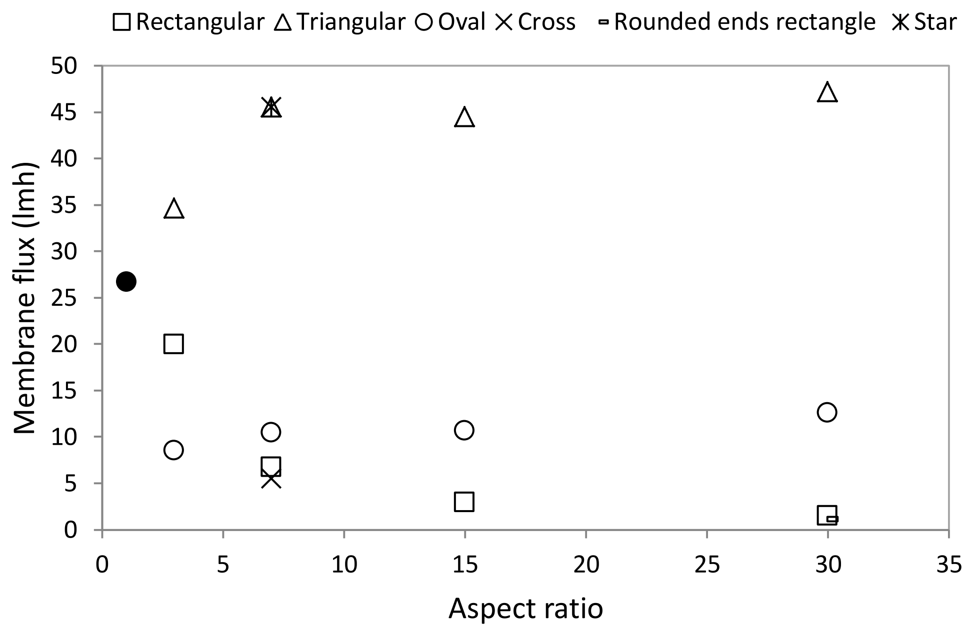

Figure 8.b) Membranes' fluxes after pore constriction by 0.025 µm particles (λ = 0.25).

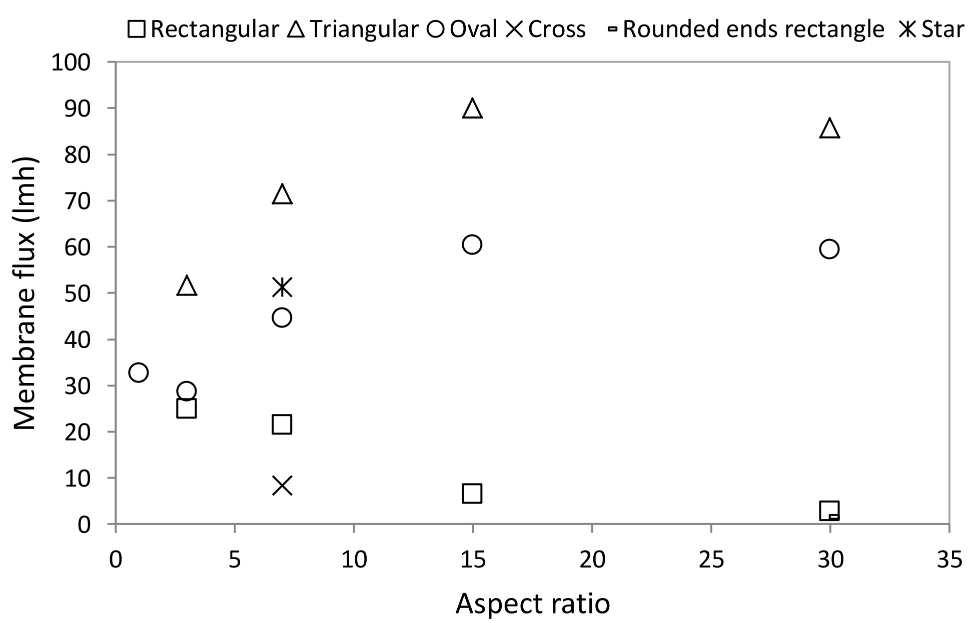

Figure 8.c) Membranes' fluxes after pore constriction by 0.05 µm particles (λ = 0.5).

Figure 8.d) shows the membranes' fluxes for particle size of 0.075 μm ($\lambda = 0.75$). As we see, all membranes with rectangular and oval geometries show a flux of 900 lmh. The clean membrane flux was also 900 lmh. It means that there was no particle penetration into the pores for these geometries at this particle size; therefore, there would be no pore constriction by particles. However, membranes with triangular, circular, cross and star shape pores are still accepting the particles into their pores, which causes a lower flux for them compared to oval and rectangular pores. This does not mean the preference of rectangular and oval pores over other geometries in the case of pore constriction since there is no particle inclusion into the pores for rectangular and oval pores in this case; but this refers to the difference in particle rejection behavior of these different geometries which is not the subject of this article's discussion.

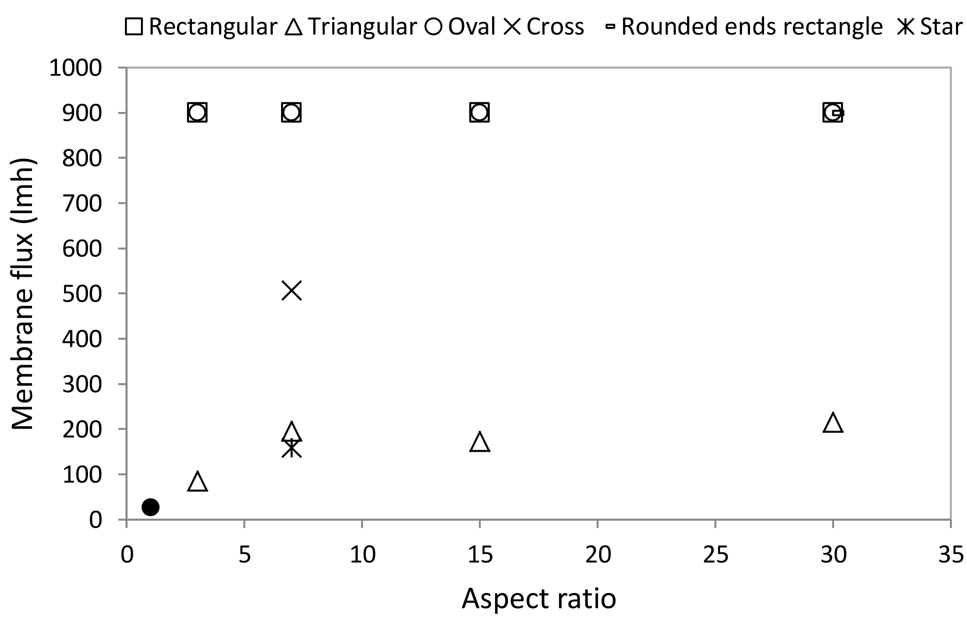

Figure 8.d) Membranes' fluxes after pore constriction by 0.075 μm particles (λ = 0.75). Rectangular and oval geometries reject the particles, showing a flux equal to clean membrane flux.

Figure 8.d) also shows that for particle size of 0.075 μm, membrane having cross shape pores show higher fluxes after pore constriction, compared to other pore constricted membranes. For a cross shape pore this situation refers to the region where $0.57 < \lambda <$

0.77; for which, the cross shape pore is constricted by just one particle at its center and most of the pore area is available for flow (see figure 2.d).

In figure 8.e) all membranes, except the one having star shape pores, reject the particles of 0.1 µm and exhibit the maximum possible flux which is the clean membrane flux. This result for membrane having star shape pore was expected since the star shape pore had shown to be available for particle deposition, for particles larger than its hydraulic diameter (figure 2.d).

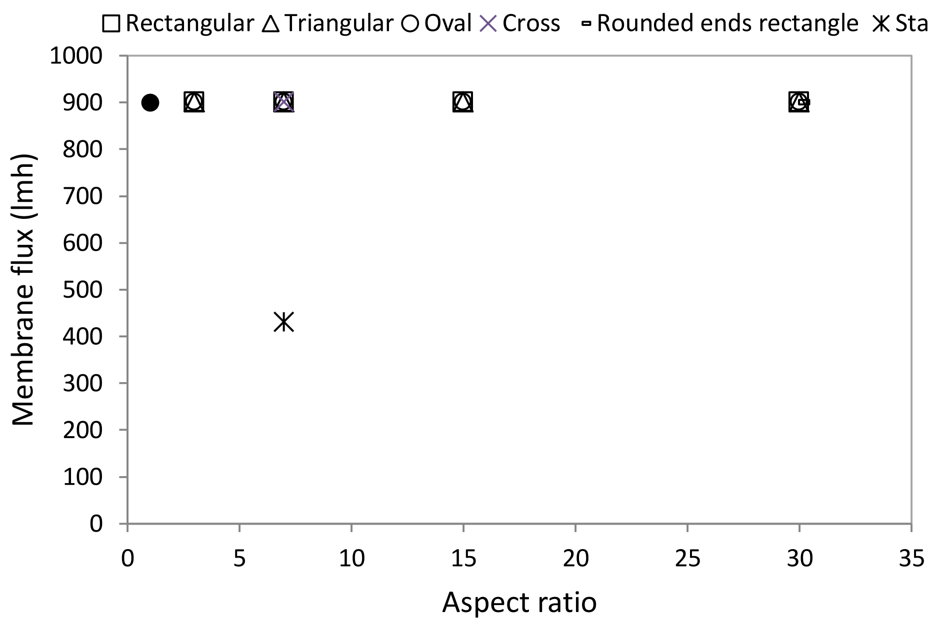

Figure 8.e) Membranes' fluxes after pore constriction by 0.1 µm particles (λ = 0.1). All geometries, except star, reject the particles, showing a flux equal to clean membrane flux.

Figures 8.a) to 8.d) also show the effect of aspect ratio on the flux of the membranes after particle deposition. As we can see, by increasing the aspect ratio of the pores, the fouled membrane flux also increases for triangular and oval geometries while it decreases for rectangular geometries. For triangular pores, this is caused by the effect of their narrow end. As we increase the aspect ratio of a triangle, the angles of the triangle become smaller which causes more open area after particle deposition into pores. The same effect can be seen at the two ends of an oval pore by increasing its aspect ratio.

3.3. The best geometry vs. λ

As mentioned before, values of α vs. λ follows different patterns for various geometries. At a given λ, the available area after maximum particle binding to a pore with a specific geometry (i.e. triangular pore) might be larger than the available area in another geometry (i.e. a rectangular pore). However this is true at a certain λ and might not be valid for another λ. In order to have a more accurate comparison between different pore geometries considering the variance of α vs. λ for a given geometry, one should consider the whole possible range of particle size to pore hydraulic diameter. For this reason, Figure 9 was sketched to compare the major groups of geometries (excluding combined geometries) at aspect ratio of 7 in every lambda. At each λ, it shows the geometry with highest value of α (α_{max}). These data are sketched only for the lambdas for which there is particle penetration into the pores. As we can see in Figure 9, circular pores show more open area after pore constriction at $0.5 < \lambda < 0.6$; However, for most of the other particle to pore size ratios, triangular pores provide higher area after particle deposition compared to rectangular, oval and circular pores.

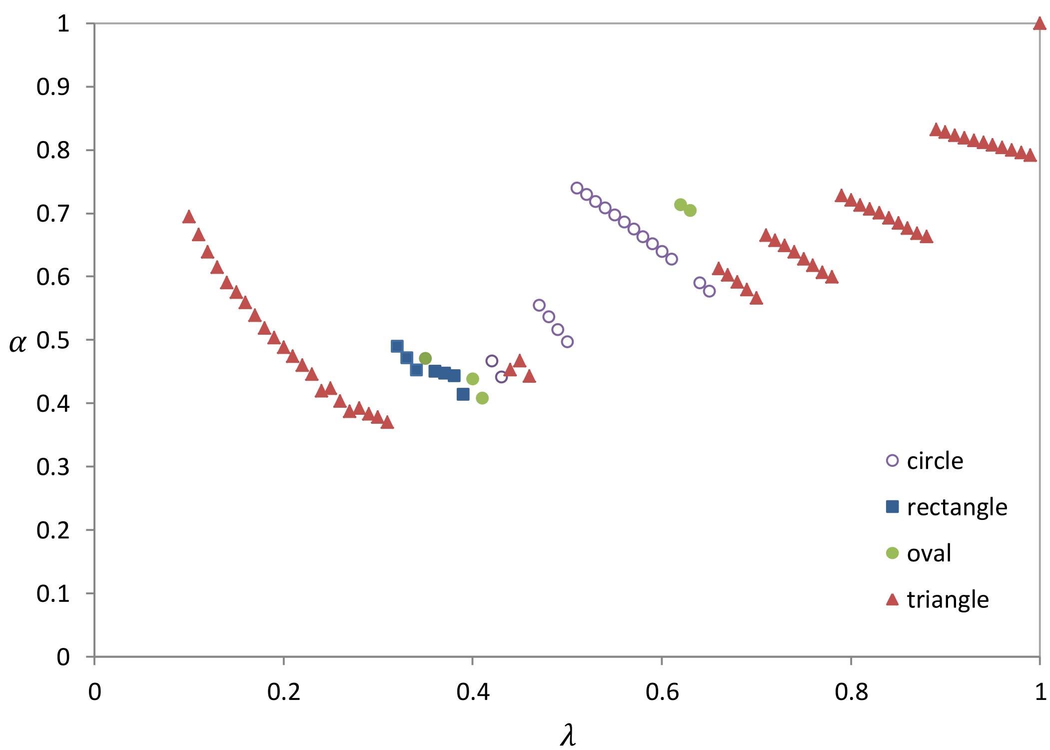

Figure 9. α_{max} vs. λ for basic geometries with aspect ratio of 7.

3.4. Possible effect of geometry on particle release by back-flushing

Periodic back-flushing is commonly used to release the blocking particles from the internal structure of the membranes. The back-flushing flow removes the particles binding to pore walls by exerting a drag force on them. In figures 2.a) to 2.d) the values of α vs. λ, for rectangular and circular pores, reaches zero at some particle to pore size ratios. As mentioned before, at these ratios, maximum particle binding to pore walls results in covering the whole surface of the pores by the particles. In such situation, the pore channel is completely blocked by the particles leaving no space for the back-flushing flow to be able to flow around the particles and dislodge them out of the pore channel. Therefore, the rectangular and circular pore geometries can undesirably affect the particle release by back-flushing as a mechanism for membrane cleaning. For triangular pores, the minimum value of α is 0.3, meaning that for all for all particle to pore size ratios, a sufficient amount of area is available for flow which can facilitate particle release by back-flushing. The improved performance of triangular pores in particle release is also shown by Brans *et al.* [14] for release of particles deposited on the entrance of the pores, under the influence of the cross flow.

Conclusion and recommendations

Pore constriction by spherical particles was approximated with maximum particle deposition onto pore walls and simulated using MATLAB image processing toolbox. α was defined as the ratio of available cross-sectional area for flow after pore constriction to initial pore cross-sectional area. β was defined as the ratio of the hydraulic diameter of the pore channel after pore constriction to initial hydraulic diameter of the pore. The values of α and β were measured, as results of the simulation, at each λ (ratio of particle diameter to clean pore hydraulic diameter). These values followed the same pattern vs. λ. The values of α were plotted against λ. For all geometries, values of α vs. λ followed the same pattern for $\lambda<0.2$. For this region of λ, different pore geometries had the same effect on the amount of area lost after pore constriction by particles. This was due to the effect of thin layer of small particles which does not change the overall geometry of the pores. For rectangular pores the value of

α drops to zero at two positions of λ; first case corresponding to particle diameters equal to half the pore width and second case corresponding to particle diameters equal to the pore width. For circular pores this situation happens when the particle is the same size as pore diameter. However, for oval, triangular, star and cross shape pores, α never drops to zero at any λ. This can be linked to facilitated particle release by back-flushing for these pore shapes. The minimum α for triangular shapes was around 0.3, and for ovals was around 0.2. The effect of aspect ratio on α at constant values of λ was investigated for three groups of geometries. Increasing the aspect ratio of the pore at a constant λ, for rectangular pores, causes α to decrease. While for triangular and oval pores, increasing the aspect ratio of the pore increases the value of α. To compare the flux of the membranes having the aforementioned pore shapes after pore constriction by particles, sixteen model membranes were considered which have the same initial flux. Using the values of α and β vs. λ, the flux of these membranes after pore constriction were calculated and compared at five different λ. For low values of λ, all membranes showed the comparably same flux due to the effect of monolayer of small particles. For intermediate values of λ, membranes having triangular pores showed the best flux which increased by increasing the aspect ratio of the pores. The overall performance of triangular after pore constriction by particles is expected to be superior compared to other geometries and the least favorable pore geometry in this regards would be the rectangular geometry.

Acknowledgement

The authors would like to acknowledge the support of the Natural Science and Engineering Research Council of Canada (NSERC).

References

[1] K. Hwang, T. Lin. Effect of morphology of polymeric membrane on the performance of cross-flow microfiltration. J.Membr.Sci., 199 (2002) 41.

[2] R.W. Baker, Membrane Technology and Applications, Membrane Technology and Research, Inc. Menlo Park, California, John Wiley & Sons Ltd, 2004.

[3] A.G. Fane, C.J.D. Fell. A review of fouling and fouling control in ultrafiltration. Desalination, 62 (1987) 117.

[4] A. Santos, P. Bedrikovetsky, and S. Fontoura. Analytical micro model for size exclusion: Pore blocking and permeability reduction. J.Membr.Sci., 308 (2008) 115.

[5] A.L. Lim, R. Bai. Membrane fouling and cleaning in microfiltration of activated sludge wastewater. J.Membr.Sci., 216 (2003) 279.

[6] Jacquemet, Valerie, Gilberte Gaval, Elena-Carmen Gherman, and Jean-Christophe Schrotter. 2006. "Deeper Understanding of Membrane Fouling Issues on a Full Scale Water Plant." Desalination 199 (1-3): 78-80.

[7] E.M.V. Hoek, J. Allred, T. Knoell, and B. Jeong. Modeling the effects of fouling on full-scale reverse osmosis processes. J.Membr.Sci., 314 (2008) 33.

[8] R. Bai, H.F. Leow. Microfiltration of activated sludge wastewater—the effect of system operation parameters. Separation and Purification Technology, 29 (2002) 189.

[9] F. Wang, V.V. Tarabara. Pore blocking mechanisms during early stages of membrane fouling by colloids. J.Colloid Interface Sci., 328 (2008) 464.

[10] C. Ho, A.L. Zydney. Effect of membrane morphology on the initial rate of protein fouling during microfiltration. J.Membr.Sci., 155 (1999) 261.

[11] A.L. Zydney, C. Ho. Effect of membrane morphology on system capacity during normal flow microfiltration. Biotechnology and Bioengineering, 83 (2003) 537.

[12] C. HO, A.L. Zydney. Theoretical Analysis of the Effect of Membrane Morphology on Fouling during Microfiltration. Sep.Sci.Technol., 34 (1999) 2461.

[13] M. Chandler, A. Zydney. Effects of membrane pore geometry on fouling behavior during yeast cell microfiltration. J.Membr.Sci., 285 (2006) 334.

[14] G. Brans, R.G.M. van der Sman, C.G.P.H. Schroën, A. van der Padt, and R.M. Boom. Optimization of the membrane and pore design for micro-machined membranes. J.Membr.Sci., 278 (2006) 239.

[15] A.D. Levine, G. Tchobanoglous, and T. Asano. Characterization of the Size Distribution of Contaminants in Wastewater: Treatment and Reuse Implications. Journal (Water Pollution Control Federation), 57 (1985) 805.

[16] A.D. Levine, G. Tchobanoglous, and T. Asano. Size distributions of particulate contaminants in wastewater and their impact on treatability. Water Res., 25 (1991) 911.

[17] A.R. Pendashteh, L.C. Abdullah, A. Fakhru'l-Razi, S.S. Madaeni, Z. Zainal Abidin, and D.R. Awang Biak. Evaluation of membrane bioreactor for hypersaline oily wastewater treatment. Process Saf.Environ.Prot., 90 (2012) 45.

[18] A. Salahi, M. Abbasi, and T. Mohammadi. Permeate flux decline during UF of oily wastewater: Experimental and modeling. Desalination, 251 (2010) 153.

[19] I. Chang, C. Chung, and S. Han. Treatment of oily wastewater by ultrafiltration and ozone. Desalination, 133 (2001) 225.

[20] H. Peng, A. Y. Tremblay, and D. E. Veinot. 2005. "The use of Backflushed Coalescing Microfiltration as a Pretreatment for the Ultrafiltration of Bilge Water." Desalination 181 (1-3): 109-120.

[21] B. Dietrich, W. Schabel, M. Kind, and H. Martin. Pressure drop measurements of ceramic sponges—Determining the hydraulic diameter. Chemical Engineering Science, 64 (2009) 3633.

[22] G. Breyiannis, S. Varoutis, and D. Valougeorgis. Rarefied gas flow in concentric annular tube: Estimation of the Poiseuille number and the exact hydraulic diameter. European Journal of Mechanics - B/Fluids, 27 (2008) 609.

[23] A. Jena, K. Gupta. (2003). Liquid extrusion techniques for pore structure evaluation of nonwovens. International Nonwovens Journal, *12*, 45-53.

[24] M. Cheryan and N. Rajagopalan, Membrane processing of oily streams: wastewater treatment and waste reduction, J. Membr. Sci., 151 (I 998) 13-28.

[25] A.L. Zydney, Chapter 15 - High Performance Ultrafiltration Membranes: Pore Geometry and Charge Effects, in Anonymous , Membrane Science and Technology, Elsevier, pp. 333-352.

CHAPTER III

Effect of pore shape and pore size distribution on particle rejection and membrane flux decline due to pore constriction

M.H. Faghihi, A.Y. Tremblay*

Department of Chemical and Biological Engineering, University of Ottawa

161 Louis Pasteur Street, Ottawa, ON, K1V 6N5, Canada

Abstract

One of the biggest challenges regarding membrane separation is irreversible flux decline which decreases useful membrane life and often affects the economic viability of membranes as a competitive separation technology. Irreversible flux decline can be linked to penetration and deposition of particles into interior structure of the membranes. The effect of pore geometry, as a morphological factor, on particle rejection and the flux decline due to pore constriction by particles was investigated in light of several pore size distributions. A range of pore sizes from 0.001µm, with an interval of 0.001µm, to 1µm and a particle size of 0.1µm was considered. For all the pores, not physically rejecting the particles, pore constriction was approximated by maximum particle deposition into membrane pore walls and simulated using MATLAB Image Processing Toolbox. Thirteen model membranes with different basic pore shapes (oval, rectangular and triangular), having different aspect ratios (1, 3, 7, 15 and 30), and a circular pore shape were examined and compared. All parameters affecting the membrane flow, such as membrane porosity, pore size distribution, membrane thickness, *etc.*, were held constant to avoid their effect on the flow and result in an identical clean membrane flux for all membranes. Membrane flux after pore constriction by particles was calculated. A part of this flux is the contribution of the pores that totally reject the particles and another part is the contribution of partially open pores. The overall flux of membranes and also the portion of each aforementioned contributions depend on the pore size distribution. Generally, for PSDs for which most of the pores are larger than the particle size, membranes having rectangular and oval pores provide higher fluxes compared to triangular and circular pores, this is mainly because rectangular pores exhibited higher rejection and thus less internal fouling. However, comparison of the portion of membranes flux contributed by partially clogged pores showed that triangular pores offers the highest flux after internal fouling has occurred. Circular and triangular pores exhibited the greatest flux decline because of lower rejection of particles. Increasing the aspect ratio of the pores enhanced fluid flow. This benefit leveled off after an aspect ratio of 15. The effect of pore aspect ratio was examined which showed that increasing the pore aspect ratio increases the rejection of rectangular and oval pores, while it does not affect the rejection of triangular pores. Increasing the aspect ratio of the pores causes an increase in the contribution of the constricted pores to the overall flux, for triangular and oval pores. However, for rectangular pores, increasing the aspect ratio decreases the contribution of constricted pores. In general, the results of this work indicate that membranes with elongated rectangular or oval pores be recommended for applications where high particle rejection is required and elongated triangular pores recommended for applications in which particle accumulation within pores is more likely to happen.

Keywords: pore constriction, particle rejection, pore geometry, aspect ratio, internal fouling

1. Introduction

Application of synthetic membranes in numerous separation processes is widely spread and is known as an economic and environmental friendly mode of separation. Membranes cross-flow filtration is used for separation of particulates, colloids and suspended matter from waste water streams, or in purification of drinking water, micro-organism removal from dairy products, to name a few. Membrane microfiltration is also used in biopharmaceutical processes, membrane pre-treatment, and food and beverage applications [1-3].

Short term and long term fouling of the membranes are considered as the major challenges of this separation process. Membrane fouling reduces the permeate flux of the membranes by increasing the overall resistance of the membrane to flow, leading to irreversible fouling and diminishing long-term membrane productivity [1-2, 4-6]. Studies have shown that several economic aspects of membrane separation such as the energy consumption of the process, membrane life and replacement costs, and consequently the overall economic viability of the process can be affected by membrane fouling [6-8].

The four traditional fouling mechanisms, defined by Hermia [9], are extensively used in modeling membrane flux decline [6, 10-11]. These mechanisms are classified as: standard pore blocking (pore constriction), complete pore blocking (pore sealing), intermediate pore blocking and cake filtration. Among these mechanisms, pore constriction (standard pore blocking) is the only one referring to the situation where particles can penetrate in the membrane pores and reduce the membrane flux by reducing the section of the pore channel.

The extent and intensity of membrane fouling and flux decline is affected by many intrinsic characteristics of the membrane and the solutes in the feed stream. Characteristics such as membrane material, morphology, porosity, pore size distribution and membrane-solute mutual interactions can affect the flux decline behavior of the membrane in a separation process [1-2, 4, 6].

Ho and Zydney [12] studied the initial rate of flux decline due to protein fouling in Ultrafiltration. Their results showed a twofold effect of porosity on the initial rate of flux decline. They showed that, for high porosities, the flux decline is not affected by porosity; however, for membranes with low porosities, by a slight increase in membrane porosity the initial rate of flux decline decreased. They also showed that, at a constant porosity, the rate of flux decline in membranes having interconnected pores is lower than the rate of flux decline for membranes having straight-through pores. In another study, using Darcy’s law, they performed the theoretical modeling of different membranes, after partial internal fouling, to compare the rate of flux decline for membranes with straight-through pores and membranes with interconnected pores. The results of their calculations show that the rate of flux decline for membranes with interconnected pores is slower due to less hydraulic resistance after partial internal fouling [13].

Chandler and Zydney [14] investigated the role of pore geometry on the flux decline and fouling behavior of micro-machined membranes used for microfiltration of yeast cells. They compared membranes with circular pores and membranes with slotted pores while both membranes had pore sizes (6 μm) smaller than the particle size range (6.5-11.5 μm). They showed that the rate of flux decline for membranes with slotted pores was slower than the rate of flux decline for membranes with circular pores. For the membrane with slotted pores, deposition of particles on the surface of the membrane covers a small portion of the pore entrance, while for the membrane having circular pores, the particles covered the whole entrance of the pores at the surface of the membrane, leading to a rapid decline in membrane flux. In another attempt to characterize the effect of pore geometry, Brans *et al.* [15] using CFD simulation, calculated the amount of drag and pressure forces exerted on particles deposited at the entrance of the pores. They compared four basic pore geometries in terms of the ease of release of the deposited particles at the entrance of the pores. Their results showed that triangular pores offer the best particle release by the cross-flow, at the entrance of the pores.

Almost all published studies in this area assume that all the pores in the membrane are smaller than particles in the feed stream. This ignores the effect of internal fouling; while it has been shown that up to 80% of membranes permeate volume can be affected by pore constriction [11] which is the direct consequence of particle penetration into the pores, leading to internal fouling of the membrane. Many membranes have a distribution of pore sizes instead of a unique pore size. In this distribution, the larger pores are few in number but they contribute to most of the flow. These pores are the ones susceptible to particle penetration which causes pore constriction. Furthermore, many feed streams, such as wastewaters, contain a mixture of particles with different sizes. These can be colloids, soot, humic acid, proteins, dissolved solids, oil droplets, suspended matter, *etc.* For example, contaminants in wastewater streams are a combination of different particulates and soluble inorganic and organic matter which covers a broad range of sizes [16]. These particles can be categorized as dissolved (<0.001μm), colloidal (0.001-1μm), supracolloidal (1-100μm) and settleable (>100μm). Particle size distribution of wastewater streams varies depending on the contaminants and the origin of the wastewater; however, a vast portion of the organic matter found in these waste streams belong to the colloidal and supracolloidal categories

[17]. Oily wastewaters are mostly produced in oil and gas industry and are highly concentrated in hydrocarbon substances and different salts [18]. There are different ranges of size reported in literature for the particles and colloids in oily wastewaters (0.07-1.5μm [19], 0.05-0.3μm [20] and 0.3-30μm [18]). Peng *et al.* [21] applied ultrafiltration and microfiltration to treat a bilge water stream comprising a bimodal particle size distribution. The smaller particle sizes were 0.07, 0.089 and 0.1μm (colloidal); while the larger particles were between 2 and 5 μm (supracolloidal). In such cases, the larger particles are rejected by membrane pores but the smaller ones can penetrate into membranes pores and constrict the pore channels. The penetrated particles can be either hydro-dynamically trapped or adsorbed onto the interior walls of the membrane's pore. The results of the pore constriction by particles is the internal fouling of the membranes which is an important contributor to irreversible decline of membrane flux, leading to costly membrane replacement [2].

The flux of ultra and microfiltration membranes drops from their initial value (clean flux) to a steady state flux, in a few moments after their first implementation. This steady state flux is usually an order of magnitude less than the initial flux of the membrane. Due to internal and external fouling, the steady state flux of the membrane decreases over time. Periodic back-flushing of the permeate helps to recover a portion of declined flux due to internal fouling; but, particles will remain physically entrapped within the reticulated geometry of membrane pores over time. Dislodging these particles needs more aggressive physical or chemical cleanings, this causes serious damage to the membrane structure, leading to substantial replacement costs.

The pore size distribution of a membrane has been shown to affect its flux and rejection behavior [22]. The effect of pore geometry on the filtration of particles at the pore entrance was investigated [12-15]; however, the effect of pore geometry on flux decline due to pore constriction and also its effect on particle rejection, are not covered in the literature to a great extent. In membranes with a distribution of pore sizes, the smaller pores reject the particles and the larger ones are responsible for internal fouling of the membrane. Studying the effects of pore geometry could help in designing membranes with improved long term flux and particle rejection, which can increase the productivity and extend the useful life of the membranes.

The objective of this study is to extend our knowledge about morphological factors affecting a membrane's performance by investigating the effect of geometrical characteristics of membrane pores such as pore shape and aspect ratio on particle rejection (for smaller pores), and the amount of flux decline due to pore constriction (for larger pores in PSD), in light of several pore size distributions.

2. Simulation and calculation method

2.1.Model membranes and constant parameters

The permeate flux of the membranes is determined by different factors such as membrane porosity, thickness, pore size distribution, viscosity of the solvent, *etc.* To accurately compare the flux of the membranes under the effect of geometry and PSD, the factors listed in Table 1 were kept constant and used in flux calculations.

Table 1. Constant parameters for flux calculations

Pressure difference across the membrane thickness (ΔP)	2 bar
Viscosity of the permeate (μ)	$1\ cP$
Membrane Thickness (l)	$50\ \mu m$
Porosity (ϵ)	20%
Particle Size (diameter)	$0.1\ \mu m$

Six pore size distributions were considered and the fluxes of the membranes having different pore geometries, after maximum particle deposition onto interior wall of the pores, were compared for each pore size distribution. Four basic geometries were considered for comparison, including four aspect ratios. Table 2 shows these geometries.

Table 2. Geometry and Aspect ratio of pores studied.

Geometry	Circular	Rectangular	oval	triangular
Aspect ratios	1	3,7,15,30	3,7,15,30	3,7,15,30

Where the aspect ratios for different geometries were defined as follows:

oval: $\frac{\text{larger diameter}}{\text{smaller diameter}}$, rectangular: $\frac{\text{length}}{\text{width}}$, triangular: $\frac{\text{height}}{\text{base}}$

2.2.Pore size range and distributions

A range of pore hydraulic diameter (D_H) from 0.001 µm to 1.00 µm with an interval (dD_H) of 0.001 µm with a log-normal distribution were considered for all model membranes. Log-normal probability density function has been extensively used in the literature to model the pore size distribution of the membranes [22-24]. A classical form of the log-normal distribution [25] can be defined as:

$$f_D(D) = \frac{1}{\sigma D_H\sqrt{2\pi}} \exp\left(-\frac{[ln(D_H) - ln(D^*)]^2}{2\sigma^2}\right) \tag{1}$$

Where σ and D^* are used to calculate the mean pore size (μ) and variance ($\hat{\sigma}^2$) as followings:

$$\mu = D^* \exp\left({\sigma^2}/{2}\right) \tag{2}$$

$$\hat{\sigma}^2 = {D^*}^2(\exp(2\sigma^2) - \exp(\sigma^2)) \tag{3}$$

Table 3 shows the parameters of the six log-normal distributions used in this study. The first three distributions have different mean and variance. The last three distributions use the same parameters as the second but are shifted in the horizontal axis. Table 3 also shows the percentage of the pores with hydraulic diameter smaller than 0.1 μm (particle diameter) in each distribution. The normalized log-normal distributions can be seen in Figure 1.

Table 3. log-normal distribution constants and percent of pores (RP) in the distribution, smaller than particle size (0.1μm)

PSD	D^*	σ	Mean	Variance	% of pores < 0.1 μm (RP)
PSD A	0.050	0.585	0.059	0.001	88.36
PSD B	0.070	0.819	0.098	0.009	67.10
PSD C	0.090	1.053	0.157	0.050	54.78
PSD D	0.070	0.819	0.198	0.009	0.00
PSD E	0.070	0.819	0.248	0.009	0.00
PSD F	0.070	0.819	0.298	0.009	0.00

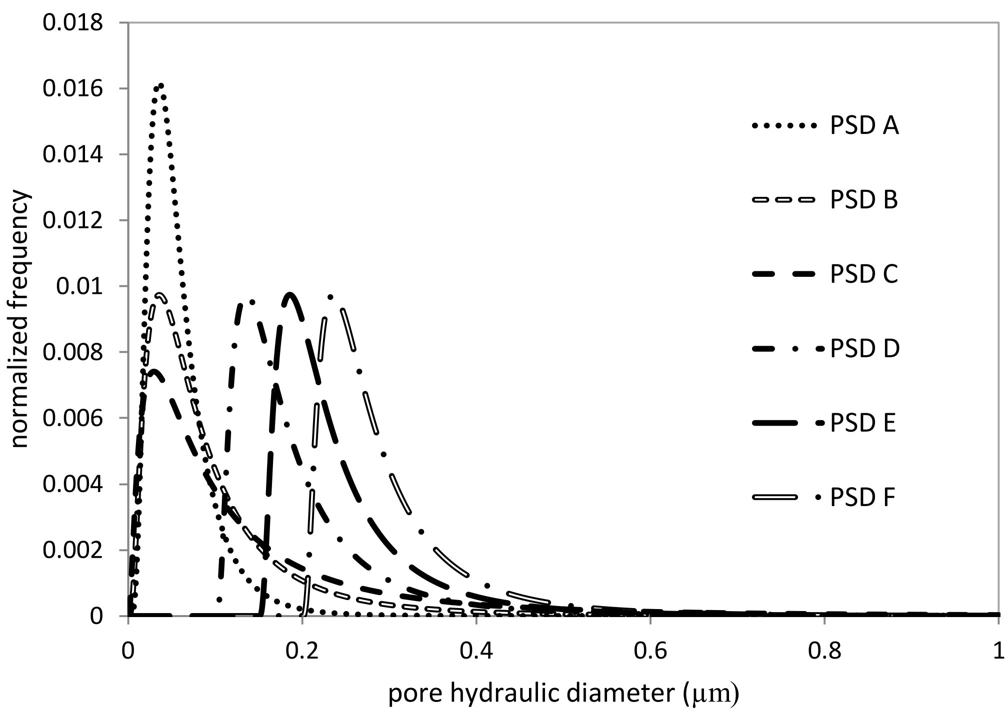

Figure 1. Pore size distributions studied in this work.

2.3.Simulation of maximum particle binding onto pore walls

Pore constriction by particles was approximated with monolayer particle deposition inside pore walls and simulated using MATLAB image analysis toolbox. The program is capable of measuring the cross sectional area and wetted perimeter of a desired pore to calculate the hydraulic diameter of the pore. Then, using a specific geometrical algorithm, which places the particles side by side on the perimeter of the pore, maximum particle deposition onto interior perimeter of pores is simulated. The available area for flow and the wetted perimeter of the pore channel, after particle deposition, are then measured and recorded for further calculation of the pore hydraulic diameter after particle deposition. Particles are assumed to be rigid and spherical (circular in 2D); therefore, in its measurement of area and wetted perimeter, the program takes into account the semi-circular profile of the particles forming the new outline of the flow channel. This procedure can be done for any desired combination of particle diameters and pore hydraulic diameters. Figure 2 shows a graphical sample of the simulation results for different pore geometries at two different particle to pore size ratios (λ). In this figure, open surfaces outlined by the space between the edges of the particles, including the convoluted shape of the adsorbed particle layer, represent the available area for flow after pore constriction. The small areas trapped between the pore wall and the borders of the particles, are considered to be unavailable for flow.

The hydraulic diameter of the pore channel, before and after particle deposition, is calculated as follows:

$$D_{H,clean} = \frac{4A_{clean}}{p_{clean}} \tag{4}$$

$$D_{H,constricted} = \frac{4A_{constricted}}{p_{constricted}} \tag{5}$$

In which D_H is pore hydraulic diameter and is defined as four times the pore area over wetted perimeter of the pore [26-27]. The pore size of membranes is usually characterized by bubble point porometry. The definition of pore hydraulic diameter, as stated above, will yield the same value of pore size measured by bubble point porometry [28].

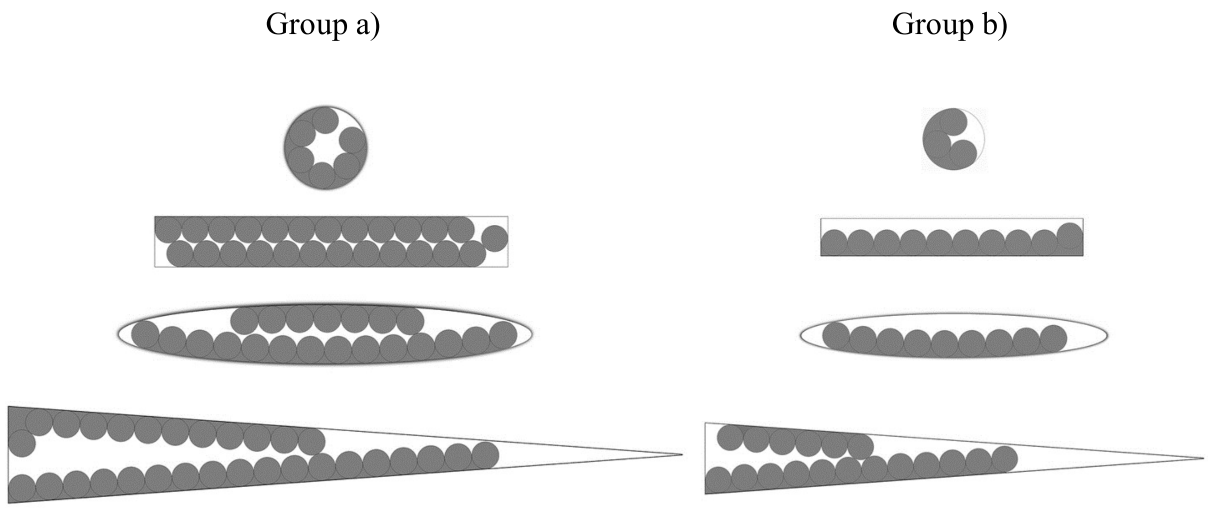

Figure 2. Sample simulation results and available area after particle binding for different geometries in two different particle to pore size ratios. a) represent particle to pore size ratio (λ) of 0.3 and b) represent particle to pore size ratio λ of 0.4. The aspect ratio is 7 for all shapes (except for the circle). The particle size is unique and identical for both groups. All geometries in a group have the same value of hydraulic diameter. The geometries and particles are drawn to scale.

In this study, as mentioned before, the pore hydraulic diameters in the range of 0.001 µm to 1 µm were considered to be present at the surface of the membranes, and the particle diameter is assumed to be 0.1 µm. The 0.1µm particles represent less concentrated smaller particles in the feed responsible for internal fouling while the supracolloidal particles in the feed (>1µm) are totally rejected by membrane pores. Simulation of pore constriction by particles is only applicable for the pore sizes that physically accept at least one particle into their geometry. In other words, if a pore is small enough to physically reject a particle, there would be no particle inclusion into the pore and consequently no pore constriction by the pores. Therefore, for all the pore sizes, with different geometries, for which the particle inclusion is possible, the hydraulic diameter and cross sectional area of the constricted pore can be calculated as a result of the simulation, and then be used for calculation of membrane flux after internal fouling.

2.4.Membrane flux calculations

Using Hagen-Poiseuille equation, the flow rate through one clean single pore can be calculated as follows:

$$Q_{i,clean} = D^2_{H\ i,clean}\ A_{i,clean}\ \frac{\Delta P}{32\mu l} \tag{6}$$

In which $Q_{i,clean}$ is the flow rate through a clean single pore, $D_{H\ i,clean}$ the pore hydraulic diameter, $A_{i,clean}$ the cross-sectional area of the pore, perpendicular to the flow, and l pore length [21]. The subscript " i " represents the pore index which alters by changing pore hydraulic diameter. It was assumed that the pore geometry does not change along the surface of a membrane. ΔP is the pressure difference across the membrane thickness and μ is the viscosity of the solvent (water). Pore length is considered as a constant parameter for all geometries. All calculations were carried out for a unit area (1 m^2) of membranes.

The clean membrane flux can be calculated as:

$$J_{clean} = \sum_{i=1}^{n} n_i\ Q_{i,clean} \tag{7}$$

Where n_i represents the number of pores of a certain size in 1 m^2 of the membrane. As mentioned previously, an identical porosity was assumed for all different membranes. Considering the fact that different geometries will have different areas at the same hydraulic diameter; the number of pores at the surface of the membrane was adjusted, following the log-normal distribution, to obtain the same porosity for all geometries.

Knowing the values for pore hydraulic diameter (D_H) and using the definition of hydraulic diameter ($4A/P$) we can calculate the clean pore area ($A_{i,clean}$). Subsequently, pore's area frequency (AF_i) can be defined as:

$$AF_i(m^2) = A_{i,clean}(m^2) \times f_i \tag{8}$$

In which f_i is the normalized frequency of pore i, So:

$$AF_i(m^2) = \frac{A_{i,clean}(m^2) \times n_i}{N} \tag{9}$$

Where n_i is the number of pore i, and N is the total number of all pores (all sizes) in the membrane. The cumulative pore area frequency (AAF) can be defined as:

$$AAF(m^2) = \sum AF_i\,(m^2) \tag{10}$$

This means:

$$AAF(m^2) = \frac{total\ area\ of\ pores\ in\ membrane\ (m^2)}{N}$$
$$= \frac{porosity \times membrane\ area\ (m^2)}{N} \tag{11}$$

By rearranging this equation we can write:

$$N = \frac{porosity \times membrane\ area\ (m^2)}{AAF(m^2)} \tag{12}$$

Having the value of N for a membrane with specific pore geometry, the number of pores at each pore size can be calculated as the following:

$$n_i = f_i \times N \tag{13}$$

The number of pores at each size is then used for calculation of clean and fouled membrane fluxes. The calculated clean flux of the membranes with different geometries for a constant pore size distribution had the same value as expected. This prepares a basis for comparison of membrane fluxes after pore constriction by particles.

As a result of pore constriction, both hydraulic diameter and cross-sectional area decrease, causing a reduction in permeate flow. The following equations can be written for an internally fouled pore:

$$Q_{i,constricted} = D^2_{H\ i,constricted}\ A_{i,constricted}\ \frac{\Delta P}{32\mu l} \tag{14}$$

$$J_{constricted} = \sum_{i=1}^{n} n_i \, Q_{i,constricted} \tag{15}$$

Where $D_{H\,i,fouled}$ and $A_{i,fouled}$ are hydraulic diameter of the pore and pore area after pore constriction which are known as a result of the simulation. It should be noted that for the pore sizes for which the particles cannot physically penetrate into the pore (rejecting pores) the values of $Q_{i,clean}$ and $Q_{i,constricted}$ are the same as there is no pore constriction occurred.

3. Results and discussion

3.1. Effect of pore shape and PSD on particle rejection

Table 4 shows the clean membrane flux of the membranes having different pore geometries at different pore size distributions, along with the total number of pores for each membrane, and the percent of these pores physically rejecting the 0.1 µm diameter particles. The clean flux of different membranes for a constant PSD is the same, as expected, due to the method of flux calculation mentioned before. The total number of pores, as a result of equations 8 to 13, varies for membranes with different pore geometries. This can be explained by the fact that different pore geometries at the same hydraulic diameter have a different cross-sectional area. Therefore, the total number of pores on the membrane surface was calculated based on the PSD, to maintain a constant porosity, and consequently a constant clean flux, for different membranes. In Table 4, RP shows the percent of the total number of the pores smaller than particle size (0.1 µm), while RP* represents the percent of the pores that physically reject the particles. It is interesting that although RP is the same for all membranes at a constant PSD, RP* is different for different pore geometries. For rectangular pores, this value is always larger than RP and increases by increasing the aspect ratio. For triangular and circular pores, RP is always the same as RP* and does not change with pore aspect ratio. For oval pores, RP* is always larger than RP, but it is less sensitive to aspect ratio, compared to rectangular geometry, as it increases with aspect ratio up to aspect ratio of 7 and remains constant for higher aspect ratios.

The effect of pore geometry on particle rejection can be better understood from Figures 3 to 5. In these figures, the contribution of different pore sizes to initial (clean) membrane flux and fouled membrane flux are plotted for membranes with different pore geometries at an aspect ratio of 7, and PSD B. The presented values take into account the number of pores of a specific size based on the PSD. As we can see in Figure 3, the contribution of different pore sizes to clean and fouled fluxes are the same for all pore sizes smaller than 0.172 μm (the first breaking point of the curve). It means that for all the pores smaller than this pore size, there is no particle inclusion into the pores. In other words, all the pores smaller than this size, are rejecting the particle size of 0.1 μm, and the pores larger than this size are constricted, due to particle penetration in the pore.. This pore will be referred as $D_{H,LRP}$ (largest rejecting pore) of the membrane, in the rest of this article. $D_{H,LRP}$ is different for different pore geometries. In fact it is the reason for different values of RP* for different membranes as explained above. The value of $D_{H,LRP}$ is determined by the particle size and the geometry of the pore and is not affected by PSD and the number of pores in the membrane. Larger values of $D_{H,LRP}$ denote better rejection of particles. As previously mentioned, all the pores larger than $D_{H,LRP}$ are constricted by particles; therefore, the location of $D_{H,LRP}$ in the PSD of the membrane will have significant effect on the portion of membrane flux unaffected by pore constriction. $D_{H,LRP}$ for different pore geometries, filtering the particle size of 0.1 μm, are also listed in Table 4.

Table 4. clean membrane flux (J_{clean}) total number of pores (N), number percent (RP) of pores smaller than particle size (0.1μm) and number percent of pores physically rejecting the particles (RP*) for membranes with different pore geometries and PSDs.

PSD		PSD A		PSD B		PSD C		PSD D		PSD E		PSD F		$D_{H,LRP}$ in the membrane (μ) for particle size of 0.1μ
Most probable size (μ)		0.036		0.036		0.030		0.136		0.186		0.236		
% of pores < 1 μ (RP)		88.36		67.10		54.78		0.00		0.00		0.00		
J_{clean} (lmh)		874		6372		13400		5650		6085		6902		
aspect ratio		N	RP* (%)	N	RP* (%)	N	RP* (%)	N	RP* (%)	N	RP* (%)	N	RP* (%)	
Rectangular	3	1.51E+13	95.46	4.23E+12	78.79	1.74E+12	65.59	1.60E+12	19.40	1.09E+12	0	7.84E+11	0.00	0.133
	7	8.83E+12	98.33	2.47E+12	86.66	1.02E+12	74.17	9.34E+11	52.42	6.36E+11	9.14	4.57E+11	0.00	0.172
	15	4.73E+12	98.78	1.32E+12	88.48	5.45E+11	76.40	5.00E+11	60.25	3.41E+11	21.35	2.45E+11	0.00	0.185
	30	2.52E+12	98.99	7.04E+11	89.45	2.90E+11	77.65	2.67E+11	64.36	1.81E+11	29.04	1.31E+11	0.00	0.192
Triangular	3	9.65E+12	88.36	2.70E+12	67.10	1.11E+12	54.78	1.02E+12	0.00	6.95E+11	0	5.00E+11	0.00	0.100
	7	5.00E+12	88.36	1.40E+12	67.10	5.76E+11	54.78	5.29E+11	0.00	3.60E+11	0	2.59E+11	0.00	0.100
	15	2.52E+12	88.36	7.03E+11	67.10	2.90E+11	54.78	2.66E+11	0.00	1.81E+11	0	1.30E+11	0.00	0.100
	30	1.30E+12	88.36	3.63E+11	67.10	1.50E+11	54.78	1.38E+11	0.00	9.37E+10	0	6.74E+10	0.00	0.100
Oval	1	2.57E+13	88.36	7.18E+12	67.10	2.96E+12	54.78	2.72E+12	0.00	1.85E+12	0	1.33E+12	0.00	0.100
	3	1.70E+13	95.46	4.76E+12	78.79	1.96E+12	65.59	1.80E+12	19.40	1.23E+12	0	8.82E+11	0.00	0.149
	7	8.56E+12	97.51	2.39E+12	83.94	9.86E+11	71.03	9.05E+11	40.55	6.17E+11	0.32	4.43E+11	0.00	0.156
	15	4.17E+12	97.51	1.16E+12	83.94	4.80E+11	71.03	4.41E+11	40.55	3.00E+11	0.32	2.16E+11	0.00	0.156
	30	2.11E+12	97.51	5.90E+11	83.94	2.43E+11	71.03	2.24E+11	40.55	1.52E+11	0.32	1.09E+11	0.00	0.156

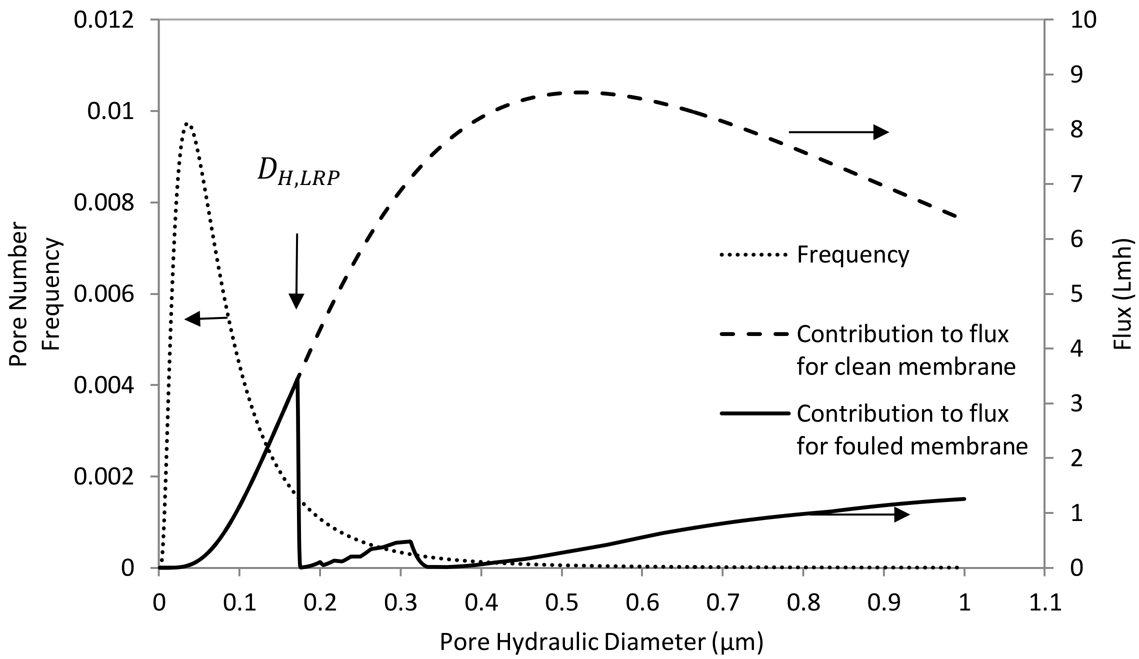

Figure 3. Contribution of different pore sizes (considering their abundance) to clean and fouled membrane flux for the membrane with rectangular pores (aspect ratio of 7:1) following PSD B

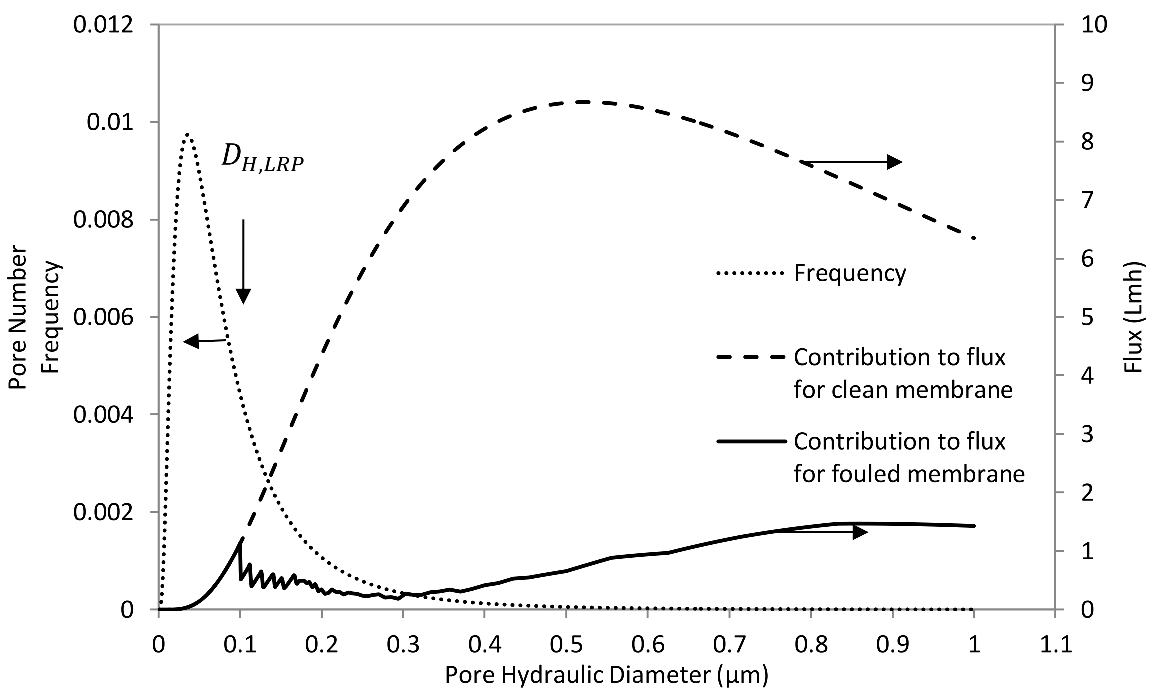

Figure 4. Contribution of different pore sizes (considering their abundance) to clean and fouled membrane flux for the membrane with triangular pores (aspect ratio of 7:1) following PSD B

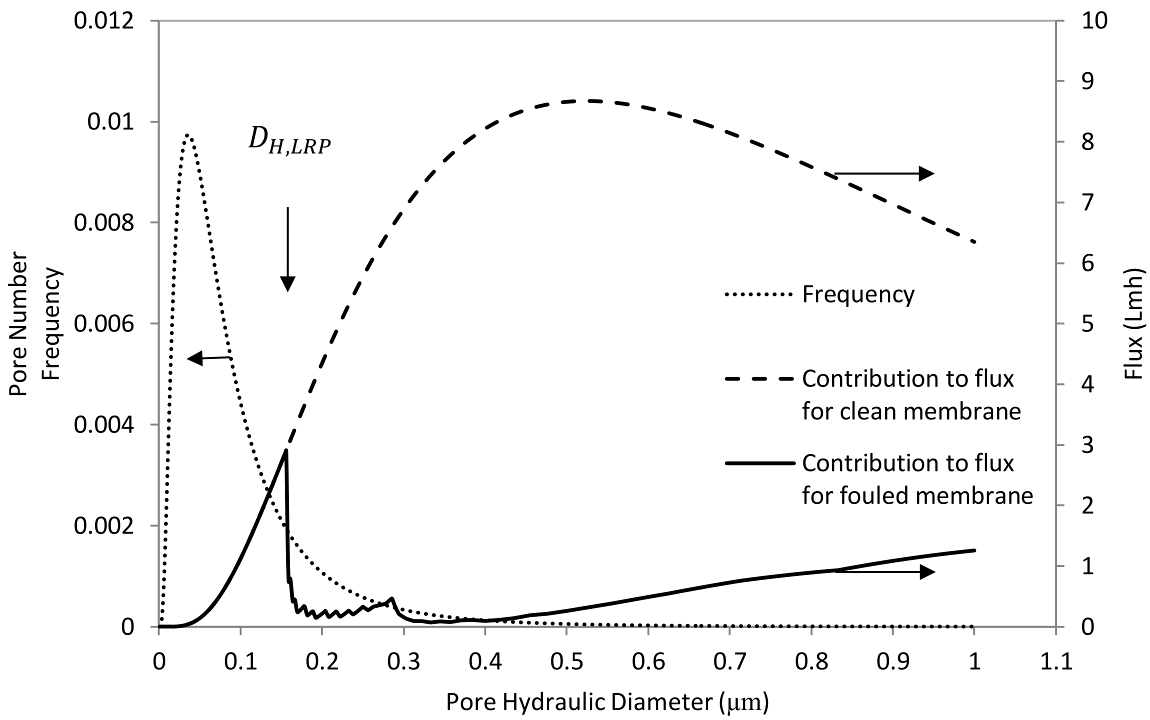

Figure 5. Contribution of different pore sizes (considering their abundance) to clean and fouled membrane flux for the membrane with oval pores (aspect ratio of 7:1) following PSD B

3.2. Contribution to flux by different pore sizes: rejecting pores and constricted pores

Based on the position of $D_{H,LRP}$ in the pore size distribution, the range of pore sizes can be divided to two sections. These two sections are rejecting pores and constricted pores. As mentioned previously, rejecting pores are all the pores smaller than $D_{H,LRP}$, for which there is no pore constriction happening since they reject the particles. On the other hand the constricted pores are all the pores larger than $D_{H,LRP}$, which are constricted by the particles. In our calculations we were focused on the effect of pore geometry on internal fouling, as a result of pore constriction, and ignored the effect of other fouling types like cake layer and pore sealing. Therefore, for all the rejecting pores, there is no fouling and thus they show the same contribution to membrane flow after fouling, as the clean membrane flux. However, for all constricted pores, the contribution to membrane flow is drastically reduced due to pore constriction.

The overall flux of the membranes was determined as the accumulation of the contribution of rejecting and constricted pores to membrane flux and depends on three parameters. First, the value of $D_{H,LRP}$ in the membrane; the larger the $D_{H,LRP}$, the higher contribution of rejecting pores in fouled membrane flux. For membranes having pore geometries with higher values of $D_{H,LRP}$ (such as rectangular and oval), there are more number of pores rejecting the particles. This increases the contribution of rejecting pores to fouled membrane flux. The second factor is the overall extent of flux decline after particle deposition into pores, which affects the contribution of constricted pores to fouled membrane flux and the third factor is the location of $D_{H,LRP}$ in the pore size distribution which determines the number of pores belonging to each group of pores (rejecting and constricted pores). Figures 6 to 11 represent the contribution of rejecting pores and constricted pores for different geometries and pore size distributions.

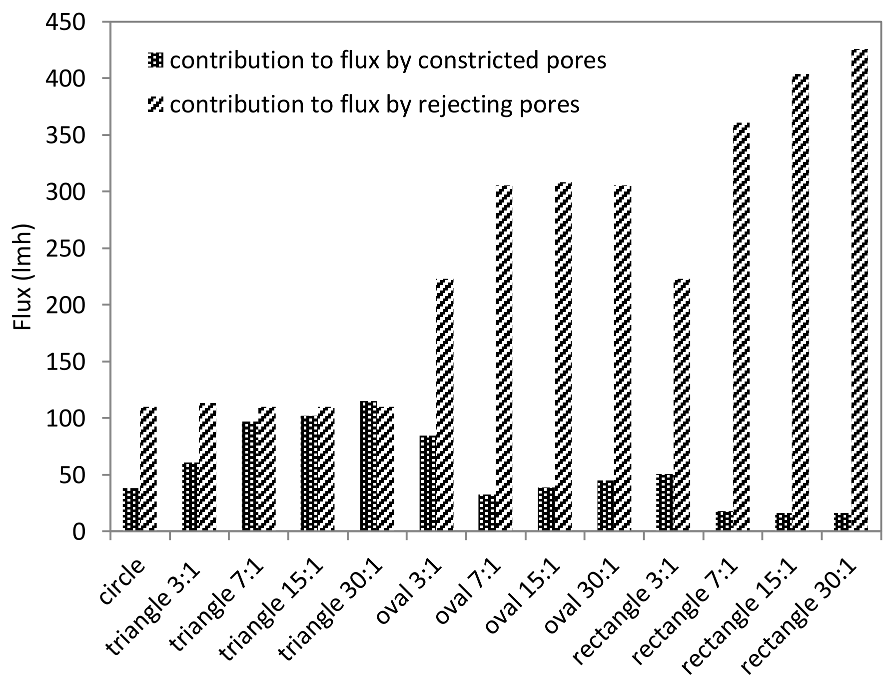

Figure 6. Contribution to fouled membrane flux by rejecting pores and constricted pores for membranes following PSD A.

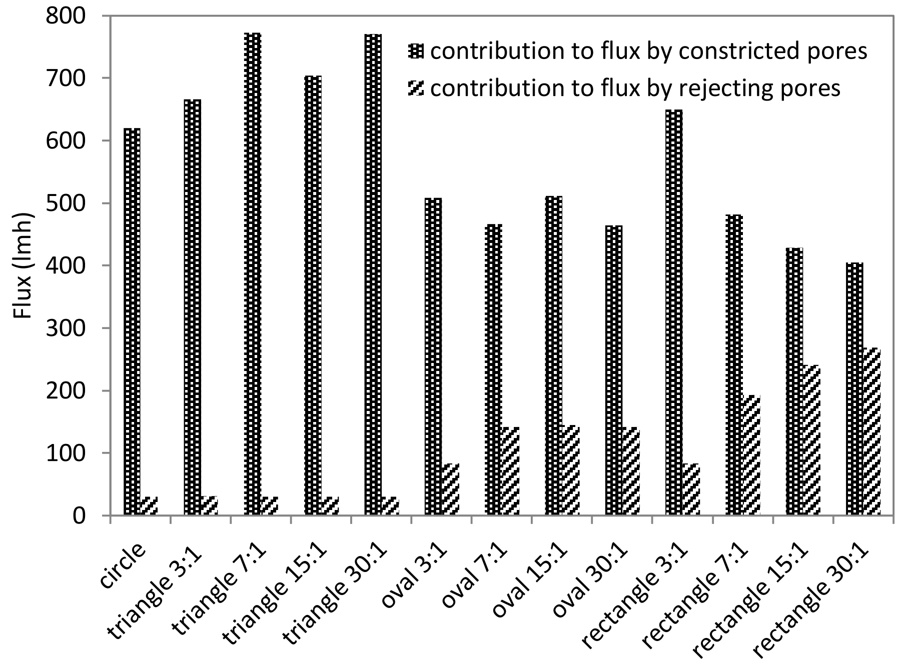

Figure 7. Contribution to fouled membrane flux by rejecting pores and constricted pores for membranes following PSD B.

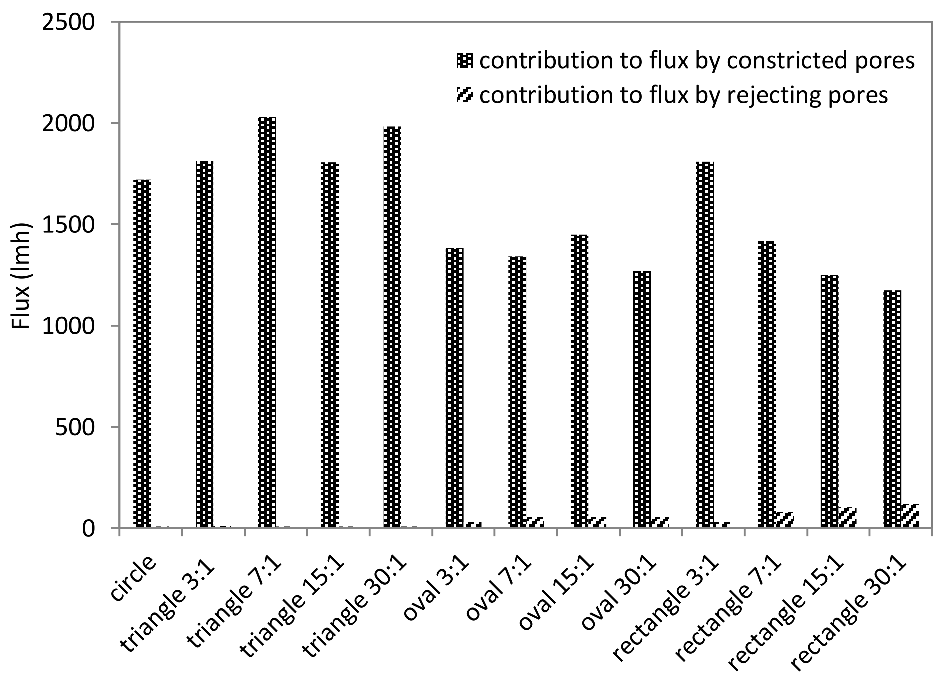

Figure 8. Contribution to fouled membrane flux by rejecting pores and constricted pores for membranes following PSD C**.**

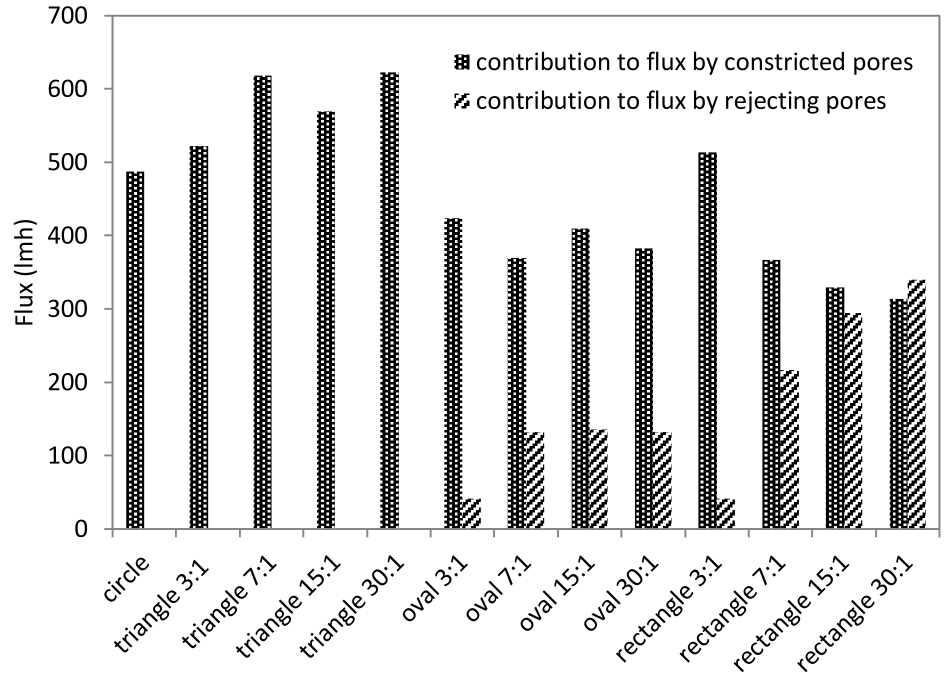

Figure 9. Contribution to fouled membrane flux by rejecting pores and constricted pores for membranes following PSD D.

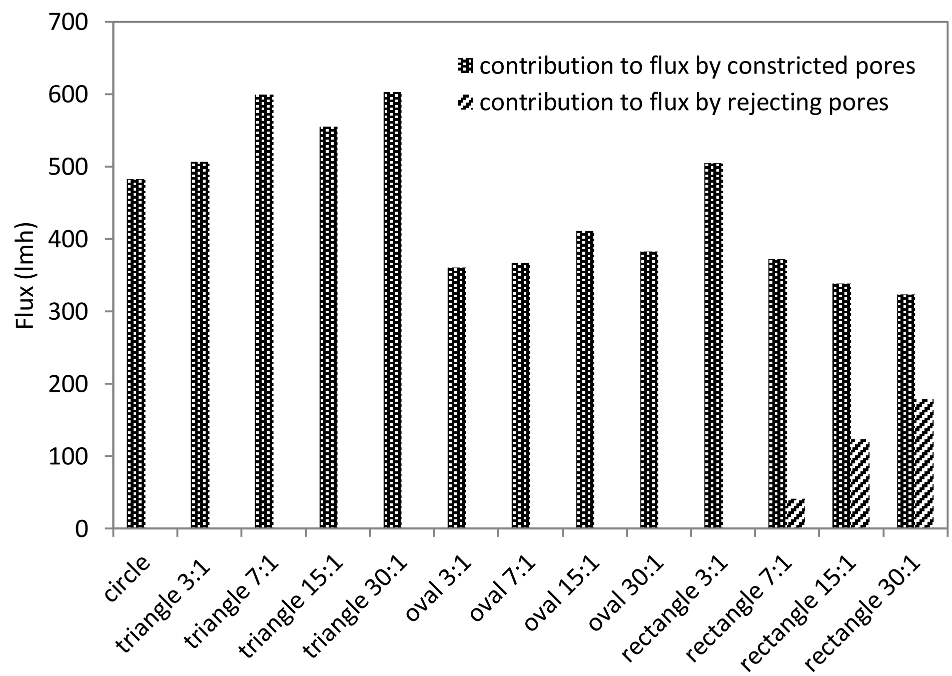

Figure 10. Contribution to fouled membrane flux by rejecting pores and constricted pores for membranes following PSD E.

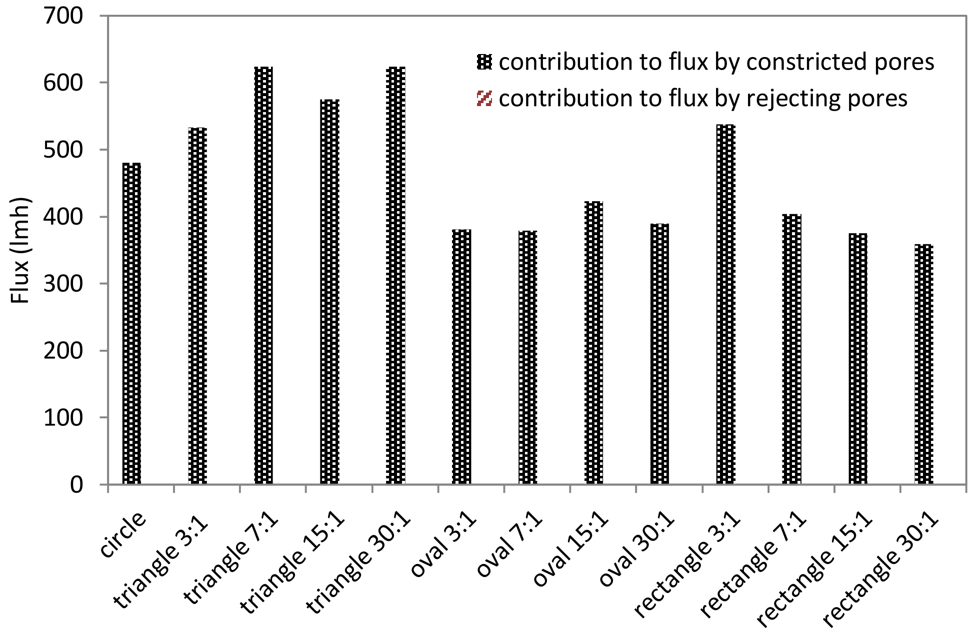

Figure 11. Contribution to fouled membrane flux by rejecting pores and constricted pores for membranes following PSD F.

3.2.1. Effect of $D_{H,LRP}$:

In Figures 6 to 11, the contribution of rejecting pores for rectangular pores is the highest compared to contribution of rejecting pores for oval and triangular. Membranes with triangular and circular pores exhibited the least contribution of rejecting pores to flux compared to other pore geometries. This is the same for all pore size distributions. This is due to the fact that rectangular pores had the largest $D_{H,LRP}$ but triangular and circular pores had the smallest $D_{H,LRP}$ among the geometries studied. The effect of aspect ratio on the contribution of rejecting pores to membrane flux is the same as the effect of aspect ratio on $D_{H,LRP}$. For rectangular pores, the contribution of rejecting pores increases by increasing pore aspect ratio; however, for triangular pores it does not change by changing the aspect ratio of the pore.

3.2.2. Effect of pore constriction:

Contribution of constricted pores for different geometries follows the same pattern at different PSDs. Comparing different geometries at a given PSD, the contribution to flux by rectangular pores was the lowest and for triangular pores was the highest. In this ranking, oval pores stand in the middle of rectangular and triangular pores. The circular pores showed a contribution of constricted pores between the values for triangular and oval. The contribution to flux by constricted pores for rectangular geometry did not change with aspect ratio. However, for triangular and oval pores, by increasing the aspect ratio, the amount of flux contributed by constricted pores increases too; which means, elongating a triangular or oval pore may reduce the amount of flux decline due to pore constriction.

3.2.3. Effect of PSD (position of $D_{H,LRP}$)

In Figure 6, the contribution of rejecting pores to flux is higher than the contribution of constricted pores for all membranes following PSD A. This is due to the narrow distribution of pore sizes for PSD A and the fact that the number of larger pores in the membrane, which are constricted by particles, is very low according to the PSD. By shifting from PSD A to the PSD B, we can see in Figure 7 that the comparative contribution of each group of pores changes dramatically. For the PSD B, the contribution of constricted pores is higher than rejecting pores. Although the most probable pore size is the same for PSDs A and B, the latter is wider; therefore, it has a greater number of larger pores compared to the PSD A. These large pores are the main contributors to flow. A small increase in the frequency of these pores in the membrane increases the portion of flux which is affected by pore constriction. The same effect can be seen by shifting from PSD B to PSD C.

PSDs B, D, E and F all have the same skewness and variance. In fact, the last three are following the same distribution as the PSD B but are shifted in “pore size” axis by values of 0.1, 0.15 and 0.2 μm. Comparing their results, in figures 7 and 9 to 11, shows that by shifting the distribution to larger pore sizes, the number of rejecting pores in all membranes decreases as expected. As a result the contribution of rejecting pores to membrane flux decreases as well.

3.3. Overall membrane flux: combined effect of particle rejection, pore constriction and PSD

Figures 12 to 17 show the overall fouled flux of the membranes having different pore geometries for different pore size distributions. The fouled flux of the membranes is affected by the combination of the three parameters listed above. In Figure 12 membranes follow the PSD A for which over 85% of the pores in all membranes are physically rejecting the particles (Table 3). In this case, the rejecting pores have dominant contribution to flux, therefore, the overall flux ranking follows the ranking for the contribution of rejecting pores in which the membranes having rectangular geometry have the highest flux, followed by membranes with oval and triangular pore. Since most of the pores are rejecting the particles, the effect of aspect ratio on the overall flux follows the same pattern as the effect of aspect ratio on rejection. By increasing the aspect ratio, the flux of the membranes with rectangular pores increases due the increase in particle rejection (less pore constriction). For membranes with oval pore geometries the flux increases in moving from aspect ratio of 7 to 15 and remains constant for higher aspect ratios. This is the same pattern seen for particle rejection (Table 3). For membranes with triangular pores we can see a slight increase in the flux by increasing the aspect ratio. This is not due to higher rejection of longer triangular pores but is due to increase in the contribution of constricted pores to overall membrane flux by increasing pore aspect ratio.

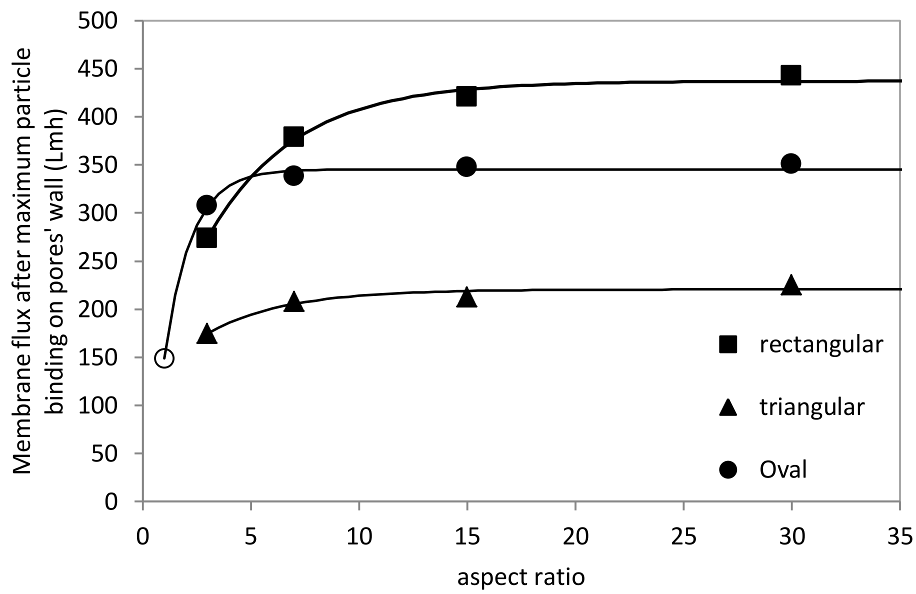

Figure 12. The overall membrane flux after maximum particle deposition into pore walls for membranes following the PSD A**.**

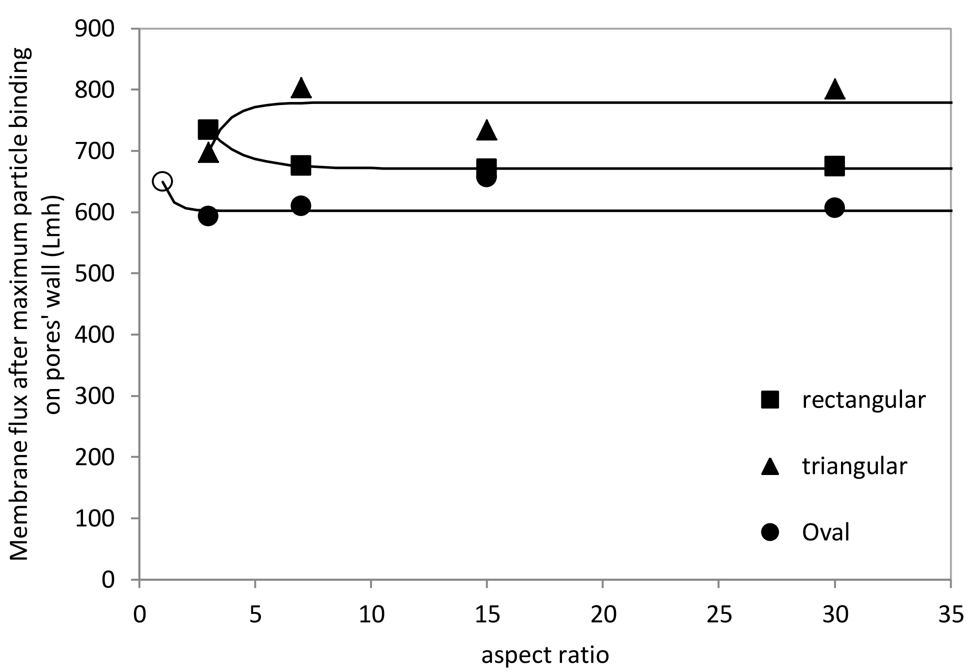

Figure 13. The overall membrane flux after maximum particle deposition into pore walls for membranes following the PSD B.

By widening the distribution to PSD B in Figure 13, there are still more than 65% of the pores that are physically rejecting the particles (Table 3) and it is expected to see the domination of rejecting pores in determining the overall flux. Here, membranes with triangular pores show the highest flux. As previously mentioned, widening the pore size distribution causes the number of larger pores, contributing to membrane flow, to increase. This increases the number of constricted pores and consequently increases the contribution of constricted pores to overall membrane flux. Therefore, the effect of constricted pores on overall flux becomes dominant and the geometry for which the flux of the constricted pores is higher would yield higher overall flux. This effect is magnified by further widening the distribution to the PSD C (Figure 14). In this case, triangular pores show the highest flux.

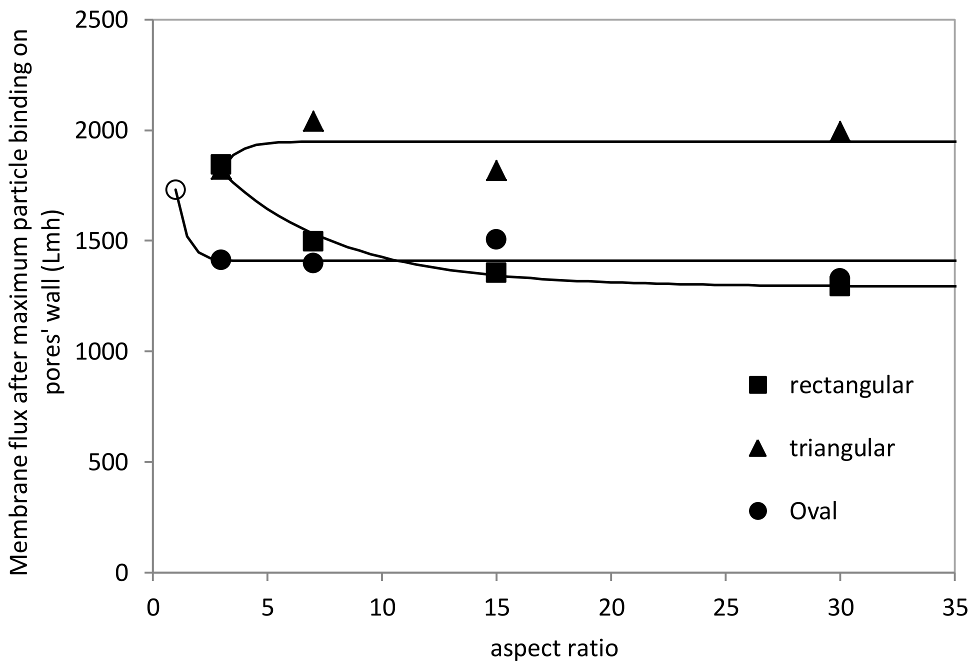

Figure 14. The overall membrane flux after maximum particle deposition into pore walls for membranes following the PSD C.

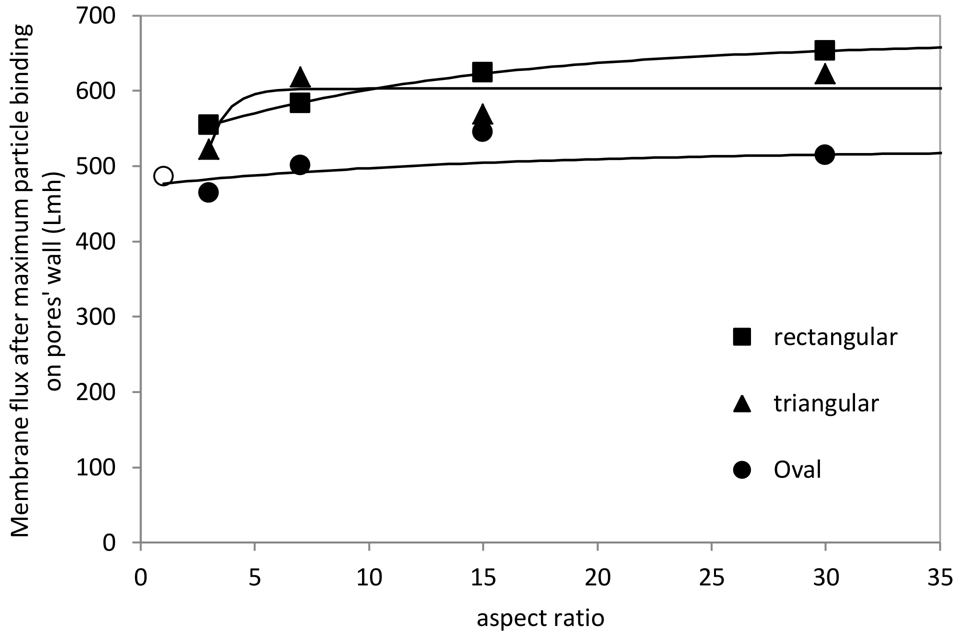

Figure 15. The overall membrane flux after maximum particle deposition into pore walls for membranes following the PSD D.

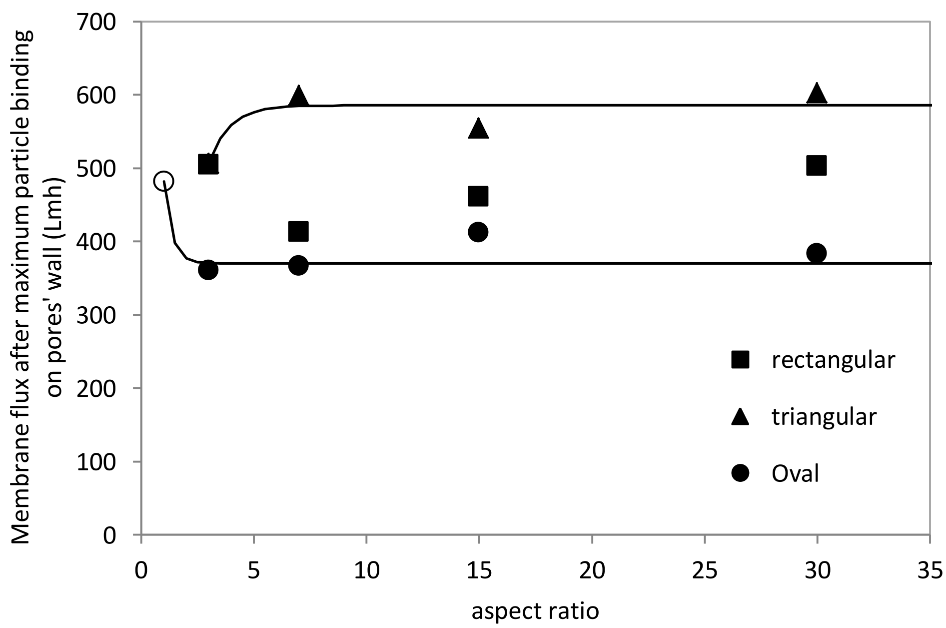

Figure 16. The overall membrane flux after maximum particle deposition into pore walls for membranes following the PSD E.

By shifting from the PSD B to PSD D (Figure 13 to Figure 15), we can see an intermediate case where there is no overall preference for any pore geometry over the other. In this case, due to the position of the PSD, all the pores for all membranes with triangular pore geometries are constricted by particles causing a reduction in overall membrane flux, while a significant portion of the pores for membranes with rectangular and oval pores are rejecting the particles (Table 3, PSD D). In such a case, the rectangular membranes show slightly higher fluxes than triangular membranes because of higher rejection of the particles (Figure 15).

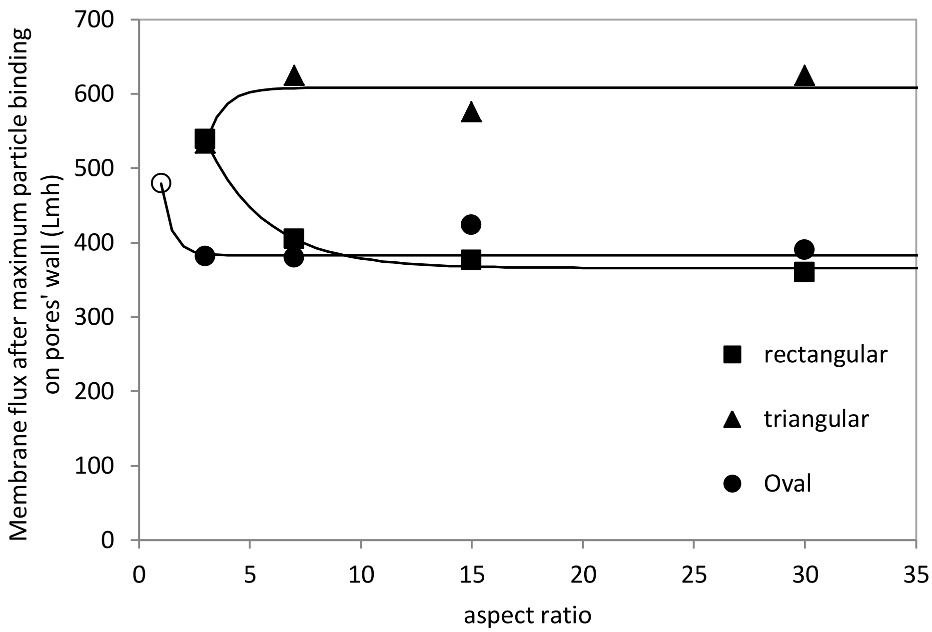

Figure 17. The overall membrane flux after maximum particle deposition into pore walls for membranes following the PSD F**.**

By shifting the PSD towards larger pores in PSD E and PSD F, the number of rejecting pores decreases. As a result, the effect of constricted pores becomes dominant and membranes having geometries which provide better flow after pore constriction, show higher overall fluxes. This effect is less visible for PSD E (Figure 16) because of the fact that there are still many rectangular pores rejecting the particles which fortifies the effect of rejecting pores in overall flux of the membranes. However, for PSD F, all the pores for all different membranes are including the particles and the effect of particle rejection is completely eliminated. In such case, membranes having triangular pores show the most desirable flux which is slightly enhanced by increasing the aspect ratio. The overall flux of the membranes with rectangular and oval pores is about 60% of the flux of membranes with triangular pores and tends to decrease by increasing the aspect ratio of their pores.

Results of this study indicate the improved performance of membranes with rectangular pores for the application where most of the pores reject the particles. This is in the same line as the results presented by Chandler and Zydney [14] in which, long slotted pores showed slower rates of flux decline, compared to circular pores, due to particle deposition on the entrance of the pores. On the other hand, for the applications where a major portion of the pores are physically larger the particles (available for particle penetration), the triangular pores are recommended because of higher flux after pore constriction. An example of such applications can be pretreatment of feed solution containing a range of particle sizes.

Conclusions and recommendations

Thirteen model membranes were considered with six different pore size distributions all following a log-normal distribution. It was observed that pore shape can affect the rejection characteristics of a membrane. Pores of identical hydraulic diameter but different geometries exhibited different rejections. Comparing different pore shapes at a constant hydraulic diameter, rectangular pores can reject larger particles than oval pores while both geometries are able to reject particles larger than their hydraulic diameter. This capability is improved by elongating these pore geometries. Circular and triangular geometries, regardless of aspect ratio, all reject the particles with the same size as their hydraulic diameter. Based on this difference in particle rejection, in a distribution of pore sizes for a membrane, the number of rejecting pores for a membrane having rectangular pores is the highest compared to other geometries at the same aspect ratio. Different rejection behavior of various geometries causes $D_{H,LRP}$ (the largest rejecting pore) vary for different membranes. Based on the position of $D_{H,LRP}$ in the PSD, the whole range of pore sizes can be divided to two parts.

One part consists of rejecting pores ($D_H < D_{H,LRP}$) and the other consists of constricted pores ($D_{H,} > D_{H,LRP}$). The total fouled membrane flux also can be split to two parts; one being the contribution to flux by rejecting pores and the other the contribution to flux by constricted pores. For a given PSD, the contribution to flux by rejecting pores is the highest for membranes with rectangular pores while the contribution of constricted pores to flux is the highest for triangular pores. Increasing the aspect ratio of pores has different effects on the contribution of constricted pores to flux for different geometries. For triangular and oval geometries, increasing the aspect ratio increases the contribution of constricted pores to flux while for rectangular geometries, it decreases the contribution of constricted pores to overall membrane flux. Generally, rectangular pores are recommended for applications for which a high rejection of particles is required and where the pore constriction by particles is less likely to happen; but, triangular geometries are recommended for applications where particle penetration into membrane pores is inevitable, such as in the case of feed solutions containing a mix of colloids and larger droplets or particles in the micron range.

Acknowledgment

The authors would like to acknowledge the support of the Natural Science and Engineering Research Council of Canada (NSERC).

References

[1] K. Hwang, T. Lin. Effect of morphology of polymeric membrane on the performance of cross-flow microfiltration. J.Membr.Sci., 199 (2002) 41.

[2] R.W. Baker, Membrane Technology and Applications, Membrane Technology and Research, Inc. Menlo Park, California, John Wiley & Sons Ltd, 2004.

[3] R.S. Barhate, C.K. Loong, and S. Ramakrishna. Preparation and characterization of nanofibrous filtering media. J.Membr.Sci., 283 (2006) 209.

[4] A.G. Fane, C.J.D. Fell. A review of fouling and fouling control in ultrafiltration. Desalination, 62 (1987) 117.

[5] A. Santos, P. Bedrikovetsky, and S. Fontoura. Analytical micro model for size exclusion: Pore blocking and permeability reduction. J.Membr.Sci., 308 (2008) 115.

[6] A.L. Lim, R. Bai. Membrane fouling and cleaning in microfiltration of activated sludge wastewater. J.Membr.Sci., 216 (2003) 279.

[7] Jacquemet, Valerie, Gilberte Gaval, Elena-Carmen Gherman, and Jean-Christophe Schrotter. 2006. "Deeper Understanding of Membrane Fouling Issues on a Full Scale Water Plant." Desalination 199 (1-3): 78-80.

[8] E.M.V. Hoek, J. Allred, T. Knoell, and B. Jeong. Modeling the effects of fouling on full-scale reverse osmosis processes. J.Membr.Sci., 314 (2008) 33.

[9] Hermia, J. 1982. "Constant Pressure Blocking Filtration Laws -“ Application to Power-Law Non-Newtonian Fluids." Trans. IChemE 60: 183.

[10] R. Bai, H.F. Leow. Microfiltration of activated sludge wastewater—the effect of system operation parameters. Separation and Purification Technology, 29 (2002) 189.

[11] F. Wang, V.V. Tarabara. Pore blocking mechanisms during early stages of membrane fouling by colloids. J.Colloid Interface Sci., 328 (2008) 464.

[12] C. Ho, A.L. Zydney. Effect of membrane morphology on the initial rate of protein fouling during microfiltration. J.Membr.Sci., 155 (1999) 261.

[13] C. HO, A.L. Zydney. Theoretical Analysis of the Effect of Membrane Morphology on Fouling during Microfiltration. Sep.Sci.Technol., 34 (1999) 2461.

[14] M. Chandler, A. Zydney. Effects of membrane pore geometry on fouling behavior during yeast cell microfiltration. J.Membr.Sci., 285 (2006) 334.

[15] G. Brans, R.G.M. van der Sman, C.G.P.H. Schroën, A. van der Padt, and R.M. Boom. Optimization of the membrane and pore design for micro-machined membranes. J.Membr.Sci., 278 (2006) 239.

[16] A.D. Levine, G. Tchobanoglous, and T. Asano. Characterization of the Size Distribution of Contaminants in Wastewater: Treatment and Reuse Implications. Journal (Water Pollution Control Federation), 57 (1985) 805.

[17] A.D. Levine, G. Tchobanoglous, and T. Asano. Size distributions of particulate contaminants in wastewater and their impact on treatability. Water Res., 25 (1991) 911.

[18] A.R. Pendashteh, L.C. Abdullah, A. Fakhru’l-Razi, S.S. Madaeni, Z. Zainal Abidin, and D.R. Awang Biak. Evaluation of membrane bioreactor for hypersaline oily wastewater treatment. Process Saf.Environ.Prot., 90 (2012) 45.

[19] A. Salahi, M. Abbasi, and T. Mohammadi. Permeate flux decline during UF of oily wastewater: Experimental and modeling. Desalination, 251 (2010) 153.

[20] I. Chang, C. Chung, and S. Han. Treatment of oily wastewater by ultrafiltration and ozone. Desalination, 133 (2001) 225.

[21] H. Peng, A. Y. Tremblay, and D. E. Veinot. 2005. "The use of Backflushed Coalescing Microfiltration as a Pretreatment for the Ultrafiltration of Bilge Water." Desalination 181 (1-3): 109-120.

[22] W.R. Bowen, J.S. Welfoot. Modelling of membrane nanofiltration—pore size distribution effects. Chemical Engineering Science, 57 (2002) 1393.

[23] S. Singh, K.C. Khulbe, T. Matsuura, and P. Ramamurthy. Membrane characterization by solute transport and atomic force microscopy. J.Membr.Sci., 142 (1998) 111.

[24] G. Belfort, P. Mikulasek, J.M. Pimbley, and K.Y. Chung. Diagnosis of membrane fouling using a rotating annular filter. 2. Dilute particle suspensions of known particle size. J.Membr.Sci., 77 (1993) 23.

[25] A.L. Zydney, P. Aimar, M. Meireles, J.M. Pimbley, and G. Belfort. Use of the log-normal probability density function to analyze membrane pore size distributions: functional forms and discrepancies. J.Membr.Sci., 91 (1994) 293.

[26] B. Dietrich, W. Schabel, M. Kind, and H. Martin. Pressure drop measurements of ceramic sponges—Determining the hydraulic diameter. Chemical Engineering Science, 64 (2009) 3633.

[27] G. Breyiannis, S. Varoutis, and D. Valougeorgis. Rarefied gas flow in concentric annular tube: Estimation of the Poiseuille number and the exact hydraulic diameter. European Journal of Mechanics - B/Fluids, 27 (2008) 609.

[28] A. Jena, K. Gupta. (2003). Liquid extrusion techniques for pore structure evaluation of nonwovens. International Nonwovens Journal, *12*, 45-53.

[29] A.L. Zydney, Chapter 15 - High Performance Ultrafiltration Membranes: Pore Geometry and Charge Effects, in Anonymous , Membrane Science and Technology, Elsevier, pp. 333-352

CHAPTER IV

Discussion

The primary objective of this thesis was to investigate the effect of pore geometry on the performance of synthetic membranes. Performance of the membranes can be defined in different aspects such as rejection behavior or molecular weight cut-off (MWCO), fouling mechanism, rate of flux decline, steady state flux of the membrane, *etc.* The effect of pore geometry as a morphological characteristic of membranes is not investigated to a great extent in the literature. This might be due to the existing difficulties for accurate determination of the effect of pore geometry. Most of the commercial membranes made by conventional preparation methods such as phase inversion, solution casting, thin film stretching, *etc.*, do not have a regular pore shape. There is no method to quantitatively define an irregular pore shape which causes a lack of basis for an accurate comparison.

Furthermore, the performance of the membranes is affected by many operational and design parameters. Operational parameters such as trans-membrane pressure (TMP), temperature and permeate viscosity, and design and morphological parameters such as membrane porosity, asymmetricity, homogeneity, PSD, and pore interconnectivity. In order to be able to determine the effect of one parameter, one should minimize the diversity of other parameters to prevent their effect on membrane flux. In this regard, manipulation of operational parameters is possible; however, designing the morphological factors at the sub-micron level, in a way that eliminates the confliction of their effects, is almost impossible.

Few published articles can be found in the literature concerning the effect of pore shape on membrane performance. These studies were concerned with the situation where particles are physically larger than the pores in the membrane and are completely rejected by the pores. However, Wang and Tarabara [2008] showed that up to 80% of the permeate flux of the membranes is affected by pore constriction which is the result of particle penetration into the pores of the membrane. The penetration and deposition of the particles into the structure of the membranes, referred as internal fouling, causes irreversible decline in membrane flux which is the main factor shortening a membrane's useful life. Therefore, it is required to improve our knowledge about the effect of pore geometry on membrane performance in the case of particle penetration into membrane pores and specifically on the pore constriction by particles. This was the main objective of this thesis.

Due to the difficulties for isolating the effect of pore geometry on membrane performance, it was decided to choose the simulation of pore constriction instead of making membranes with different geometries. Fortunately, due to recent developments in imaging techniques and image processing software, there are enough tools available for such simulations. One of the well-known and commonly used image processing programs is provided by MATLAB, also known as MATLAB image processing toolbox (MIPT).

This toolbox has many useful predefined functions and a high level of flexibility which facilitates the simulation procedure and specific measurement to be done on the image. Another interesting feature of MIPT is that the predefined functions can be coupled with and be used at the same time with any specific external algorithm. Therefore, MIPT was used to simulate maximum particle deposition onto pore walls, representing pore constriction by particles. Two other small programs were also developed for measurement of the cross-sectional area and hydraulic diameter of the clean and constricted pores. In the design of the codes and algorithms, additional effort was used to generate a general program which is able to simulate pore constriction for any regular or irregular pore geometries. Although the program is also applicable to irregular geometries, it was used for simulation of basic geometries in this thesis. An advantage of using the simulation, instead of making membranes, for this study was the fact that we were able to set all the parameters affecting the membrane flux to constant values to eliminate their effect on the flux of the membranes.

Sixteen geometries were considered for the simulation of pore constriction by particles. For each geometry, first the initial cross-sectional area and hydraulic diameter of the geometry were measured and recorded (in pixels). Next, the pore constriction was simulated. Then the cross-sectional area and hydraulic diameter after pore constriction were measured and recorded (in pixels). The next step was calculating the ratios of available area and hydraulic diameter after pore constriction to initial area and hydraulic diameter (α and β). Therefore, α

and β are dimensionless and can be used for further calculation of area and hydraulic diameter of a constricted pore (with a specific shape).

Previous studies to date, concerning the shrinkage in pore diameter and cross-sectional area of circular pores considered a thin uniform adsorbed layer within the pore reducing its diameter and area. In this work, a fine microscopic model gives particles a spherical shape that creates a convoluted outline within the pore. This outline is taken into account in modeling the reduced area and hydraulic diameter of the pore for different pore geometries.

The simulation of pore constriction by particles showed that for small particles compared to pore hydraulic diameter ($\lambda < 0.2$) there is no significant difference in the results of α and β for different geometries. This is believed to be due to the effect of thin layer of particles for the range of $\lambda < 0.2$. The result of pore constriction for the mentioned range of λ is a thin layer of particles covering the interior perimeter of the pores. This layer does not change the overall characteristic of the geometries and thus the amount of area lost by deposition of these particles, will be the same for different geometries, resulting in the same values of α and β vs. λ for $\lambda < 0.2$.

The effect of different pore geometries was seen for $\lambda > 0.2$. Rectangular pores showed two minimums for α and β vs. λ. The first minimum corresponds to the particle where the whole surface of the rectangular pore being covered by two rows of particles along the pore length. The second minimum corresponds to the situation where the pore is totally covered by one row of particles. These are the most undesirable situations for rectangular pores since there is no space left in the pore for the flow of the permeate or the back-flushing flow (α and $\beta \rightarrow 0$).

Triangular pores showed one minimum of α and β vs. λ for $\lambda \approx 0.35$. Unlike rectangular geometries, the available area and hydraulic diameter for triangular pores never reaches zero, meaning that there is always a certain amount of area available for permeate or back-flushing flow. The minimum value of α for triangular geometries was 0.3. Triangular pores showed the maximum amount of available area after constriction by particle, between the basic geometries having the same pore aspect ratio (PAR), for most of the studied values of λ. This suggests a facilitated particle release by back-flushing since there is always a certain amount of area available for back-flushing flow in the cross-section of the pore after constriction by the particle. This is in agreement with the facilitated release of the particles for triangular pores, when the particles are trapped on the entrance of the pores, shown by Brans *et al.* [2006].

Oval pores showed results in between rectangular and triangular. The values of α and β vs. λ never reached zero for oval shapes; however, the minimum value of α for these geometries was less than minimum α for triangular. The minimum α for oval pores was around 0.2. Results for circular pore were not following the same pattern as the ovals. For circular pores, there are two major minimums of α and β vs. λ at $\lambda \approx 0.4$ and 1. The latter refers to the situation where the whole surface of the pore is covered by one particle, which is the worst case for pore cleaning by back-flushing.

Results of α and β vs. λ showed that different geometries reject particles at different values of λ. It means that for a given pore size (hydraulic diameter) some geometries are able to reject smaller particles. The fact that pore hydraulic diameter is the same value resulted by bubble point porometry, which is extensively used in membrane pore size characterization, makes these results more useful. These results can be used for designing membranes for specific applications where a high level of separation is required.

Rectangular and oval pores showed to be able to reject the particles larger than their hydraulic diameter. This ability was improved by elongating these pore shapes. In other words, comparing two rectangular pores with PAR of 7 and 15 shows that for a constant pore hydraulic diameter, rectangular pores with PAR of 15 are able to reject larger particles that rectangular pores with PAR of 7. Circular and triangular pores start rejecting the particles with the same size as their hydraulic diameter. For triangular pores, the rejection behavior did not change by changing the PAR. Star shaped pore however showed to be constricted even by particle larger than its hydraulic diameter. For a star shaped pore, rejection of particles started at $\lambda \approx 1.24$. These results suggest that for separation processes for which a high level of separation is required, rectangular pores are recommended as they showed superior rejection compared to other geometries. Superior performance of rectangular pores in the case where particles are physically rejected by the pores was also shown by Chandler and Zydney [2006].

The combined effect of different rejection and constriction behavior of pores with different geometries was investigated in the 2nd paper (chapter III) for the membranes following the same pore size distribution (PSD). It was shown that the flux of the membranes can be divided to two portions. One is the contribution of pores that physically reject the particles, and the other is the contribution of pores that are constricted by particles. By changing the PSD, it was shown that the comparative values of these contributions for a given membrane will change due to the change in the position of $D_{H,LRP}$ in the PSD. This can affect preference of a membrane with a specific pore shape over another shape. However, for all different PSDs, the contribution of constricted pores to membrane flux was the highest for membranes having triangular shapes. This suggests that for processes for which the penetration of particles into the membrane pores is most likely to happen, triangular shaped pores are recommended. An example of such processes can be MF pretreatment of the feed streams with a range of particle sizes such as wastewater streams.

References

Brans, G., R. G. M. van der Sman, C. G. P. H. Schroën, A. van der Padt, and R. M. Boom. 2006. "Optimization of the Membrane and Pore Design for Micro-Machined Membranes." *Journal of Membrane Science* 278 (1–2): 239-250.

Chandler, Martin and Andrew Zydney. 2006. "Effects of Membrane Pore Geometry on Fouling Behavior during Yeast Cell Microfiltration." *Journal of Membrane Science* 285 (1–2): 334-342.

Wang, Fulin and Volodymyr V. Tarabara. 2008. "Pore Blocking Mechanisms during Early Stages of Membrane Fouling by Colloids." *Journal of Colloid and Interface Science* 328 (2): 464-469.

CHAPTER V

Conclusion

Pore constriction by spherical particles was simulated using MATLAB image processing toolbox. In the simulation, pore constriction was approximated with maximum particle deposition onto pore walls. The simulation of pore constriction was carried out for 16 different basic geometries with different pore aspect ratios (PAR). The studies pore geometries are rectangular, triangular and oval at PARs of 3, 7, 15 and 30, circle, star, cross and rounded ends rectangle. The values of α and β were measured, following the simulation for different values of λ (ratio of particle diameter to clean pore hydraulic diameter). These values (α and β) followed the same pattern vs. λ, with slight difference, for a given pore geometry.

The values of α were plotted against λ for different geometries. For λ<0.2, where particles are small compared to pore hydraulic diameter, it was observed that different geometries exhibited the same values of α vs. λ. Therefore, it was concluded that for λ<0.2 pore geometry does not have any significant effect on the amount of pore area lost due to pore constriction. The effect of different pore geometries was observed for λ>0.2.

For rectangular pores the value of α reaches zero at two locations of λ. first case corresponding to λ for which the particle diameter equals the pore width. In this case row of the constricting particles covers the whole cross-sectional area of the pore. The second case corresponds to λ where particle diameter equals to half the pore width in which the whole cross-sectional area of the pore is covered by two rows of constricting particles. For circular pores this situation happens when the particle is the same size as pore diameter. Complete coverage of the pore surface by the particles is the worst case for pore cleaning by back-flushing since there is no space available for back-flushing fluid to flow and exert the required external force on the particles to dislodge them. However, for oval, triangular, star and cross shape pores, the value of α never drops to zero for any λ. This suggests a facilitated particle release by back-flushing for these pore shapes.

The minimum α for triangular pores was around 0.3, and for ovals was around 0.2. The effect of PAR on α at a constant λ was investigated for three groups of geometries. For rectangular pores, increasing the PAR causes a decrease in α for a constant λ. However, for triangular and oval pores, by increasing the PAR, the value of α increases for a given λ.

Comparative results of α and β for different geometries were different for different values of λ. Comparing basic geometries (rectangular, triangular, oval and circular) at aspect ratio of 7 shows that for a few values of λ, rectangular pores provide the highest α and β but for most of the values of λ triangular and circular pores offer the highest α and β.

Sixteen model membranes with pore size of $0.1\mu m$ and having similar initial flux were considered to compare the flux of the membranes having different pore shapes after pore constriction by particles. The fluxes of these membranes, after pore constriction were calculated using the values of α and β vs. λ for different geometries at five different λ. For low values of λ (small particles compared to membrane pores), membranes showed almost the same values of flux. However, for intermediate particle sizes (intermediate values of λ), membranes having triangular and star shaped pores showed the highest flux. The flux of membranes with triangular pores was increased by increasing the aspect ratio of the pores. Membranes having rectangular pores showed the least values of flux after pore constriction. The flux of these membranes was decreased by increasing the aspect ratio of the pores.

It was observed that different pore geometries physically rejected the particles at different values of λ. To investigate the combined effect of pore geometry on particle rejection and pore constriction, thirteen model membranes having different pore geometries and distribution of pore sizes were considered. These include rectangular, triangular and oval pores, at different PARs, and circular pores. Six different log-normal pore size distributions (PSD) were considered and the fluxes of different membranes after pore constriction were calculated and compared at each PSD. The clean flux of all different membranes was the same for a given PSD.

It was observed that pores of identical hydraulic diameter but different geometries exhibited different rejections. Rectangular pores reject larger particles than oval pores while both geometries can reject particles larger than their hydraulic diameter. This ability was improved by increasing the PAR. Triangular and circular geometries, regardless of PAR, all reject the particles with the same size as their hydraulic diameter.

In the range of pore sizes available in the membrane, some pores are physically smaller than particles (called as rejecting pores) which are responsible for particle rejection. The rest of the pores are physically larger than particles and are constricted by them. These pores are called constricted pores. Due to the difference in particle rejection for different geometries, the largest rejecting pore ($D_{H,LRP}$), in the pore size range of a membrane, is different for membranes having different geometries. The total number of pores in the membranes that physically reject the particles will also be different following the distribution of pore sizes. The number of rejecting pores for a membrane having rectangular pores is the highest compared to other geometries at a given PAR.

Based on the location of $D_{H,LRP}$ in the pore size distribution, the whole range of pore sizes in the membrane can be split into two parts. One portion includes the rejecting pores for which $D_H < D_{H,LRP}$ and the other includes the constricted pores for which $D_{H,} > D_{H,LRP}$. Therefore, the overall flux of the membrane after pore constriction can be divided to two parts. One is the contribution of rejecting pores to flux and the other is the contribution of constricted pores to flux. It was observed that, at a constant PSD, the contribution of rejecting pores to flux was the highest for membranes with rectangular pores while the contribution of constricted pores to flux was the highest for triangular pores. Increasing the PAR had different effects on the contribution of constricted pores to flux for different membranes. For membranes having triangular and oval pores, increasing the PAR increases the contribution of constricted pores to membranes flux. However, for membranes with rectangular pore geometries, it decreases the contribution of constricted pores to membrane flux.

Calculation of the flux of the membranes after pore constriction, for membranes with a distribution of pore sizes, showed that the comparative values of the flux of the membranes with different geometries are affected by three parameters. These are the rejection behavior ($D_{H,LRP}$), the constriction behavior and the shape of PSD. Based on the results of this thesis, generally, for separation processes for which a high level of separation is required, rectangular pores are recommended as they showed superior rejection compared to other geometries. On the other hand, for processes for which the penetration of particles into the membrane pores is most likely to happen, triangular and star shaped pores are recommended as they showed larger amount of available area for flow after being constricted by particles. An example of such processes can be pretreatment of feed streams with a range of particle sizes such as wastewater streams.

CHAPTERVI

Recommendations for Further work

Based on the results of this thesis the following steps are recommended for further investigation of the effect of pore geometry on membrane performance:

1. Using recently developed membrane preparation techniques (such as micro-machined membrane manufacturing) to create membranes with triangular geometries for experimental investigation of the effect of this pore geometry on membrane performance.
2. Investigating the effect of pore geometry on other types of fouling (complete pore blocking, intermediate pore blocking and cake filtration) and combining the result with the results of this thesis to determine the best geometry to meet the requirements of a specific process.
3. Extend this work to irregularly shaped pores defined by a shape factor (SH) or angularity factor (AF) and determine if any predictable performance is obtainable for these factors. This will provide the basis for comparing different irregular pore geometries found in commercial membranes.

APPENDIX A

General applicability of pore characterization and constricted pore geometries using the MATLAB Image Processing Toolbox (MIPT)

Imaging techniques and image processing approaches have been used in the characterization of synthetic membranes. Pore size, pore size distribution, porosity, pore shape, *etc.* can all be measured and characterized using these techniques. SEM micrographs of the surface of the membranes are used as the basic image for the calculations. In MIPT each image is defined by a matrix containing information on pixel location, intensity and color. A basic example can be a binary image. For a binary image the constituting pixels can be either white or black. The matrix representing this binary image consists of elements equal to 0 or 1, representing black or white pixels respectively. The size of the matrix is the same as the image size. For example a binary image of 800 x 600 (horizontal x vertical) pixels, will result in a one dimensional matrix with 800 columns and 600 rows. For a grayscale image the representing matrix will be a one dimensional matrix while the value of the elements shows the intensity of black or white. An RGB image (colorful) can be represented as a 3 dimensional matrix (red, green and blue) where the values of elements in each dimension show the intensity of the color corresponding to that specific dimension. Therefore, by converting an image to a matrix, the location of all the pixels forming the whole image is known and can be used for required calculations. The designed codes represented in appendix B uses the location of the pixels and some predefined functions provided by MIPT, along with a specific geometrical algorithm to simulate the maximum particle deposition onto pore walls. The program was used to model pore constriction of the basic pore geometries in this thesis and is applicable to any irregularly shaped pore geometry.

Predefined functions in MIPT

MIPT offers a wide range of predefined functions for image processing. Some of these functions are used in this research for measurement of pore characteristics such as pore cross-sectional area and wetted perimeter which are used to calculate the hydraulic diameter of the pores.

In this case, SEM (scanning electron microscopy) or TEM (transmission electron microscopy) micrographs can be used for processing. These images are usually in grayscale. Membrane pores are usually darker and the bulk of the membrane is brighter. Figure 1, shows a TEM micrograph of an ultrathin section of Vycor 7980 silica glass of average pore size of 7 nm (Levits et al., 1991). By using a predefined function, we can convert a grayscale image to a binary image where the pores are all black and the bulk of the membrane is white (Figures 1 and 2). Using predefined functions in MIPT for object tracking, we are able to isolate a desired pore for further measurement of its desired characteristics.

Figure A-1. TEM micrograph of the surface of a vycore glass membrane (grayscale)

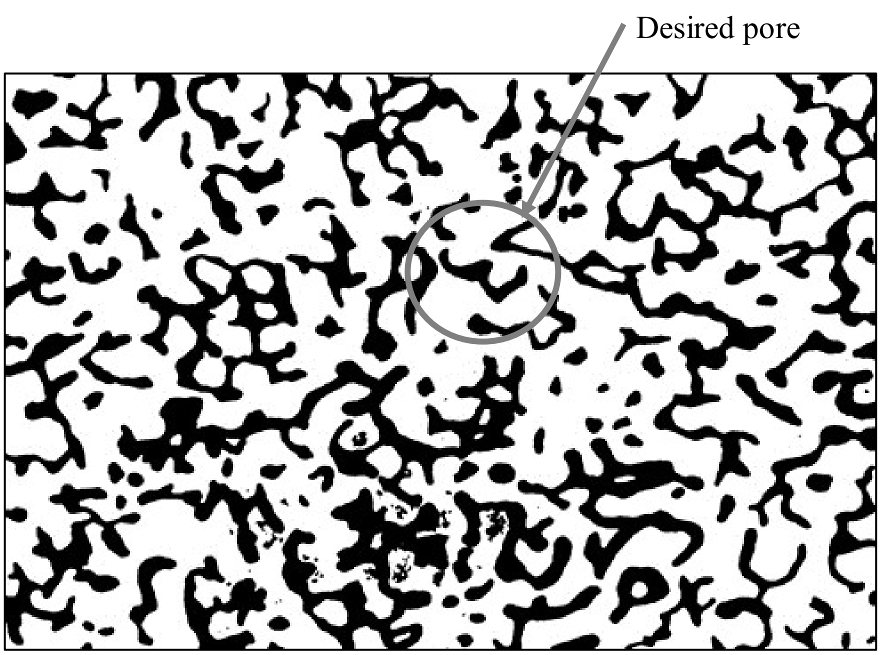

Figure A-2. Binary image of the surface of a vycore glass membrane showing the desired pore

Figure 3, shows a binary image of the isolated pore. In the matrix representing this image, the number of elements equaling 0, is actually the cross sectional area of the pore. The number of element of a specific value can be calculated using a simple code in MATLAB (APPENDIX B).

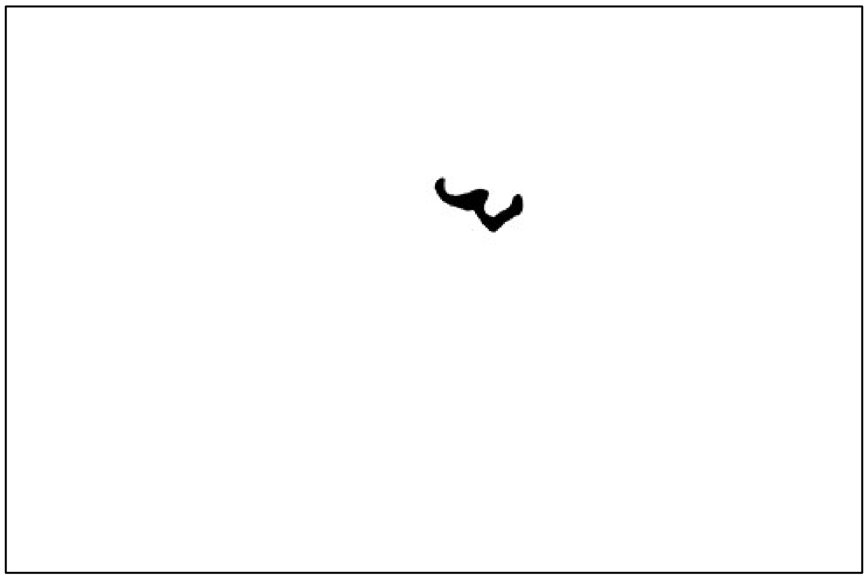

Figure A-3. Binary image of the isolated pore

MIPT also provides a series of predefined functions for edge detection. Figure 4.a) shows the binary image of the edges of all the pores in the micrograph. Figure 4.b) shows the edges of the desired pore. In the matrix representing this image, the number of elements equaling 0, is essentially the wetted perimeter of the desired pore.

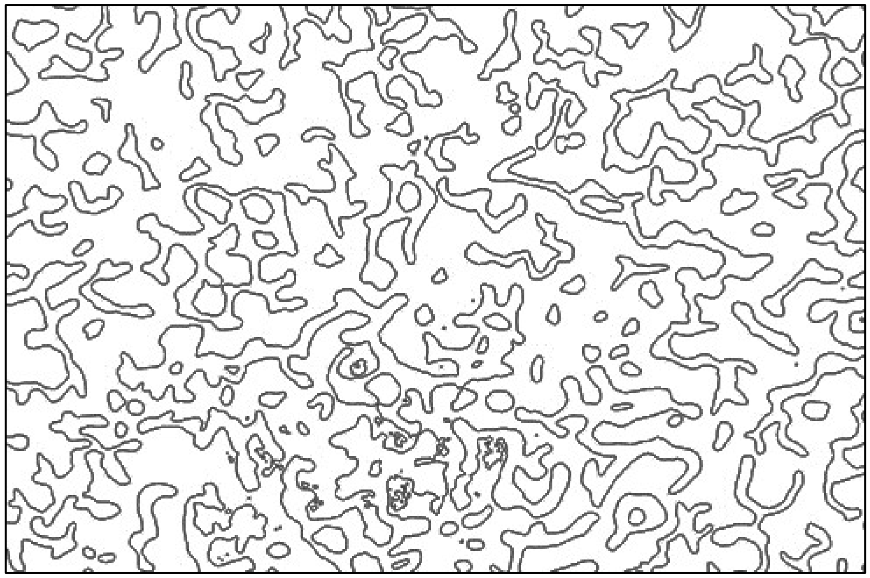

Figure A-4.a. Binary image of the edges of all the pores

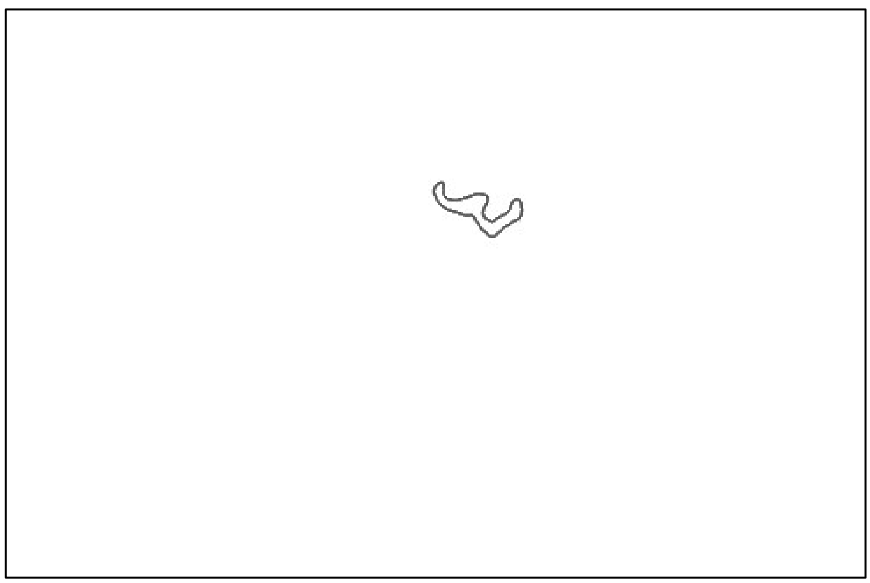

Figure A-4.b. Binary image of the edges of the desired pore

References

Levitz, P., G. Ehret, S. K. Sinha, and J. M. Drake. 1991. "Porous Vycor Glass: The Microstructure as Probed by Electron Microscopy, Direct Energy Transfer, Small-Angle Scattering, and Molecular Adsorption." *The Journal of Chemical Physics* 95 (8): 6151-6161.

APPENDIX B

Simulation and measurement codes

Measurement of area and Perimeter of clean pore

The following code was developed and can be debugged in MATLAB.

```
function clean_area_primeter

%initial parameters
defaultarea = 1;
defaultdiam = 1;

%reading the image
I = imread('triangle 151.jpg');
Isize = size(size(I));

if Isize(1,2)~=2
    I = rgb2gray(I);
end;

Ibin = im2bw(I,0.5);

Isize = size(Ibin);

for i = 1:Isize(1)
    for j = 1:Isize(2)
        if Ibin(i,j)==1
            Ibin(i,j) = 0;
        else
            Ibin(i,j) = 1;
        end
    end
end
Ibinsel = Ibin;

[Ibinsel,idx] = bwselect(Ibin,4);
Iseledge = edge(Ibinsel,'canny');
[J,I] = find(Iseledge);

perimeter = size(J,1);
%disp('the wetted perimeter is:');
%disp(perimeter);

%finding the area of the selected pore
porearea = 0;
for i = 1:size(Ibinsel,1)
    for j = 1:size(Ibinsel,2)
        if Ibinsel(i,j) ==1
            porearea = porearea + 1;
        end
    end
end

disp('the pore area ratio is:');
disp(porearea);

%calculating hydrolic diameter
hydrodiameter = 4*porearea/perimeter;
disp('the hydrolic diameter ratio is:');
disp(hydrodiameter);
imshow(Ibinsel);
```

Maximum particle deposition onto pore wall

The following code was developed and can be debugged in MATLAB.

```
function mono_layer

DH = 2.5916e+003;          %pore hydraulic diameter, input
ratio =  0.1;              %ratio of particle diameter to DH, input
counterlimit = 88 ;        %number of particles desired to deposite

% by a few trial and error the monolayer deposition of particles
% can be acheived

dp = round(ratio*DH);
r = round(dp/2);           %radius of particle

stuckat1st = 0;


% Read the desired image of membrane surface from directory
% in this case, "ellipse71.jpg" is the file's name in directory
I = imread('ellipse71.jpg');
Isize = size(size(I));


% Converting the image to grayscale
if Isize(1,2)~=2
    I = rgb2gray(I);
end;


% Converting the image to binary
Ibin = im2bw(I,0.5);

Isize = size(Ibin);
for i = 1:Isize(1)
    for j = 1:Isize(2)
        if Ibin(i,j)==1
            Ibin(i,j) = 0;
        else
            Ibin(i,j) = 1;
        end
    end
end


% Selecting the desired pore in the image
[Ibinsel,idx] = bwselect(Ibin,4);
Iseledge = edge(Ibinsel,'canny'); % Detects the edges of the selected pore
[J,I] = find(Iseledge);


%initial values of the calculation parameters
coordx = zeros(3,1);
coordy = zeros(3,1);
m = 1;

% Section 1: Placing the 1st particle
for i = (r+2):size(Ibinsel,2)-r-2
    for j = size(Ibinsel,1)-r-2:-1:(r+2)
        cond = 1;
```

```
        if  Ibinsel(j+r-1,i)==1  &  Ibinsel(j-r+1,i)==1  &  Ibinsel(j,i-r+1)==1  &
Ibinsel(j,i+r-1)==1
        for jj = (j - r):(j + r)
        for ii = (i-round(sqrt((r)^2 - (jj - j)^2))):(i + round(sqrt((r)^2 - (jj -
j)^2)))
            if Ibinsel(jj,ii)==0
                cond=0;
                break
            end
        end
        if cond==0
            break
        end
        end
        else
            cond=0;
        end
        if cond == 1
            %the command inside "if" is used for drawing the circles
            %and is used numerous times in the whole code
            Ibinsel(j,i) = 0;
            xc = j;
            yc = i;
            radius = r;
            value = 0;

            x = 0;
            y = radius;
            d = 1 - radius;

            Ibinsel(xc, yc+y) = value;
            Ibinsel(xc, yc-y) = value;
            Ibinsel(xc+y, yc) = value;
            Ibinsel(xc-y, yc) = value;

            while ( x < y - 1 )
                x = x + 1;
                if ( d < 0 )
                    d = d + x + x + 1;
                else
                    y = y - 1;
                    a = x - y + 1;
                    d = d + a + a;
                end
            Ibinsel( x+xc,  y+yc) = value;
            Ibinsel( y+xc,  x+yc) = value;
            Ibinsel( y+xc, -x+yc) = value;
            Ibinsel( x+xc, -y+yc) = value;
            Ibinsel(-x+xc, -y+yc) = value;
            Ibinsel(-y+xc, -x+yc) = value;
            Ibinsel(-y+xc,  x+yc) = value;
            Ibinsel(-x+xc,  y+yc) = value;
            end
            counter = 1;  %shows the number of drawn particles
            break

        end

    end
    if cond == 1
        break
    end
```

```
end

%after this section, if "counter" equals zero, it means that particle
%deposition into pore is impossible and the pore is rejecting
%this particle size


%section 2: placing the rest of circles
%if there is at least one particle drawn before, it tries to draw another


Xcenters = zeros(100,1);
Ycenters = zeros(100,1);
revfrom  = zeros(100,1);
revto    = zeros(100,1);
Xcenters(1,1) = yc;
lastx = yc;
lasty = xc;
Ycenters(1,1) = xc;
condition = 3;
xcapp = yc - round((dp+1)*cos(pi/4));
ycapp = xc + round((dp+1)*sin(pi/4));
i = 1;
j = 0;
reverse = 0;
finishit = 0;
m = 1;
finishit = 0;
counter = 1;


while counter < counterlimit



%this part gets xcapp and ycapp from the last part and either draws or
%finishes without drawing
% changing xcapp and ycapp

%1st condition
if condition==1
    nxtcircle = 0;
    %1st quarter
    while (xcapp > lastx-round((dp+1)*cos(pi/4)) ) & (nxtcircle==0)
        xcapp = xcapp - 1;
        ycapp = lasty - round(sqrt((dp+1)^2-(xcapp-lastx)^2));
        cond = 1;
        for jj = (ycapp - r+1):(ycapp + r-1)
        for  ii  =  (xcapp-round(sqrt((r-1)^2  -  (jj  -  ycapp)^2))):(xcapp  +
round(sqrt((r-1)^2 - (jj - ycapp)^2)))
            if Ibinsel(jj,ii)==0
                cond=0;
                break
            end
        end
        if cond==0
            break
        end
        end
        if cond == 1
            Ibinsel(ycapp,xcapp) = 0;
            xc = ycapp;
yc = xcapp;
```

```
radius = r;
value = 0;

x = 0;
y = radius;
d = 1 - radius;

Ibinsel(xc, yc+y) = value;
Ibinsel(xc, yc-y) = value;
Ibinsel(xc+y, yc) = value;
Ibinsel(xc-y, yc) = value;

while ( x < y - 1 )
    x = x + 1;
    if ( d < 0 )
        d = d + x + x + 1;
    else
        y = y - 1;
        a = x - y + 1;
        d = d + a + a;
    end
    Ibinsel( x+xc,  y+yc) = value;
    Ibinsel( y+xc,  x+yc) = value;
    Ibinsel( y+xc, -x+yc) = value;
    Ibinsel( x+xc, -y+yc) = value;
    Ibinsel(-x+xc, -y+yc) = value;
    Ibinsel(-y+xc, -x+yc) = value;
    Ibinsel(-y+xc,  x+yc) = value;
    Ibinsel(-x+xc,  y+yc) = value;
end
counter = counter + 1;
nxtcircle = 1;
        end
    end

    %2nd quarter
    while (ycapp < lasty + round((dp+1)*sin(pi/4))) & (nxtcircle==0)
        ycapp = ycapp + 1;
        xcapp = lastx - round(sqrt((dp+1)^2-(ycapp-lasty)^2));
        cond = 1;
        for jj = (ycapp - r+1):(ycapp + r-1)
        for  ii  =  (xcapp-round(sqrt((r-1)^2  -  (jj  -  ycapp)^2))):(xcapp  +
round(sqrt((r-1)^2 - (jj - ycapp)^2)))
            if Ibinsel(jj,ii)==0
                cond=0;
                break
            end
        end
        if cond==0
            break
        end
        end
        if cond == 1
            Ibinsel(ycapp,xcapp) = 0;
            xc = ycapp;
yc = xcapp;
radius = r;
value = 0;

x = 0;
y = radius;
d = 1 - radius;
```

```
Ibinsel(xc, yc+y) = value;
Ibinsel(xc, yc-y) = value;
Ibinsel(xc+y, yc) = value;
Ibinsel(xc-y, yc) = value;

while ( x < y - 1 )
    x = x + 1;
    if ( d < 0 )
        d = d + x + x + 1;
    else
        y = y - 1;
        a = x - y + 1;
        d = d + a + a;
    end
    Ibinsel( x+xc,  y+yc) = value;
    Ibinsel( y+xc,  x+yc) = value;
    Ibinsel( y+xc, -x+yc) = value;
    Ibinsel( x+xc, -y+yc) = value;
    Ibinsel(-x+xc, -y+yc) = value;
    Ibinsel(-y+xc, -x+yc) = value;
    Ibinsel(-y+xc,  x+yc) = value;
    Ibinsel(-x+xc,  y+yc) = value;
end
counter = counter + 1;
nxtcircle = 1;
        end
    end

    %3rd quarter
    while (xcapp < lastx + round((dp+1)*cos(pi/4))) & (nxtcircle==0)
        xcapp = xcapp + 1;
        ycapp = lasty + round(sqrt((dp+1)^2-(xcapp-lastx)^2));
        cond = 1;
        for jj = (ycapp - r+1):(ycapp + r-1)
        for  ii  =  (xcapp-round(sqrt((r-1)^2  -  (jj  -  ycapp)^2))):(xcapp  +
round(sqrt((r-1)^2 - (jj - ycapp)^2)))
            if Ibinsel(jj,ii)==0
                cond=0;
                break
            end
        end
        if cond==0
            break
        end
        end
        if cond == 1
            Ibinsel(ycapp,xcapp) = 0;
            xc = ycapp;
yc = xcapp;
radius = r;
value = 0;

x = 0;
y = radius;
d = 1 - radius;

Ibinsel(xc, yc+y) = value;
Ibinsel(xc, yc-y) = value;
Ibinsel(xc+y, yc) = value;
Ibinsel(xc-y, yc) = value;

while ( x < y - 1 )
    x = x + 1;
```

```
    if ( d < 0 )
        d = d + x + x + 1;
    else
        y = y - 1;
        a = x - y + 1;
        d = d + a + a;
    end
    Ibinsel( x+xc,  y+yc) = value;
    Ibinsel( y+xc,  x+yc) = value;
    Ibinsel( y+xc, -x+yc) = value;
    Ibinsel( x+xc, -y+yc) = value;
    Ibinsel(-x+xc, -y+yc) = value;
    Ibinsel(-y+xc, -x+yc) = value;
    Ibinsel(-y+xc,  x+yc) = value;
    Ibinsel(-x+xc,  y+yc) = value;
end
counter = counter + 1;
nxtcircle = 1;
        end
    end

        %4th quarter
        while (ycapp > lasty - round((dp+1)*sin(pi/4))) & (nxtcircle==0)
            ycapp = ycapp - 1;
            xcapp = lastx + round(sqrt((dp+1)^2-(ycapp-lasty)^2));
        cond = 1;
        for jj = (ycapp - r+1):(ycapp + r-1)
        for  ii  =  (xcapp-round(sqrt((r-1)^2  -  (jj  -  ycapp)^2))):(xcapp  +
round(sqrt((r-1)^2 - (jj - ycapp)^2)))
            if Ibinsel(jj,ii)==0
                cond=0;
                break
            end
        end
        if cond==0
            break
        end
        end
        if cond == 1
            Ibinsel(ycapp,xcapp) = 0;
            xc = ycapp;
yc = xcapp;
radius = r;
value = 0;

x = 0;
y = radius;
d = 1 - radius;

Ibinsel(xc, yc+y) = value;
Ibinsel(xc, yc-y) = value;
Ibinsel(xc+y, yc) = value;
Ibinsel(xc-y, yc) = value;

while ( x < y - 1 )
    x = x + 1;
    if ( d < 0 )
        d = d + x + x + 1;
    else
        y = y - 1;
        a = x - y + 1;
        d = d + a + a;
    end
```

```
    Ibinsel( x+xc,  y+yc) = value;
    Ibinsel( y+xc,  x+yc) = value;
    Ibinsel( y+xc, -x+yc) = value;
    Ibinsel( x+xc, -y+yc) = value;
    Ibinsel(-x+xc, -y+yc) = value;
    Ibinsel(-y+xc, -x+yc) = value;
    Ibinsel(-y+xc,  x+yc) = value;
    Ibinsel(-x+xc,  y+yc) = value;
end
counter = counter + 1;
nxtcircle = 1;
        end
        end
end




%2nd condition
if condition==2
    nxtcircle = 0;
    %1st quarter
    while (ycapp < lasty + round((dp+1)*sin(pi/4))) & (nxtcircle==0)
        ycapp = ycapp + 1;
        xcapp = lastx - round(sqrt((dp+1)^2-(ycapp-lasty)^2));
        cond = 1;
        for jj = (ycapp - r+1):(ycapp + r-1)
        for  ii  =  (xcapp-round(sqrt((r-1)^2  -  (jj  -  ycapp)^2))):(xcapp  +
round(sqrt((r-1)^2 - (jj - ycapp)^2)))
            if Ibinsel(jj,ii)==0
                cond=0;
                break
            end
        end
        if cond==0
            break
        end
        end
        if cond == 1
            Ibinsel(ycapp,xcapp) = 0;
            xc = ycapp;
yc = xcapp;
radius = r;
value = 0;

x = 0;
y = radius;
d = 1 - radius;

Ibinsel(xc, yc+y) = value;
Ibinsel(xc, yc-y) = value;
Ibinsel(xc+y, yc) = value;
Ibinsel(xc-y, yc) = value;

while ( x < y - 1 )
    x = x + 1;
    if ( d < 0 )
        d = d + x + x + 1;
    else
        y = y - 1;
        a = x - y + 1;
        d = d + a + a;
    end
```

```
    Ibinsel( x+xc,  y+yc) = value;
    Ibinsel( y+xc,  x+yc) = value;
    Ibinsel( y+xc, -x+yc) = value;
    Ibinsel( x+xc, -y+yc) = value;
    Ibinsel(-x+xc, -y+yc) = value;
    Ibinsel(-y+xc, -x+yc) = value;
    Ibinsel(-y+xc,  x+yc) = value;
    Ibinsel(-x+xc,  y+yc) = value;
end
counter = counter + 1;
nxtcircle = 1;
        end
    end

    %2nd quarter
    while (xcapp < lastx + round((dp+1)*cos(pi/4))) & (nxtcircle==0)
        xcapp = xcapp + 1;
        ycapp = lasty + round(sqrt((dp+1)^2-(xcapp-lastx)^2));
        cond = 1;
        for jj = (ycapp - r+1):(ycapp + r-1)
        for  ii  =  (xcapp-round(sqrt((r-1)^2  -  (jj  -  ycapp)^2))):(xcapp  +
round(sqrt((r-1)^2 - (jj - ycapp)^2)))
            if Ibinsel(jj,ii)==0
                cond=0;
                break
            end
        end
        if cond==0
            break
        end
        end
        if cond == 1
            Ibinsel(ycapp,xcapp) = 0;
            xc = ycapp;
yc = xcapp;
radius = r;
value = 0;

x = 0;
y = radius;
d = 1 - radius;

Ibinsel(xc, yc+y) = value;
Ibinsel(xc, yc-y) = value;
Ibinsel(xc+y, yc) = value;
Ibinsel(xc-y, yc) = value;

while ( x < y - 1 )
    x = x + 1;
    if ( d < 0 )
        d = d + x + x + 1;
    else
        y = y - 1;
        a = x - y + 1;
        d = d + a + a;
    end
    Ibinsel( x+xc,  y+yc) = value;
    Ibinsel( y+xc,  x+yc) = value;
    Ibinsel( y+xc, -x+yc) = value;
    Ibinsel( x+xc, -y+yc) = value;
    Ibinsel(-x+xc, -y+yc) = value;
    Ibinsel(-y+xc, -x+yc) = value;
    Ibinsel(-y+xc,  x+yc) = value;
```

```
    Ibinsel(-x+xc,  y+yc) = value;
end
counter = counter + 1;
nxtcircle = 1;
        end
    end

        %3rd quarter
        while (ycapp > lasty - round((dp+1)*sin(pi/4))) & (nxtcircle==0)
            ycapp = ycapp - 1;
            xcapp = lastx + round(sqrt((dp+1)^2-(ycapp-lasty)^2));
        cond = 1;
        for jj = (ycapp - r+1):(ycapp + r-1)
        for  ii  =  (xcapp-round(sqrt((r-1)^2  -  (jj  -  ycapp)^2))):(xcapp  +
round(sqrt((r-1)^2 - (jj - ycapp)^2)))
            if Ibinsel(jj,ii)==0
                cond=0;
                break
            end
        end
        if cond==0
            break
        end
        end
        if cond == 1
            Ibinsel(ycapp,xcapp) = 0;
            xc = ycapp;
yc = xcapp;
radius = r;
value = 0;

x = 0;
y = radius;
d = 1 - radius;

Ibinsel(xc, yc+y) = value;
Ibinsel(xc, yc-y) = value;
Ibinsel(xc+y, yc) = value;
Ibinsel(xc-y, yc) = value;

while ( x < y - 1 )
    x = x + 1;
    if ( d < 0 )
        d = d + x + x + 1;
    else
        y = y - 1;
        a = x - y + 1;
        d = d + a + a;
    end
    Ibinsel( x+xc,  y+yc) = value;
    Ibinsel( y+xc,  x+yc) = value;
    Ibinsel( y+xc, -x+yc) = value;
    Ibinsel( x+xc, -y+yc) = value;
    Ibinsel(-x+xc, -y+yc) = value;
    Ibinsel(-y+xc, -x+yc) = value;
    Ibinsel(-y+xc,  x+yc) = value;
    Ibinsel(-x+xc,  y+yc) = value;
end
counter = counter + 1;
nxtcircle = 1;
        end
        end
```

```
        %4rth quarter
        while (xcapp > lastx-round((dp+1)*cos(pi/4)) ) & (nxtcircle==0)
        xcapp = xcapp - 1;
        ycapp = lasty - round(sqrt((dp+1)^2-(xcapp-lastx)^2));
        cond = 1;
        for jj = (ycapp - r+1):(ycapp + r-1)
        for   ii   =   (xcapp-round(sqrt((r-1)^2   -   (jj   -   ycapp)^2))):(xcapp   +
round(sqrt((r-1)^2 - (jj - ycapp)^2)))
            if Ibinsel(jj,ii)==0
                cond=0;
                break
            end
        end
        if cond==0
            break
        end
        end
        if cond == 1
            Ibinsel(ycapp,xcapp) = 0;
            xc = ycapp;
yc = xcapp;
radius = r;
value = 0;

x = 0;
y = radius;
d = 1 - radius;

Ibinsel(xc, yc+y) = value;
Ibinsel(xc, yc-y) = value;
Ibinsel(xc+y, yc) = value;
Ibinsel(xc-y, yc) = value;

while ( x < y - 1 )
    x = x + 1;
    if ( d < 0 )
        d = d + x + x + 1;
    else
        y = y - 1;
        a = x - y + 1;
        d = d + a + a;
    end
    Ibinsel( x+xc,  y+yc) = value;
    Ibinsel( y+xc,  x+yc) = value;
    Ibinsel( y+xc, -x+yc) = value;
    Ibinsel( x+xc, -y+yc) = value;
    Ibinsel(-x+xc, -y+yc) = value;
    Ibinsel(-y+xc, -x+yc) = value;
    Ibinsel(-y+xc,  x+yc) = value;
    Ibinsel(-x+xc,  y+yc) = value;
end
counter = counter + 1;
nxtcircle = 1;
        end
    end
end




%3rd condition
if condition==3
```

```
    nxtcircle = 0;
    %1st quarter
    while (xcapp < lastx + round((dp+1)*cos(pi/4))) & (nxtcircle==0)
        xcapp = xcapp + 1;
        ycapp = lasty + round(sqrt((dp+1)^2-(xcapp-lastx)^2));
        cond = 1;
        for jj = (ycapp - r+1):(ycapp + r-1)
        for ii = (xcapp-round(sqrt((r-1)^2 - (jj - ycapp)^2))):(xcapp + round(sqrt((r-1)^2 - (jj - ycapp)^2)))
            if Ibinsel(jj,ii)==0
                cond=0;
                break
            end
        end
        if cond==0
            break
        end
        end
        if cond == 1
            Ibinsel(ycapp,xcapp) = 0;
            xc = ycapp;
yc = xcapp;
radius = r;
value = 0;

x = 0;
y = radius;
d = 1 - radius;

Ibinsel(xc, yc+y) = value;
Ibinsel(xc, yc-y) = value;
Ibinsel(xc+y, yc) = value;
Ibinsel(xc-y, yc) = value;

while ( x < y - 1 )
    x = x + 1;
    if ( d < 0 )
        d = d + x + x + 1;
    else
        y = y - 1;
        a = x - y + 1;
        d = d + a + a;
    end
    Ibinsel( x+xc,  y+yc) = value;
    Ibinsel( y+xc,  x+yc) = value;
    Ibinsel( y+xc, -x+yc) = value;
    Ibinsel( x+xc, -y+yc) = value;
    Ibinsel(-x+xc, -y+yc) = value;
    Ibinsel(-y+xc, -x+yc) = value;
    Ibinsel(-y+xc,  x+yc) = value;
    Ibinsel(-x+xc,  y+yc) = value;
end
counter = counter + 1;
nxtcircle = 1;
        end
    end

        %2nd quarter
        while (ycapp > lasty - round((dp+1)*sin(pi/4))) & (nxtcircle==0)
            ycapp = ycapp - 1;
            xcapp = lastx + round(sqrt((dp+1)^2-(ycapp-lasty)^2));
        cond = 1;
        for jj = (ycapp - r+1):(ycapp + r-1)
```

```
        for  ii   =   (xcapp-round(sqrt((r-1)^2   -   (jj   -   ycapp)^2))):(xcapp   +
round(sqrt((r-1)^2 - (jj - ycapp)^2)))
            if Ibinsel(jj,ii)==0
                cond=0;
                break
            end
        end
        if cond==0
            break
        end
        end
        if cond == 1
            Ibinsel(ycapp,xcapp) = 0;
            xc = ycapp;
yc = xcapp;
radius = r;
value = 0;

x = 0;
y = radius;
d = 1 - radius;

Ibinsel(xc, yc+y) = value;
Ibinsel(xc, yc-y) = value;
Ibinsel(xc+y, yc) = value;
Ibinsel(xc-y, yc) = value;

while ( x < y - 1 )
    x = x + 1;
    if ( d < 0 )
        d = d + x + x + 1;
    else
        y = y - 1;
        a = x - y + 1;
        d = d + a + a;
    end
    Ibinsel( x+xc,  y+yc) = value;
    Ibinsel( y+xc,  x+yc) = value;
    Ibinsel( y+xc, -x+yc) = value;
    Ibinsel( x+xc, -y+yc) = value;
    Ibinsel(-x+xc, -y+yc) = value;
    Ibinsel(-y+xc, -x+yc) = value;
    Ibinsel(-y+xc,  x+yc) = value;
    Ibinsel(-x+xc,  y+yc) = value;
end
counter = counter + 1;
nxtcircle = 1;
        end
        end

        %3rd quarter
        while (xcapp > lastx - round((dp+1)*cos(pi/4)) ) & (nxtcircle==0)
        xcapp = xcapp - 1;
        ycapp = lasty - round(sqrt((dp+1)^2-(xcapp-lastx)^2));
        cond = 1;
        for jj = (ycapp - r+1):(ycapp + r-1)
        for  ii   =   (xcapp-round(sqrt((r-1)^2   -   (jj   -   ycapp)^2))):(xcapp   +
round(sqrt((r-1)^2 - (jj - ycapp)^2)))
            if Ibinsel(jj,ii)==0
                cond=0;
                break
            end
        end
```

```
        if cond==0
            break
        end
        end
        if cond == 1
            Ibinsel(ycapp,xcapp) = 0;
            xc = ycapp;
yc = xcapp;
radius = r;
value = 0;

x = 0;
y = radius;
d = 1 - radius;

Ibinsel(xc, yc+y) = value;
Ibinsel(xc, yc-y) = value;
Ibinsel(xc+y, yc) = value;
Ibinsel(xc-y, yc) = value;

while ( x < y - 1 )
    x = x + 1;
    if ( d < 0 )
        d = d + x + x + 1;
    else
        y = y - 1;
        a = x - y + 1;
        d = d + a + a;
    end
    Ibinsel( x+xc,  y+yc) = value;
    Ibinsel( y+xc,  x+yc) = value;
    Ibinsel( y+xc, -x+yc) = value;
    Ibinsel( x+xc, -y+yc) = value;
    Ibinsel(-x+xc, -y+yc) = value;
    Ibinsel(-y+xc, -x+yc) = value;
    Ibinsel(-y+xc,  x+yc) = value;
    Ibinsel(-x+xc,  y+yc) = value;
end
counter = counter + 1;
nxtcircle = 1;
        end
        end
    %4th quarter
    while (ycapp < lasty + round((dp+1)*sin(pi/4))) & (nxtcircle==0)
        ycapp = ycapp + 1;
        xcapp = lastx - round(sqrt((dp+1)^2-(ycapp-lasty)^2));
        cond = 1;
        for jj = (ycapp - r+1):(ycapp + r-1)
        for  ii  =  (xcapp-round(sqrt((r-1)^2  -  (jj  -  ycapp)^2))):(xcapp  +
round(sqrt((r-1)^2 - (jj - ycapp)^2)))
            if Ibinsel(jj,ii)==0
                cond=0;
                break
            end
        end
        if cond==0
            break
        end
        end
        if cond == 1
            Ibinsel(ycapp,xcapp) = 0;
            xc = ycapp;
yc = xcapp;
```

```
radius = r;
value = 0;

x = 0;
y = radius;
d = 1 - radius;

Ibinsel(xc, yc+y) = value;
Ibinsel(xc, yc-y) = value;
Ibinsel(xc+y, yc) = value;
Ibinsel(xc-y, yc) = value;

while ( x < y - 1 )
    x = x + 1;
    if ( d < 0 )
        d = d + x + x + 1;
    else
        y = y - 1;
        a = x - y + 1;
        d = d + a + a;
    end
    Ibinsel( x+xc,  y+yc) = value;
    Ibinsel( y+xc,  x+yc) = value;
    Ibinsel( y+xc, -x+yc) = value;
    Ibinsel( x+xc, -y+yc) = value;
    Ibinsel(-x+xc, -y+yc) = value;
    Ibinsel(-y+xc, -x+yc) = value;
    Ibinsel(-y+xc,  x+yc) = value;
    Ibinsel(-x+xc,  y+yc) = value;
end
counter = counter + 1;
nxtcircle = 1;
        end
    end
end




%4th condition
if condition==4
    nxtcircle = 0;
    %1st quarter
        while (ycapp > lasty - round((dp+1)*sin(pi/4))) & (nxtcircle==0)
            ycapp = ycapp - 1;
            xcapp = lastx + round(sqrt((dp+1)^2-(ycapp-lasty)^2));
        cond = 1;
        for jj = (ycapp - r+1):(ycapp + r-1)
        for  ii  =  (xcapp-round(sqrt((r-1)^2  -  (jj  -  ycapp)^2))):(xcapp  +
round(sqrt((r-1)^2 - (jj - ycapp)^2)))
            if Ibinsel(jj,ii)==0
                cond=0;
                break
            end
        end
        if cond==0
            break
        end
        end
        if cond == 1
            Ibinsel(ycapp,xcapp) = 0;
```

```
            xc = ycapp;
yc = xcapp;
radius = r;
value = 0;

x = 0;
y = radius;
d = 1 - radius;

Ibinsel(xc, yc+y) = value;
Ibinsel(xc, yc-y) = value;
Ibinsel(xc+y, yc) = value;
Ibinsel(xc-y, yc) = value;

while ( x < y - 1 )
    x = x + 1;
    if ( d < 0 )
        d = d + x + x + 1;
    else
        y = y - 1;
        a = x - y + 1;
        d = d + a + a;
    end
    Ibinsel( x+xc,  y+yc) = value;
    Ibinsel( y+xc,  x+yc) = value;
    Ibinsel( y+xc, -x+yc) = value;
    Ibinsel( x+xc, -y+yc) = value;
    Ibinsel(-x+xc, -y+yc) = value;
    Ibinsel(-y+xc, -x+yc) = value;
    Ibinsel(-y+xc,  x+yc) = value;
    Ibinsel(-x+xc,  y+yc) = value;
end
counter = counter + 1;
nxtcircle = 1;
        end
        end

        %2nd quarter
        while (xcapp > lastx - round((dp+1)*cos(pi/4)) ) & (nxtcircle==0)
        xcapp = xcapp - 1;
        ycapp = lasty - round(sqrt((dp+1)^2-(xcapp-lastx)^2));
        cond = 1;
        for jj = (ycapp - r+1):(ycapp + r-1)
        for  ii  =  (xcapp-round(sqrt((r-1)^2  -  (jj  -  ycapp)^2))):(xcapp  +
round(sqrt((r-1)^2 - (jj - ycapp)^2)))
            if Ibinsel(jj,ii)==0
                cond=0;
                break
            end
        end
        if cond==0
            break
        end
        end
        if cond == 1
            Ibinsel(ycapp,xcapp) = 0;
            xc = ycapp;
yc = xcapp;
radius = r;
value = 0;

x = 0;
y = radius;
```

```
d = 1 - radius;

Ibinsel(xc, yc+y) = value;
Ibinsel(xc, yc-y) = value;
Ibinsel(xc+y, yc) = value;
Ibinsel(xc-y, yc) = value;

while ( x < y - 1 )
    x = x + 1;
    if ( d < 0 )
        d = d + x + x + 1;
    else
        y = y - 1;
        a = x - y + 1;
        d = d + a + a;
    end
    Ibinsel( x+xc,  y+yc) = value;
    Ibinsel( y+xc,  x+yc) = value;
    Ibinsel( y+xc, -x+yc) = value;
    Ibinsel( x+xc, -y+yc) = value;
    Ibinsel(-x+xc, -y+yc) = value;
    Ibinsel(-y+xc, -x+yc) = value;
    Ibinsel(-y+xc,  x+yc) = value;
    Ibinsel(-x+xc,  y+yc) = value;
end
counter = counter + 1;
nxtcircle = 1;
        end
        end
    %3rd quarter
    while (ycapp < lasty + round((dp+1)*sin(pi/4))) & (nxtcircle==0)
        ycapp = ycapp + 1;
        xcapp = lastx - round(sqrt((dp+1)^2-(ycapp-lasty)^2));
        cond = 1;
        for jj = (ycapp - r+1):(ycapp + r-1)
        for  ii  =  (xcapp-round(sqrt((r-1)^2  -  (jj  -  ycapp)^2))):(xcapp  +
round(sqrt((r-1)^2 - (jj - ycapp)^2)))
            if Ibinsel(jj,ii)==0
                cond=0;
                break
            end
        end
        if cond==0
            break
        end
        end
        if cond == 1
            Ibinsel(ycapp,xcapp) = 0;
            xc = ycapp;
yc = xcapp;
radius = r;
value = 0;

x = 0;
y = radius;
d = 1 - radius;

Ibinsel(xc, yc+y) = value;
Ibinsel(xc, yc-y) = value;
Ibinsel(xc+y, yc) = value;
Ibinsel(xc-y, yc) = value;

while ( x < y - 1 )
```

```
    x = x + 1;
    if ( d < 0 )
        d = d + x + x + 1;
    else
        y = y - 1;
        a = x - y + 1;
        d = d + a + a;
    end
    Ibinsel( x+xc,  y+yc) = value;
    Ibinsel( y+xc,  x+yc) = value;
    Ibinsel( y+xc, -x+yc) = value;
    Ibinsel( x+xc, -y+yc) = value;
    Ibinsel(-x+xc, -y+yc) = value;
    Ibinsel(-y+xc, -x+yc) = value;
    Ibinsel(-y+xc,  x+yc) = value;
    Ibinsel(-x+xc,  y+yc) = value;
end
counter = counter + 1;
nxtcircle = 1;
        end
    end

    %4th quarter
    while (xcapp < lastx + round((dp+1)*cos(pi/4))) & (nxtcircle==0)
        xcapp = xcapp + 1;
        ycapp = lasty + round(sqrt((dp+1)^2-(xcapp-lastx)^2));
        cond = 1;
        for jj = (ycapp - r+1):(ycapp + r-1)
        for  ii  =  (xcapp-round(sqrt((r-1)^2  -  (jj  -  ycapp)^2))):(xcapp  +
round(sqrt((r-1)^2 - (jj - ycapp)^2)))
            if Ibinsel(jj,ii)==0
                cond=0;
                break
            end
        end
        if cond==0
            break
        end
        end
        if cond == 1
            Ibinsel(ycapp,xcapp) = 0;
            xc = ycapp;
yc = xcapp;
radius = r;
value = 0;

x = 0;
y = radius;
d = 1 - radius;

Ibinsel(xc, yc+y) = value;
Ibinsel(xc, yc-y) = value;
Ibinsel(xc+y, yc) = value;
Ibinsel(xc-y, yc) = value;

while ( x < y - 1 )
    x = x + 1;
    if ( d < 0 )
        d = d + x + x + 1;
    else
        y = y - 1;
        a = x - y + 1;
        d = d + a + a;
```

```
    end
    Ibinsel( x+xc,  y+yc) = value;
    Ibinsel( y+xc,  x+yc) = value;
    Ibinsel( y+xc, -x+yc) = value;
    Ibinsel( x+xc, -y+yc) = value;
    Ibinsel(-x+xc, -y+yc) = value;
    Ibinsel(-y+xc, -x+yc) = value;
    Ibinsel(-y+xc,  x+yc) = value;
    Ibinsel(-x+xc,  y+yc) = value;
end
counter = counter + 1;
nxtcircle = 1;
        end
    end
end



%after these 4 conditions which just one of them will processed in each
%cycle, we have nxtcircle=0 or =1



    if nxtcircle == 1

       i = i + 1;
       j = i - 1;
       Xcenters(i,1) = yc;
       Ycenters(i,1) = xc;

       if reverse ~= 0
           revfrom(m,1) = i - reverse - 1;
           revto(m,1)   = i;
           m = m + 1;
       end

       dx    = Xcenters(i,1) - Xcenters(i-reverse-1,1);
       dy    = Ycenters(i,1) - Ycenters(i-reverse-1,1);
       lastx = yc;
       lasty = xc;
       reverse = 0;


    else

        reverse = reverse + 1;
            for k = 1:size(revto,1);

                if j == revto(k,1)
                    n = revfrom(k,1);
                    break
                else
                    n = j - 1;
                end

            end

            dx    = Xcenters(j,1) - Xcenters(n,1);
            dy    = Ycenters(j,1) - Ycenters(n,1);
            lastx = Xcenters(j,1);
            lasty = Ycenters(j,1);
            j = j - 1;
            if j==1
```

```
                finishit=1;
            end

    end

    if dy > 0 & dx <= 0
        condition = 1;
        xcapp = lastx + round((dp+1)*cos(pi/4));
        ycapp = lasty - round((dp+1)*sin(pi/4));

    elseif dy >= 0 & dx > 0
        condition = 2;
        xcapp = lastx - round((dp+1)*cos(pi/4));
        ycapp = lasty - round((dp+1)*sin(pi/4));

    elseif dy < 0 & dx >= 0
        condition = 3;
        xcapp = lastx - round((dp+1)*cos(pi/4));
        ycapp = lasty + round((dp+1)*sin(pi/4));

    elseif dy <= 0 & dx < 0
        condition = 4;
        xcapp = lastx + round((dp+1)*cos(pi/4));
        ycapp = lasty + round((dp+1)*sin(pi/4));
    end
end

imshow(Ibinsel);

imwrite(Ibinsel,'before.jpg');
```

Measurement of area and perimeter of constricted pore

The following code was developed and can be debugged in MATLAB.

```
function cons_area_primeter


defaultarea = 15271743; %previously measured
defaultdiam = 2.5916e+003; %previously measured

%reading the image
I = imread('triangle 151.jpg');
Isize = size(size(I));

if Isize(1,2)~=2
    I = rgb2gray(I);
end;

Ibin = im2bw(I,0.5);

Isize = size(Ibin);

Ibinsel = Ibin;

[Ibinsel,idx] = bwselect(Ibin,4);
Iseledge = edge(Ibinsel,'canny');
[J,I] = find(Iseledge);

perimeter = size(J,1);
%disp('the wetted perimeter is:');
%disp(perimeter);

%finding the area of the selected pore
porearea = 0;
for i = 1:size(Ibinsel,1)
    for j = 1:size(Ibinsel,2)
        if Ibinsel(i,j) ==1
            porearea = porearea + 1;
        end
    end
end

arearatio = porearea/defaultarea;
disp('the pore area ratio is:');
disp(arearatio);

%calculating hydrolic diameter
hydrodiameter = 4*porearea/perimeter;
diamratio = hydrodiameter/defaultdiam;
disp('the hydrolic diameter ratio is:');
disp(diamratio);
imshow(Ibinsel);
imwrite(Ibinsel,'after.jpg');
```

APPENDIX C

Simulation results for different geometries

Table C-1. Values of α and β vs. λ for rectangular geometries (continues)

λ	Rectangle 3:1		Rectangle 7:1		Rectangle 15:1		Rectangle 30:1	
	α	β	α	β	α	β	α	β
0.10	0.673	0.582	0.662	0.546	0.654	0.523	0.650	0.510
0.11	0.643	0.556	0.628	0.515	0.620	0.490	0.614	0.482
0.12	0.614	0.534	0.595	0.483	0.585	0.458	0.580	0.445
0.13	0.585	0.520	0.564	0.462	0.552	0.437	0.546	0.428
0.14	0.557	0.500	0.533	0.441	0.519	0.416	0.510	0.400
0.15	0.529	0.477	0.504	0.419	0.486	0.388	0.476	0.374
0.16	0.493	0.463	0.475	0.396	0.453	0.359	0.442	0.342
0.17	0.462	0.442	0.441	0.370	0.419	0.335	0.408	0.319
0.18	0.439	0.408	0.408	0.343	0.384	0.311	0.373	0.293
0.19	0.419	0.390	0.379	0.322	0.352	0.285	0.339	0.267
0.20	0.400	0.380	0.351	0.300	0.324	0.261	0.305	0.239
0.21	0.370	0.349	0.321	0.277	0.294	0.237	0.272	0.212
0.22	0.339	0.327	0.290	0.254	0.256	0.209	0.239	0.187
0.23	0.309	0.323	0.282	0.229	0.228	0.188	0.206	0.163
0.24	0.298	0.302	0.274	0.204	0.192	0.155	0.173	0.136
0.25	0.297	0.273	0.227	0.182	0.169	0.138	0.139	0.109
0.26	0.325	0.250	0.181	0.159	0.134	0.110	0.007	0.087
0.27	0.325	0.227	0.153	0.135	0.013	0.155	0.005	0.135
0.28	0.268	0.202	0.126	0.111	0.024	0.235	0.513	0.447
0.29	0.266	0.194	0.100	0.137	0.488	0.445	0.489	0.433
0.30	0.291	0.195	0.074	0.163	0.471	0.430	0.465	0.418
0.31	0.211	0.168	0.282	0.267	0.461	0.414	0.455	0.402
0.32	0.160	0.147	0.490	0.371	0.451	0.399	0.444	0.387
0.33	0.168	0.137	0.472	0.378	0.441	0.391	0.428	0.374
0.34	0.183	0.133	0.453	0.385	0.430	0.383	0.412	0.361
0.35	0.201	0.133	0.452	0.372	0.410	0.364	0.389	0.343
0.36	0.412	0.341	0.450	0.359	0.390	0.346	0.366	0.325
0.37	0.545	0.472	0.447	0.357	0.379	0.324	0.357	0.315
0.38	0.520	0.449	0.444	0.354	0.369	0.303	0.348	0.304
0.39	0.485	0.438	0.414	0.329	0.347	0.290	0.332	0.290
0.40	0.444	0.432	0.385	0.303	0.326	0.277	0.315	0.275
0.41	0.502	0.455	0.387	0.306	0.315	0.262	0.300	0.262
0.42	0.532	0.463	0.390	0.309	0.303	0.247	0.285	0.250
0.43	0.510	0.441	0.361	0.284	0.282	0.239	0.262	0.229
0.44	0.487	0.419	0.331	0.259	0.260	0.231	0.239	0.208
0.45	0.464	0.398	0.342	0.267	0.249	0.221	0.228	0.199
0.46	0.439	0.376	0.352	0.275	0.238	0.212	0.216	0.189
0.47	0.415	0.354	0.306	0.259	0.229	0.204	0.195	0.170
0.48	0.390	0.332	0.260	0.242	0.221	0.197	0.174	0.152
0.49	0.351	0.316	0.231	0.214	0.215	0.192	0.167	0.145
0.50	0.306	0.302	0.300	0.282	0.210	0.188	0.161	0.140
0.51	0.406	0.366	0.274	0.257	0.179	0.160	0.128	0.111
0.52	0.466	0.402	0.248	0.232	0.148	0.132	1.000	1.000
0.53	0.445	0.383	0.221	0.206	0.116	0.103	1.000	1.000
0.54	0.424	0.364	0.194	0.180	1.000	1.000	1.000	1.000
0.55	0.402	0.345	0.166	0.154	1.000	1.000	1.000	1.000

λ: ratio of particle diameter to pore hydraulic diameter
α: ratio of pore cross-sectional area after particle deposition onto pore wall, to initial pore area
β: ratio of pore hydraulic diameter after particle deposition onto pore wall, to initial hydraulic diameter

Table C-1. (continued) Values of α and β vs. λ for rectangular geometries

λ	Rectangle 3:1		Rectangle 7:1		Rectangle 15:1		Rectangle 30:1	
	α	β	α	β	α	β	α	β
0.56	0.380	0.325	0.138	0.128	1.000	1.000	1.000	1.000
0.57	0.358	0.305	0.102	0.105	1.000	1.000	1.000	1.000
0.58	0.335	0.285	1.000	1.000	1.000	1.000	1.000	1.000
0.59	0.312	0.265	1.000	1.000	1.000	1.000	1.000	1.000
0.60	0.289	0.245	1.000	1.000	1.000	1.000	1.000	1.000
0.61	0.265	0.224	1.000	1.000	1.000	1.000	1.000	1.000
0.62	0.241	0.203	1.000	1.000	1.000	1.000	1.000	1.000
0.63	0.216	0.181	1.000	1.000	1.000	1.000	1.000	1.000
0.64	0.191	0.159	1.000	1.000	1.000	1.000	1.000	1.000
0.65	0.166	0.138	1.000	1.000	1.000	1.000	1.000	1.000
0.66	0.322	0.276	1.000	1.000	1.000	1.000	1.000	1.000
0.67	0.449	0.394	1.000	1.000	1.000	1.000	1.000	1.000
0.68	0.518	0.469	1.000	1.000	1.000	1.000	1.000	1.000
0.69	0.587	0.545	1.000	1.000	1.000	1.000	1.000	1.000
0.70	0.656	0.621	1.000	1.000	1.000	1.000	1.000	1.000
0.71	0.725	0.697	1.000	1.000	1.000	1.000	1.000	1.000
0.72	0.793	0.773	1.000	1.000	1.000	1.000	1.000	1.000
0.73	0.862	0.848	1.000	1.000	1.000	1.000	1.000	1.000
0.74	0.931	0.924	1.000	1.000	1.000	1.000	1.000	1.000
0.75	1.000	1.000	1.000	1.000	1.000	1.000	1.000	1.000
0.76	1.000	1.000	1.000	1.000	1.000	1.000	1.000	1.000
0.77	1.000	1.000	1.000	1.000	1.000	1.000	1.000	1.000
0.78	1.000	1.000	1.000	1.000	1.000	1.000	1.000	1.000
0.79	1.000	1.000	1.000	1.000	1.000	1.000	1.000	1.000
0.80	1.000	1.000	1.000	1.000	1.000	1.000	1.000	1.000
0.81	1.000	1.000	1.000	1.000	1.000	1.000	1.000	1.000
0.82	1.000	1.000	1.000	1.000	1.000	1.000	1.000	1.000
0.83	1.000	1.000	1.000	1.000	1.000	1.000	1.000	1.000
0.84	1.000	1.000	1.000	1.000	1.000	1.000	1.000	1.000
0.85	1.000	1.000	1.000	1.000	1.000	1.000	1.000	1.000
0.86	1.000	1.000	1.000	1.000	1.000	1.000	1.000	1.000
0.87	1.000	1.000	1.000	1.000	1.000	1.000	1.000	1.000
0.88	1.000	1.000	1.000	1.000	1.000	1.000	1.000	1.000
0.89	1.000	1.000	1.000	1.000	1.000	1.000	1.000	1.000
0.90	1.000	1.000	1.000	1.000	1.000	1.000	1.000	1.000
0.91	1.000	1.000	1.000	1.000	1.000	1.000	1.000	1.000
0.92	1.000	1.000	1.000	1.000	1.000	1.000	1.000	1.000
0.93	1.000	1.000	1.000	1.000	1.000	1.000	1.000	1.000
0.94	1.000	1.000	1.000	1.000	1.000	1.000	1.000	1.000
0.95	1.000	1.000	1.000	1.000	1.000	1.000	1.000	1.000
0.96	1.000	1.000	1.000	1.000	1.000	1.000	1.000	1.000
0.97	1.000	1.000	1.000	1.000	1.000	1.000	1.000	1.000
0.98	1.000	1.000	1.000	1.000	1.000	1.000	1.000	1.000
0.99	1.000	1.000	1.000	1.000	1.000	1.000	1.000	1.000
1.00	1.000	1.000	1.000	1.000	1.000	1.000	1.000	1.000

λ: ratio of particle diameter to pore hydraulic diameter
α: ratio of pore cross-sectional area after particle deposition onto pore wall, to initial pore area
β: ratio of pore hydraulic diameter after particle deposition onto pore wall, to initial hydraulic diameter

Table C-2. Values of α and β vs. λ for triangular geometries (continues)

λ	Triangle 3:1		Triangle 7:1		Triangle 15:1		Triangle 30:1	
	α	β	α	β	α	β	α	β
0.10	0.676	0.565	0.694	0.569	0.695	0.554	0.688	0.583
0.11	0.652	0.547	0.666	0.564	0.670	0.527	0.663	0.557
0.12	0.628	0.529	0.639	0.558	0.646	0.501	0.639	0.531
0.13	0.603	0.502	0.615	0.534	0.623	0.488	0.616	0.516
0.14	0.578	0.476	0.591	0.511	0.600	0.475	0.593	0.501
0.15	0.556	0.464	0.575	0.481	0.579	0.457	0.572	0.481
0.16	0.535	0.452	0.559	0.452	0.558	0.439	0.552	0.460
0.17	0.515	0.439	0.539	0.448	0.539	0.428	0.534	0.448
0.18	0.496	0.425	0.519	0.444	0.520	0.418	0.516	0.436
0.19	0.483	0.397	0.504	0.419	0.505	0.404	0.499	0.419
0.20	0.470	0.369	0.488	0.394	0.491	0.390	0.482	0.403
0.21	0.456	0.358	0.474	0.384	0.474	0.380	0.469	0.395
0.22	0.443	0.347	0.460	0.374	0.457	0.371	0.461	0.383
0.23	0.430	0.333	0.446	0.375	0.446	0.361	0.447	0.373
0.24	0.417	0.318	0.420	0.360	0.434	0.351	0.434	0.362
0.25	0.415	0.304	0.423	0.346	0.421	0.343	0.422	0.353
0.26	0.414	0.290	0.403	0.329	0.410	0.339	0.413	0.344
0.27	0.388	0.301	0.387	0.316	0.399	0.336	0.409	0.342
0.28	0.384	0.301	0.393	0.334	0.392	0.331	0.400	0.338
0.29	0.385	0.271	0.383	0.326	0.385	0.327	0.391	0.331
0.30	0.365	0.287	0.378	0.324	0.380	0.323	0.384	0.324
0.31	0.376	0.279	0.370	0.306	0.376	0.319	0.381	0.323
0.32	0.387	0.270	0.371	0.309	0.373	0.318	0.376	0.320
0.33	0.332	0.260	0.374	0.324	0.370	0.317	0.374	0.319
0.34	0.410	0.287	0.394	0.263	0.363	0.315	0.369	0.318
0.35	0.352	0.277	0.350	0.303	0.356	0.313	0.366	0.318
0.36	0.298	0.272	0.372	0.293	0.363	0.314	0.380	0.324
0.37	0.363	0.249	0.393	0.326	0.369	0.311	0.378	0.330
0.38	0.317	0.231	0.390	0.324	0.373	0.325	0.386	0.335
0.39	0.367	0.234	0.386	0.317	0.374	0.326	0.388	0.338
0.40	0.385	0.265	0.388	0.326	0.379	0.332	0.394	0.344
0.41	0.340	0.268	0.408	0.342	0.386	0.341	0.392	0.346
0.42	0.404	0.277	0.416	0.349	0.397	0.351	0.404	0.354
0.43	0.458	0.314	0.427	0.359	0.389	0.349	0.407	0.358
0.44	0.432	0.295	0.453	0.331	0.406	0.360	0.424	0.375
0.45	0.406	0.276	0.467	0.359	0.426	0.379	0.433	0.384
0.46	0.352	0.281	0.443	0.374	0.425	0.379	0.445	0.395
0.47	0.451	0.305	0.466	0.396	0.451	0.404	0.446	0.398
0.48	0.517	0.384	0.441	0.373	0.454	0.407	0.462	0.416
0.49	0.497	0.367	0.486	0.352	0.460	0.416	0.482	0.433
0.50	0.475	0.348	0.514	0.393	0.496	0.449	0.490	0.441
0.51	0.455	0.331	0.486	0.391	0.499	0.454	0.505	0.453
0.52	0.434	0.315	0.528	0.451	0.532	0.505	0.516	0.465
0.53	0.375	0.337	0.508	0.433	0.531	0.472	0.546	0.494
0.54	0.533	0.345	0.550	0.471	0.525	0.501	0.561	0.517
0.55	0.516	0.333	0.523	0.478	0.530	0.471	0.562	0.519

λ: ratio of particle diameter to pore hydraulic diameter
α: ratio of pore cross-sectional area after particle deposition onto pore wall, to initial pore area
β: ratio of pore hydraulic diameter after particle deposition onto pore wall, to initial hydraulic diameter

Table C-2. (continued) Values of α and β vs. λ for triangular geometries

λ	Triangle 3:1		Triangle 7:1		Triangle 15:1		Triangle 30:1	
	α	β	α	β	α	β	α	β
0.56	0.498	0.320	0.594	0.477	0.548	0.487	0.564	0.521
0.57	0.481	0.308	0.573	0.492	0.531	0.475	0.567	0.525
0.58	0.592	0.428	0.553	0.507	0.553	0.493	0.571	0.530
0.59	0.578	0.414	0.536	0.489	0.537	0.480	0.556	0.516
0.60	0.564	0.399	0.600	0.554	0.562	0.502	0.561	0.521
0.61	0.549	0.387	0.587	0.540	0.547	0.488	0.568	0.528
0.62	0.535	0.374	0.575	0.526	0.576	0.515	0.576	0.537
0.63	0.520	0.363	0.560	0.512	0.562	0.502	0.585	0.546
0.64	0.505	0.351	0.545	0.497	0.594	0.532	0.572	0.535
0.65	0.652	0.529	0.531	0.492	0.581	0.520	0.583	0.548
0.66	0.641	0.518	0.613	0.569	0.568	0.508	0.596	0.561
0.67	0.631	0.509	0.602	0.558	0.606	0.544	0.609	0.576
0.68	0.620	0.500	0.592	0.548	0.594	0.532	0.598	0.564
0.69	0.609	0.489	0.579	0.536	0.582	0.523	0.613	0.580
0.70	0.597	0.477	0.566	0.525	0.625	0.562	0.630	0.597
0.71	0.585	0.466	0.666	0.623	0.614	0.551	0.620	0.587
0.72	0.572	0.454	0.657	0.614	0.603	0.541	0.639	0.607
0.73	0.559	0.443	0.649	0.606	0.652	0.587	0.629	0.597
0.74	0.547	0.432	0.638	0.596	0.646	0.567	0.650	0.619
0.75	0.534	0.421	0.628	0.587	0.640	0.548	0.641	0.611
0.76	0.522	0.410	0.617	0.576	0.687	0.620	0.665	0.634
0.77	0.510	0.398	0.607	0.565	0.679	0.612	0.690	0.661
0.78	0.765	0.615	0.599	0.557	0.671	0.603	0.682	0.653
0.79	0.759	0.609	0.728	0.687	0.671	0.575	0.710	0.682
0.80	0.753	0.602	0.720	0.680	0.725	0.655	0.705	0.675
0.81	0.746	0.596	0.713	0.674	0.718	0.649	0.698	0.668
0.82	0.740	0.590	0.707	0.667	0.712	0.642	0.729	0.700
0.83	0.734	0.583	0.700	0.660	0.705	0.635	0.722	0.693
0.84	0.728	0.577	0.692	0.652	0.776	0.705	0.756	0.729
0.85	0.721	0.571	0.684	0.643	0.771	0.699	0.751	0.723
0.86	0.715	0.564	0.676	0.636	0.766	0.694	0.788	0.762
0.87	0.708	0.557	0.669	0.628	0.760	0.688	0.783	0.757
0.88	0.701	0.550	0.663	0.626	0.755	0.683	0.777	0.752
0.89	0.695	0.543	0.832	0.794	0.838	0.763	0.818	0.795
0.90	0.688	0.536	0.828	0.789	0.834	0.759	0.814	0.791
0.91	0.681	0.529	0.823	0.784	0.831	0.756	0.858	0.837
0.92	0.674	0.523	0.819	0.780	0.814	0.783	0.855	0.834
0.93	0.667	0.516	0.815	0.776	0.797	0.811	0.852	0.831
0.94	0.660	0.510	0.812	0.772	0.782	0.858	0.900	0.883
0.95	0.653	0.503	0.808	0.768	0.904	0.879	0.898	0.881
0.96	0.645	0.496	0.804	0.764	0.902	0.877	0.896	0.878
0.97	0.638	0.489	0.799	0.759	0.900	0.875	0.948	0.934
0.98	0.631	0.482	0.796	0.755	0.898	0.873	0.947	0.933
0.99	1.000	1.000	0.792	0.751	0.896	0.870	0.946	0.932
1.00	1.000	1.000	1.000	1.000	1.000	1.000	1.000	1.000

λ: ratio of particle diameter to pore hydraulic diameter
α: ratio of pore cross-sectional area after particle deposition onto pore wall, to initial pore area
β: ratio of pore hydraulic diameter after particle deposition onto pore wall, to initial hydraulic diameter

Table C-3. Values of α and β vs. λ for oval geometries (continues)

λ	Oval 3:1		Oval 7:1		Oval 15:1		Oval 30:1	
	α	β	α	β	α	β	α	β
0.10	0.644	0.534	0.643	0.555	0.648	0.564	0.654	0.514
0.11	0.616	0.511	0.619	0.508	0.616	0.526	0.621	0.488
0.12	0.588	0.488	0.594	0.461	0.583	0.487	0.587	0.462
0.13	0.555	0.461	0.564	0.441	0.552	0.469	0.557	0.435
0.14	0.522	0.435	0.533	0.420	0.521	0.451	0.526	0.407
0.15	0.493	0.412	0.499	0.396	0.490	0.426	0.496	0.387
0.16	0.463	0.389	0.466	0.373	0.470	0.376	0.465	0.366
0.17	0.441	0.352	0.437	0.351	0.439	0.358	0.443	0.345
0.18	0.418	0.315	0.409	0.329	0.410	0.343	0.420	0.323
0.19	0.402	0.290	0.388	0.308	0.386	0.315	0.397	0.304
0.20	0.387	0.265	0.368	0.286	0.363	0.295	0.374	0.286
0.21	0.354	0.296	0.332	0.273	0.345	0.271	0.350	0.270
0.22	0.340	0.250	0.326	0.260	0.335	0.265	0.326	0.255
0.23	0.271	0.227	0.304	0.233	0.312	0.246	0.310	0.241
0.24	0.313	0.232	0.283	0.218	0.294	0.229	0.295	0.227
0.25	0.260	0.191	0.272	0.207	0.269	0.210	0.285	0.222
0.26	0.261	0.205	0.281	0.221	0.272	0.213	0.275	0.217
0.27	0.261	0.195	0.278	0.219	0.256	0.200	0.266	0.208
0.28	0.279	0.205	0.251	0.198	0.257	0.202	0.259	0.203
0.29	0.220	0.164	0.258	0.211	0.250	0.199	0.258	0.207
0.30	0.250	0.172	0.241	0.198	0.248	0.196	0.271	0.217
0.31	0.273	0.206	0.265	0.219	0.288	0.229	0.282	0.225
0.32	0.231	0.170	0.270	0.221	0.317	0.254	0.301	0.246
0.33	0.269	0.202	0.306	0.252	0.313	0.346	0.346	0.286
0.34	0.427	0.325	0.368	0.291	0.395	0.373	0.402	0.382
0.35	0.389	0.295	0.471	0.390	0.478	0.411	0.473	0.405
0.36	0.453	0.402	0.438	0.367	0.472	0.405	0.466	0.404
0.37	0.417	0.374	0.433	0.361	0.442	0.378	0.460	0.399
0.38	0.387	0.345	0.429	0.356	0.439	0.375	0.448	0.384
0.39	0.346	0.313	0.408	0.335	0.437	0.375	0.446	0.387
0.40	0.458	0.415	0.439	0.362	0.438	0.376	0.445	0.387
0.41	0.428	0.388	0.409	0.336	0.440	0.379	0.436	0.376
0.42	0.399	0.362	0.377	0.313	0.413	0.354	0.423	0.366
0.43	0.379	0.315	0.420	0.346	0.419	0.360	0.429	0.374
0.44	0.360	0.268	0.390	0.322	0.427	0.369	0.419	0.366
0.45	0.316	0.261	0.360	0.301	0.401	0.344	0.434	0.377
0.46	0.271	0.254	0.426	0.351	0.413	0.355	0.427	0.374
0.47	0.456	0.349	0.399	0.327	0.429	0.370	0.421	0.368
0.48	0.432	0.329	0.372	0.302	0.405	0.348	0.421	0.368
0.49	0.408	0.309	0.441	0.365	0.424	0.366	0.440	0.386
0.50	0.383	0.289	0.418	0.344	0.447	0.388	0.440	0.387
0.51	0.358	0.268	0.396	0.324	0.425	0.367	0.444	0.390
0.52	0.333	0.249	0.374	0.304	0.452	0.393	0.446	0.393
0.53	0.307	0.229	0.459	0.378	0.431	0.373	0.477	0.424
0.54	0.277	0.206	0.437	0.359	0.463	0.403	0.483	0.430
0.55	0.514	0.384	0.416	0.342	0.500	0.438	0.494	0.440

λ: ratio of particle diameter to pore hydraulic diameter
α: ratio of pore cross-sectional area after particle deposition onto pore wall, to initial pore area
β: ratio of pore hydraulic diameter after particle deposition onto pore wall, to initial hydraulic diameter

Table C-3. (continued) Values of α and β vs. λ for oval geometries

λ	Oval 3:1		Oval 7:1		Oval 15:1		Oval 30:1	
	α	β	α	β	α	β	α	β
0.56	0.496	0.368	0.517	0.429	0.481	0.420	0.504	0.450
0.57	0.478	0.353	0.500	0.414	0.523	0.459	0.546	0.493
0.58	0.459	0.338	0.481	0.397	0.569	0.503	0.564	0.508
0.59	0.440	0.323	0.468	0.385	0.554	0.488	0.580	0.526
0.60	0.421	0.308	0.591	0.491	0.606	0.538	0.633	0.579
0.61	0.402	0.293	0.576	0.477	0.662	0.592	0.690	0.635
0.62	0.381	0.276	0.714	0.602	0.722	0.651	0.717	0.664
0.63	0.361	0.260	0.704	0.589	0.787	0.715	0.819	0.770
0.64	0.696	0.504	1.000	1.000	1.000	1.000	1.000	1.000
0.65	0.686	0.494	1.000	1.000	1.000	1.000	1.000	1.000
0.66	0.677	0.484	1.000	1.000	1.000	1.000	1.000	1.000
0.67	1.000	1.000	1.000	1.000	1.000	1.000	1.000	1.000
0.68	1.000	1.000	1.000	1.000	1.000	1.000	1.000	1.000
0.69	1.000	1.000	1.000	1.000	1.000	1.000	1.000	1.000
0.70	1.000	1.000	1.000	1.000	1.000	1.000	1.000	1.000
0.71	1.000	1.000	1.000	1.000	1.000	1.000	1.000	1.000
0.72	1.000	1.000	1.000	1.000	1.000	1.000	1.000	1.000
0.73	1.000	1.000	1.000	1.000	1.000	1.000	1.000	1.000
0.74	1.000	1.000	1.000	1.000	1.000	1.000	1.000	1.000
0.75	1.000	1.000	1.000	1.000	1.000	1.000	1.000	1.000
0.76	1.000	1.000	1.000	1.000	1.000	1.000	1.000	1.000
0.77	1.000	1.000	1.000	1.000	1.000	1.000	1.000	1.000
0.78	1.000	1.000	1.000	1.000	1.000	1.000	1.000	1.000
0.79	1.000	1.000	1.000	1.000	1.000	1.000	1.000	1.000
0.80	1.000	1.000	1.000	1.000	1.000	1.000	1.000	1.000
0.81	1.000	1.000	1.000	1.000	1.000	1.000	1.000	1.000
0.82	1.000	1.000	1.000	1.000	1.000	1.000	1.000	1.000
0.83	1.000	1.000	1.000	1.000	1.000	1.000	1.000	1.000
0.84	1.000	1.000	1.000	1.000	1.000	1.000	1.000	1.000
0.85	1.000	1.000	1.000	1.000	1.000	1.000	1.000	1.000
0.86	1.000	1.000	1.000	1.000	1.000	1.000	1.000	1.000
0.87	1.000	1.000	1.000	1.000	1.000	1.000	1.000	1.000
0.88	1.000	1.000	1.000	1.000	1.000	1.000	1.000	1.000
0.89	1.000	1.000	1.000	1.000	1.000	1.000	1.000	1.000
0.90	1.000	1.000	1.000	1.000	1.000	1.000	1.000	1.000
0.91	1.000	1.000	1.000	1.000	1.000	1.000	1.000	1.000
0.92	1.000	1.000	1.000	1.000	1.000	1.000	1.000	1.000
0.93	1.000	1.000	1.000	1.000	1.000	1.000	1.000	1.000
0.94	1.000	1.000	1.000	1.000	1.000	1.000	1.000	1.000
0.95	1.000	1.000	1.000	1.000	1.000	1.000	1.000	1.000
0.96	1.000	1.000	1.000	1.000	1.000	1.000	1.000	1.000
0.97	1.000	1.000	1.000	1.000	1.000	1.000	1.000	1.000
0.98	1.000	1.000	1.000	1.000	1.000	1.000	1.000	1.000
0.99	1.000	1.000	1.000	1.000	1.000	1.000	1.000	1.000
1.00	1.000	1.000	1.000	1.000	1.000	1.000	1.000	1.000

λ: ratio of particle diameter to pore hydraulic diameter
α: ratio of pore cross-sectional area after particle deposition onto pore wall, to initial pore area
β: ratio of pore hydraulic diameter after particle deposition onto pore wall, to initial hydraulic diameter

Table C-4. Values of α and β vs. λ for combined geometries and circle (continues)

λ	Circle		Cross 7:1		Star 7:1		Rounded ends 30:1	
	α	β	α	β	α	β	α	β
0.10	0.683	0.550	0.660	0.533	0.697	0.516	0.641	0.520
0.11	0.646	0.529	0.627	0.510	0.671	0.496	0.607	0.488
0.12	0.629	0.522	0.595	0.485	0.650	0.478	0.576	0.459
0.13	0.603	0.503	0.563	0.456	0.629	0.460	0.537	0.424
0.14	0.562	0.469	0.531	0.435	0.609	0.445	0.503	0.397
0.15	0.551	0.467	0.499	0.417	0.588	0.431	0.470	0.372
0.16	0.518	0.442	0.467	0.390	0.570	0.419	0.437	0.348
0.17	0.488	0.418	0.436	0.360	0.551	0.407	0.400	0.317
0.18	0.462	0.404	0.413	0.325	0.533	0.394	0.362	0.284
0.19	0.444	0.390	0.388	0.290	0.514	0.381	0.327	0.255
0.20	0.429	0.382	0.364	0.255	0.505	0.372	0.298	0.232
0.21	0.422	0.378	0.353	0.238	0.496	0.364	0.262	0.205
0.22	0.423	0.385	0.335	0.219	0.482	0.354	0.227	0.177
0.23	0.366	0.337	0.304	0.196	0.468	0.343	0.197	0.154
0.24	0.377	0.344	0.276	0.176	0.462	0.338	0.164	0.128
0.25	0.322	0.304	0.248	0.157	0.456	0.333	0.129	0.100
0.26	0.346	0.328	0.227	0.142	0.435	0.316	0.104	0.079
0.27	0.294	0.282	0.197	0.139	0.415	0.299	0.299	0.223
0.28	0.335	0.320	0.160	0.160	0.421	0.305	0.507	0.377
0.29	0.283	0.276	0.287	0.247	0.427	0.312	0.493	0.368
0.30	0.229	0.227	0.487	0.368	0.426	0.312	0.474	0.353
0.31	0.293	0.288	0.498	0.370	0.426	0.312	0.455	0.340
0.32	0.244	0.243	0.493	0.371	0.425	0.310	0.439	0.327
0.33	0.191	0.197	0.488	0.373	0.424	0.309	0.424	0.314
0.34	0.287	0.282	0.475	0.365	0.366	0.312	0.408	0.301
0.35	0.239	0.241	0.460	0.353	0.309	0.316	0.391	0.289
0.36	0.188	0.197	0.431	0.327	0.385	0.326	0.372	0.274
0.37	0.095	0.190	0.414	0.313	0.462	0.336	0.355	0.262
0.38	0.276	0.273	0.421	0.321	0.431	0.311	0.342	0.253
0.39	0.228	0.233	0.417	0.320	0.401	0.287	0.323	0.238
0.40	0.186	0.197	0.410	0.315	0.478	0.348	0.313	0.231
0.41	0.045	0.139	0.386	0.290	0.452	0.326	0.288	0.213
0.42	0.468	0.228	0.360	0.265	0.427	0.306	0.268	0.197
0.43	0.442	0.213	0.322	0.240	0.495	0.353	0.261	0.192
0.44	0.416	0.198	0.336	0.244	0.499	0.367	0.251	0.185
0.45	0.389	0.182	0.337	0.263	0.475	0.345	0.220	0.162
0.46	0.362	0.168	0.321	0.239	0.451	0.326	0.205	0.151
0.47	0.556	0.307	0.305	0.224	0.464	0.336	0.184	0.136
0.48	0.537	0.294	0.303	0.227	0.478	0.354	0.170	0.125
0.49	0.517	0.280	0.292	0.213	0.498	0.363	0.154	0.113
0.50	0.497	0.270	0.256	0.190	0.477	0.346	0.148	0.110
0.51	0.740	0.510	0.264	0.189	0.538	0.410	0.470	0.451
0.52	0.730	0.499	0.251	0.183	0.520	0.394	1.000	1.000
0.53	0.719	0.489	0.239	0.166	0.500	0.377	1.000	1.000
0.54	0.708	0.479	0.529	0.439	0.481	0.361	1.000	1.000
0.55	0.698	0.468	0.732	0.857	0.511	0.389	1.000	1.000

λ: ratio of particle diameter to pore hydraulic diameter
α: ratio of pore cross-sectional area after particle deposition onto pore wall, to initial pore area
β: ratio of pore hydraulic diameter after particle deposition onto pore wall, to initial hydraulic diameter

Table C-4. (continued) Values of α and β vs. λ for combined geometries and circle

λ	Circle		Cross 7:1		Star 7:1		Rounded ends 30:1	
	α	β	α	β	α	β	α	β
0.56	0.686	0.458	0.936	0.853	0.545	0.419	1.000	1.000
0.57	0.675	0.448	0.932	0.849	0.583	0.449	1.000	1.000
0.58	0.664	0.438	0.930	0.845	0.569	0.438	1.000	1.000
0.59	0.652	0.427	0.928	0.841	0.555	0.425	1.000	1.000
0.60	0.640	0.418	0.926	0.837	0.540	0.414	1.000	1.000
0.61	0.628	0.407	0.924	0.833	0.525	0.400	1.000	1.000
0.62	0.616	0.396	0.921	0.829	0.509	0.388	1.000	1.000
0.63	0.603	0.386	0.919	0.826	0.560	0.426	1.000	1.000
0.64	0.590	0.376	0.916	0.822	0.546	0.418	1.000	1.000
0.65	0.578	0.365	0.913	0.818	0.603	0.460	1.000	1.000
0.66	0.564	0.355	0.910	0.814	0.590	0.448	1.000	1.000
0.67	0.551	0.345	0.907	0.810	0.577	0.437	1.000	1.000
0.68	0.538	0.335	0.904	0.806	0.642	0.491	1.000	1.000
0.69	0.524	0.325	0.901	0.802	0.628	0.490	1.000	1.000
0.70	0.510	0.315	0.897	0.798	0.620	0.466	1.000	1.000
0.71	0.496	0.304	0.894	0.795	0.613	0.455	1.000	1.000
0.72	0.482	0.294	0.891	0.791	0.684	0.522	1.000	1.000
0.73	0.467	0.283	0.889	0.788	0.676	0.513	1.000	1.000
0.74	0.452	0.273	0.886	0.784	0.668	0.503	1.000	1.000
0.75	0.438	0.264	0.924	0.780	0.653	0.518	1.000	1.000
0.76	0.422	0.253	0.962	0.912	0.638	0.533	1.000	1.000
0.77	0.407	0.242	1.000	1.000	0.635	0.508	1.000	1.000
0.78	0.392	0.232	1.000	1.000	0.632	0.483	1.000	1.000
0.79	0.376	0.222	1.000	1.000	0.624	0.469	1.000	1.000
0.80	0.360	0.212	1.000	1.000	0.616	0.455	1.000	1.000
0.81	0.344	0.201	1.000	1.000	0.802	0.698	1.000	1.000
0.82	0.328	0.191	1.000	1.000	0.800	0.659	1.000	1.000
0.83	0.311	0.181	1.000	1.000	0.795	0.654	1.000	1.000
0.84	0.294	0.170	1.000	1.000	0.790	0.649	1.000	1.000
0.85	0.278	0.160	1.000	1.000	0.785	0.644	1.000	1.000
0.86	0.260	0.150	1.000	1.000	0.890	0.802	1.000	1.000
0.87	0.243	0.140	1.000	1.000	0.887	0.798	1.000	1.000
0.88	0.226	0.129	1.000	1.000	0.885	0.793	1.000	1.000
0.89	0.208	0.119	1.000	1.000	0.882	0.789	1.000	1.000
0.90	0.190	0.109	1.000	1.000	0.879	0.785	1.000	1.000
0.91	0.172	0.098	1.000	1.000	0.877	0.781	1.000	1.000
0.92	0.154	0.088	1.000	1.000	0.874	0.777	1.000	1.000
0.93	0.135	0.078	1.000	1.000	0.871	0.774	1.000	1.000
0.94	0.116	0.068	1.000	1.000	0.868	0.771	1.000	1.000
0.95	0.098	0.056	1.000	1.000	0.866	0.767	1.000	1.000
0.96	0.078	0.047	1.000	1.000	0.863	0.764	1.000	1.000
0.97	0.059	0.037	1.000	1.000	0.860	0.760	1.000	1.000
0.98	0.040	0.026	1.000	1.000	0.857	0.757	1.000	1.000
0.99	0.020	0.016	1.000	1.000	0.854	0.753	1.000	1.000
1.00	1.000	1.000	1.000	1.000	0.851	0.750	1.000	1.000

λ: ratio of particle diameter to pore hydraulic diameter
α: ratio of pore cross-sectional area after particle deposition onto pore wall, to initial pore area
β: ratio of pore hydraulic diameter after particle deposition onto pore wall, to initial hydraulic diameter

APPENDIX D

Sample calculations

Calculation of pore cross-sectional area based on the hydraulic diameter

For the defined geometries we can calculate the cross-sectional area of the pore based on the definition of hydraulic diameter. The following shows the calculations for a rectangular pore with aspect ratio of 7.

$$D_H = 0.1\ \mu m = \frac{4A}{p}$$

Where A and p are the cross-sectional area and the wetted perimeter of the rectangular pore. Therefore, for a rectangular pore with aspect ratio of 7, where a and b are the width and the length of the rectangle respectively, one can write:

$$A = a \times b = 7a^2$$

$$p = 2 \times (a + b) = 16a$$

Therefore:

$$D_H = \frac{4 \times 7a^2}{16a} = \frac{7a}{4} = 0.1\ \mu m$$

So a and A can be calculated as follows:

$$a = 0.057 \mu m$$

$$A = 7a^2 = 0.023\ (\mu m)^2$$

Calculation of the flow through a clean pore and a constricted pore

For a clean rectangular pore with aspect ratio of 7 and the following constant parameters:

$\Delta P = 2\ bar = 2 \times 10^5\ pa, \qquad \mu = 1\ cP = 0.001\ pa.s, \qquad l = 50\ \mu m = 5 \times 10^{-5} m$

$D_H = 0.1 \mu m = 10^{-7} m, \qquad Particle\ diameter = 0.025\ \mu m = 2.5 \times 10^{-8} m,$

$\lambda = 0.25$

$A = 0.023\ (\mu m)^2 = 2.3 \times 10^{-14} m$

Using the Hagen-Poiseuille equation, the flow rate through one clean single pore can be calculated as follows:

$$Q_{clean} = D_{H\ clean}^2\ A_{clean}\ \frac{\Delta P}{32 \mu l} = (10^{-7})^2 \times 2.3 \times 10^{-14} \times \frac{2 \times 10^5}{32 \times 0.001 \times 5 \times 10^{-5}}$$

$$= 2.875 \times 10^{-17}\ {m^3}/{s}$$

For a rectangular pore with aspect ratio of 7, results of the pore constriction simulation at λ = 0.25 are:

$\alpha = 0.227 \qquad and \qquad \beta = 0.182$

Therefore:

$A_{constricted} = \alpha \times A_{clean} = 0.227 \times 2.3 \times 10^{-14} = 5.221 \times 10^{-15}$

$D_{H\ constricted} = \beta \times D_{H\ clean} = 0.182 \times 10^{-7}$

Using the same equation for a constricted pore yields:

$$Q_{constricted} = D_{H\ constricted}^2\ A_{constricted}\ \frac{\Delta P}{32 \mu l} = 2.140 \times 10^{-19}\ {m^3}/{s}$$

Calculation of the number of pores in the membrane

For a membrane having rectangular pores with aspect ratio of 7, Following PSD B (chapter III), calculation of the total number of pores, and the number of pores of a specific size ($0.1\mu m$), is as the followings:

$$AF_i = A_{i,clean} \times f_i = 2.3 \times 10^{-14} * 0.00443 = 1.0127 \times 10^{-16} m^2$$

In which, f_i is the normalized frequency of the pore hydraulic diameter of $0.1\mu m$ derived from the log-normal distribution.

The equation can be written for all the pore sizes available in the membrane. Then the accumulative area frequency (*AAF*) is calculated as:

$$AAF = \sum AF_i = 4.0536 \times 10^{-11} m^2$$

Using the equation (12) in chapter III, the total number of pores (of all sizes) in the membrane can be calculated:

$$N = \frac{porosity \times membrane\ area}{AAF} = \frac{0.2 \times 1m^2}{4.0536 \times 10^{-11} m^2} = 2.4655 \times 10^{12}$$

The total number of pores of the specific size of $0.1\mu m$ can be calculated as:

$$n_i = f_i \times N = 0.00443 \times 2.4655 \times 10^{12} = 1.0922 \times 10^{10}$$